THE APPLICATION OF OSCILLATION TO THE DEFORMATION OF AN ELASTO-VISCOPLASTIC MATERIAL

By

ZHIHONG HUANG

THESIS SUBMITTED TO THE FACULTY OF ENGINEERING OF
UNIVERSITY OF GLASGOW FOR
THE DEGREE OF DOCTOR OF PHILOSOPHY

OCTOBER 2000

ABSTRACT

The research reported in this thesis demonstrates the benefits of applying coaxial vibration to forming tools in soft solid forming processes using Plasticine as a model material. In the study of vibration assisted upsetting and indentation (conical and spherical), finite element models under kinematic loading were first developed to gain insight into interface mechanics. FE simulation of the model material included the effects of elasticity, viscoplasticity, strain rate, large strains and a coulombic stress boundary condition in the presence of a lubricant. Agreement was achieved between the FE results and those obtained from upsetting and indentation experiments with respect to the force-displacement curves and deformed configurations for a range of friction coefficients, specimen sizes and platen velocities. The FE models, subsequently developed to simulate processes under superimposed vibration loading of the forming tool, predicted an apparent reduction in the mean forming force. The reduction in mean force is largely dependent on the vibration amplitude and shows a weak dependence on frequency. The results illustrate the phenomenon of stress superposition, where a cyclic stress is superimposed on a non-oscillatory stress. However, a reduction in the mean force alone is not necessarily beneficial since the maximum stress under idealised superimposed vibration loading will follow the same stress-strain curve as under static loading, with both the mean and minimum stresses following paths parallel

to the non-oscillatory stress-strain curve. In fact, in the case of strain rate dependent materials, the maximum stress can be greater under vibration loading, and this overstress is correctly predicted by the FE model. However, more importantly, experiments under vibration loading using Plasticine have shown both a reduction in the mean forming force, and a maximum stress which is less than the static stress. The reduction in maximum stress achieved is related to the friction condition at the die/specimen interface. The relationship between vibration condition and soft solid material flow is investigated. It is established that vibration assisted forming can result in a significant reduction in resistance of the forming material to deformation, by a combination of stress superposition effect and a reduction in interface friction.

ACKNOWLEDGEMENTS

My gratitude and sincere thanks go to my supervisor, Dr Margaret Lucas for her supervision, advice, guidance and encouragement throughout the research work. Her support and encouragement both launched and sustained me in the study and the writing of this thesis.

Thanks are also due to the following:

Professor Michael J. Adams, for his guidance, constructive discussions and advice.

Professor John W. Hancock, Head of the Mechanical Engineering Department, for the use of departmental facilities and for his professional advice.

The technical staff of the Department of Mechanical Engineering, in particular Mr Alex Torry, for their help, preparation of equipment and assistance in the experimental work.

The University of Glasgow and Unilever Port Sunlight Research, for funding me throughout the study.

The work was carried out in the Department of Mechanical Engineering at University of Glasgow, where the support of secretarial staff and computing service staff is gratefully acknowledged.

Finally, I am very indebted to my family for their support, patience, and encouragement throughout the research.

CONTENTS

NOTATION

τ	shear stress
p	normal wall stress
μ	coefficient of friction
m	friction factor
τ_0	shear yield stress
$\overline{\sigma}$	effective stress
$\overline{\dot{\varepsilon}}^{vp}$	effective strain rate
σ_0	uniaxial yield stress
n	flow index
$\dot{\varepsilon}_{ij}^{el}$	elastic component of strain rate tensor
$\dot{\varepsilon}_{ij}^{vp}$	viscoplastic component of strain rate tensor
D, p	material property parameters
k_{sc}	shear plastic flow consistency
k	uniaxial plastic flow consistency
$\overline{p}$	mean squeeze flow pressure
R	cylindrical specimen's radius
h	specimen's height
$[M]$	mass matrix

$[K]$	stiffness matrix
$[C]$	damping matrix
φ	eigenvalue
$\{\phi\}$	eigenvector
ω	circular frequency
$\dot{\varepsilon}_0$	constant static strain rate
ε_A	vibration strain amplitude
σ_s	flow stress without vibration
$\hat{\sigma}$	maximum oscillatory stress amplitude
V_T	upper die velocity
V_L	lower die velocity
A	oscillation displacement amplitude
T	oscillation periodic time
D_L	lower die displacement during oscillation
D_T	upper die displacement
E	elastic modulus
C	sound velocity of material
P	applied load
m, N	geometric and material property factors
S	contact stiffness
E_r	reduced elastic modulus
υ	Poisson's ratio
H	hardness

ξ	geometric factor
h_p	contact depth
θ	semi-angle of conical indenter
β	angle of inclination of indenter to specimen surface
a	contact radius
h_0	zero error
δ	tip defect
d_j	sphere displacement approach
u_i	surface point deformation of specimen

CHAPTER 1

INTRODUCTION

1.1 Background

Soft solid processing operations that rely on the transmission of forces by the walls of equipment, sometimes in combination with heating, are employed widely in the food industry. Typically, such operations include rolling, cutting, forming, biscuiting and many types of extrusion processes. The feed materials, and indeed products, which show solid-like rather than fluid-like behaviour, are generically described as granules and pastes. Pastes are commonly processed in unit operations such as stamping, coining and a variety of traction induced forming operations such as in rolling and screw extrusion. The generalised bulk responses to the imposed action of the equipment walls are shown schematically in figure 1.1 in terms of the velocity, stress, thermal and physico-chemical fields [1]. It is these fields that govern the operational performance of a given process. For example the mixing quality and the throughput all depend on the prevailing velocity field. A knowledge of the stress field allows such parameters as the machine torque and the local pressures to be calculated. The thermal field governs the product temperature which is important, for example, in the post-extrusion aeration of the product. The velocity, stress and thermal fields also control the induced physico-chemical changes or the instituted cooking processes such as hydration, phase changes or chemical degradation.

The selection, optimisation and integration of these operations, in order to develop a manufacturing line capable of delivering a product with the required properties and cost, has become progressively more demanding due to a combination of factors which include the following [1]:

- an increasing diversity of equipment currently available which is coupled with a limited technical basis for selection;
- the introduction of more speciality products with complex microstructures;
- the requirement for greater raw material and compositional flexibility;
- the general need for shorter process development time-scales;
- the demand for increasing production efficiencies and reliability;
- the trend towards large batch or continuous scale production;
- the requirement for improvements in product quality consistencies.

The design of processing equipment for soft solid materials or the control and optimisation of processing operations requires knowledge of both the feed soft solid material being used and boundary conditions associated with the walls of the equipment. Therefore measurement and prediction of the bulk and wall rheological properties is necessary for further optimisation.

Soft solid materials or pastes may be defined as highly concentrated dispersions of solid particles in a viscous liquid medium. The common feature is the two phase composition of rather rigid, small particles combined with a viscous fluid. Generally paste-like properties (appreciable plastic as well as viscous response) occur when the solid fraction exceeds 40 %. Other common features among many real paste materials are that their rheological responses are strongly dependent upon their microstructures and associated features, such as the solid volume fraction and the particle-particle interface [2-4].

To study the deformation and flow of material it has become common practice to use some form of small scale test adopted from metal manufacturing. By this means, the optimal conditions with regard to both workability and microstructure

development are readily identified. In addition, such tests provide estimates of the dependence of flow stress on the level of deformation, deformation rate, and temperature, information which is valuable in selecting equipment as well as in the control and optimisation of performance and tooling via increasingly popular numerical techniques.

One of these small scale tests is the uniaxial compression test, in which a soft solid cylinder is loaded axially between two rigid platens. The uniaxial compression configuration, also known as upsetting in metalworking practice, has been widely used in the metal deforming industries for evaluation of the flow stress of plastically deforming materials and their interactions. In this study, this test has been undertaken and analysed with static and vibration loading. The soft solid or paste used in this study is known commercially as Plasticine. Plasticine is a plastic solid material which comprises clay particles and an inert mineral oil. It is commonly used as a model material to simulate the plastic flow of pastes, such as French mustard, cheese, butter and chocolate, in fundamental experimental studies of upsetting, extrusion and rolling processes [1,5,6]. The rheological characteristics of Plasticine, such as strain rate effects and stress-strain behaviour, have been demonstrated to be very similar to such materials [7]. Plasticine is therefore adopted as the generic soft solid material in this study.

During the static compression test, pastes exhibit an elastic deformation behaviour at very low strains followed by an additional complication of plastic flow. Furthermore, the transmission of stress in pastes is also greatly influenced by the wall boundary conditions. In the case of lubricated platens (low wall friction), deformation is nominally seen to be homogeneous in character. However, when a no-slip wall boundary condition is applied, the frictional interface constraints at the platens prevents the wall slip developed in the wall lubricated case and no homogeneous flow is apparent. In this case, two conical wedge zones are formed adjacent to the platens and cause plastic flow of the remaining material which

involves barrelling and folding of the free edge onto the platen surfaces [8]. This behaviour is shown schematically in figure 1.2.

The static upsetting method has been being investigated in some detail as a possible procedure for deriving the governing equations for Plasticine [6,8,9,10]. A range of parameters may be measured for cylindrical specimens at a given strain during this procedure including the mean pressure, the radial wall pressure distribution and also the diameter of the specimen at the wall and at a vertical distance that corresponds to the half-height. In principle, this should provide sufficient information to specify the governing equations and associated material parameters. Both analytical and numerical approaches are being examined in this study as a means to achieve this goal.

The oscillatory compression test, shown in figure 1.3, illustrates that whenever cyclic strain is superimposed on unidirectional loading, the inherent asymmetry of plastic deformation causes an apparent decrease in the externally observable load. An experimental result in figure 1.4 shows how dramatic this effect can be. A Plasticine specimen was tested in compression at a constant cross-head velocity. Shortly after the onset of plastic flow, the specimen is subjected at B to oscillation at 100 Hz. Immediately the mean deforming force level drops and when the oscillatory excitation is discontinued at D, the specimen again follows an elastic line until it reaches E, the point on the force-displacement curve that it would have followed in a purely static test (shown as a broken line). At F the oscillation is superimposed again, the force level drops to G. At H the oscillation is again discontinued, the specimen follows an elastic line and, after having reached the static force-displacement curve at J, continues along it. Paths BEFJ and CDGH are parallel.

The facilitation of deformation by the application of oscillations has mainly been demonstrated previously for low ultrasonic frequency excitation of metal forming processes, where some benefits were reported [11,12]. The application of high

power ultrasonic oscillatory energy to the plastic deformation of metals was widely investigated in the 1960's and 1970's, for operations such as forging, wire and tube drawing and extrusion [13-16, 17-23]. Investigations at that time were severely restricted by lack of accurate measurement technology and experimental evidence was often inconclusive. In fact, major disagreements in the literature between established research groups demonstrated the deficiencies in their supporting evidence [19]. However, it was postulated that changes in the coefficient of friction could arise as a result of a separation of the surfaces, softening of asperities, pumping of lubricant and chemical activation of the lubricant [17], but none of these mechanisms was sufficiently validated. Studies of friction under superimposed low frequency oscillations have also been published but even the most recent study [24], which attempts to relate friction trends to the behaviour of asperities, only offers possible explanations of the frictional changes measured under oscillation loading. With advances in finite element analysis, more accurate determination of the realistic constitutive models has become feasible for establishing mechanisms of improved interfacial conditions. This provides a major objective of this research.

Previous investigations of the effects of vibration on forming processes have largely been conducted at low ultrasonic frequencies (20-40 kHz) [11-13,25, 15,16,21,22,26,27,28-34]. These have been impeded by the fact that a uniform and controllable oscillation amplitude is difficult to achieve at ultrasonic frequencies even when a vibration system comprising highly tuned transmission elements and dies is used. Moreover, the beneficial mechanisms at ultrasonic frequencies are complex and attempts to characterise them have led to some disagreement in the published literature [18]. This seems to suggest that the oscillation effects could be better investigated at low frequencies as an initial research strategy, where vibration loading can be incorporated without driving the tooling or specimen into resonance. The deformation can be more homogeneous within the specimen and load, strain and stress are easily monitored. Therefore, this study concentrated on

low frequency, low amplitude vibration in the first instance, due to the relative ease of control and measurement of vibration.

Other types of deformation configuration have been examined in this study, namely indentation hardness with cones and spheres. Traditional methods of measuring mechanical properties such as elastic modulus and hardness use quasi-static indentation methods. These involve pressing a stiff, hard indenter of known geometry – pyramidal, conical or spherical – into the surface and the size of the plastic (permanent) indentation formed for a given load is measured using optical microscopy after the sample is unloaded. The modulus is found by examining the unloading curve and the hardness from knowledge of the load and projected area of the deformation.

Recently the advent of depth sensing indentation techniques has enabled the load-indentation depth to be continuously monitored during loading and unloading with high precision and accuracy and has enabled the mechanical properties to be studies as a continuous function of displacement. This innovation has significantly extended the range of test capabilities. It also provides a simple method, which can be updated, for the study of the effect of superimposition of oscillation on the static load.

1.2 Objectives

The purpose of this research programme is to investigate the application of oscillation in the forming of the model material, Plasticine. The aim is to establish a fundamental understanding of the benefits of stress superposition and improved interfacial conditions in vibration assisted processing of generic soft solid material.

The investigation, using both experimental and finite element techniques, is in three parts. The first is a study of static deformation in upsetting processes to obtain detailed knowledge of the flow behaviour of the forming model material,

Plasticine, and thus develop a suitable finite element model to predict the deformation history and force-displacement relationships under oscillatory assisted forming.

The second is a study of the upsetting process, in which a specimen is compressed with the lower die oscillated axially while the upper die provides a static compressive load. This is an investigation into volume and surface effects, studying the interaction of the applied low frequency oscillation stress to a deformation process. In order to develop an understanding of the underlying mechanics of the process, the mechanics of axisymmetric upsetting with one axially oscillated die was studied. A series of upsetting tests was conducted, studying the effects on the magnitude of induced cyclic stress, of such variables as amplitude and frequency of oscillation, deformation rate and wall interfacial boundary condition.

The third part is a study of the indentation process with and without axial oscillations applied to the indenter. This investigation focuses on volume and surface effects, again studying the interaction of applied low frequency oscillatory stress to the deformation.

This thesis also describes and discusses the historical development of the technology of applying oscillations to metalworking processes, and details the research undertaken in the field of soft solid material deformation processes and optimisation.

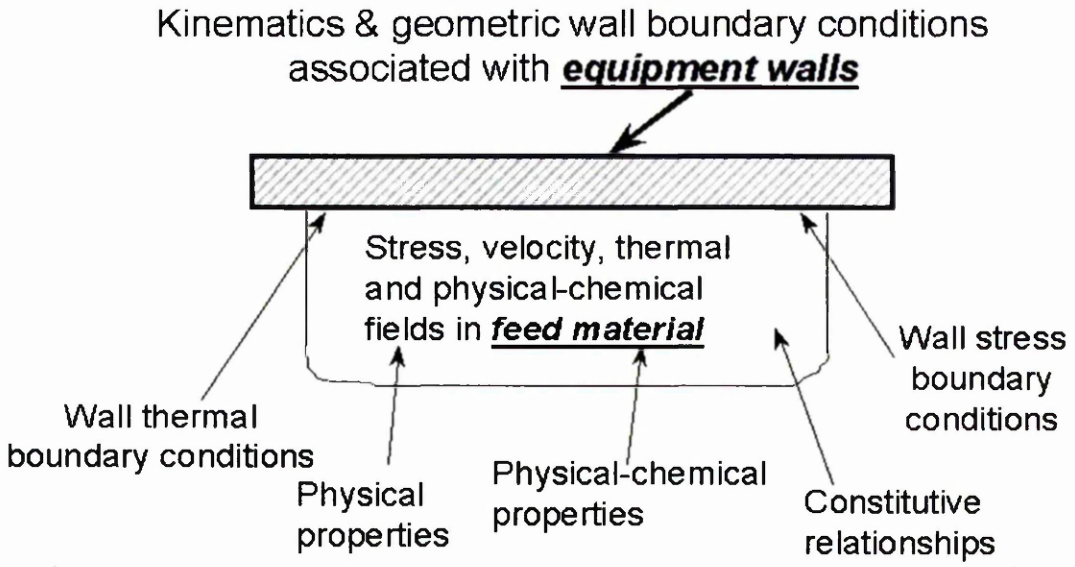

Figure 1.1 Schematic representation of the various factors that produce a given bulk response in feed materials being acted upon by equipment walls (reprinted from Adams and Briscoe [1]).

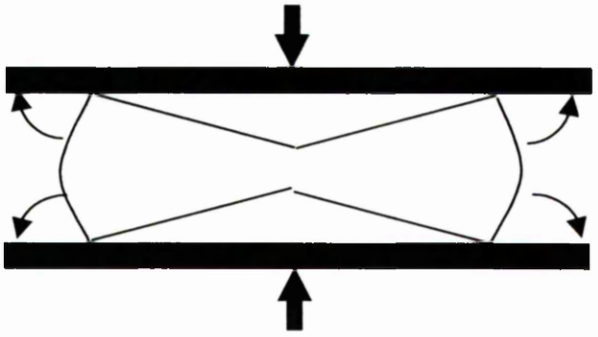

Figure 1.2 Schematic diagram of the deformation field in a cylindrical specimen developed during the upsetting of a plastic solid for large values of the platen friction. (reprinted from Adams *et al.* [8])

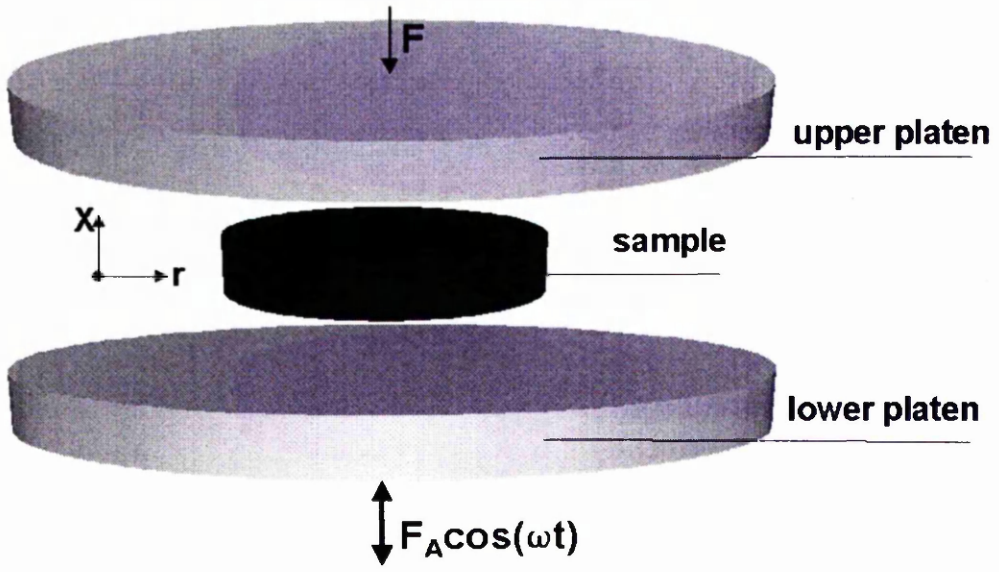

Figure 1.3 Schematic of oscillatory axisymmetric upsetting.

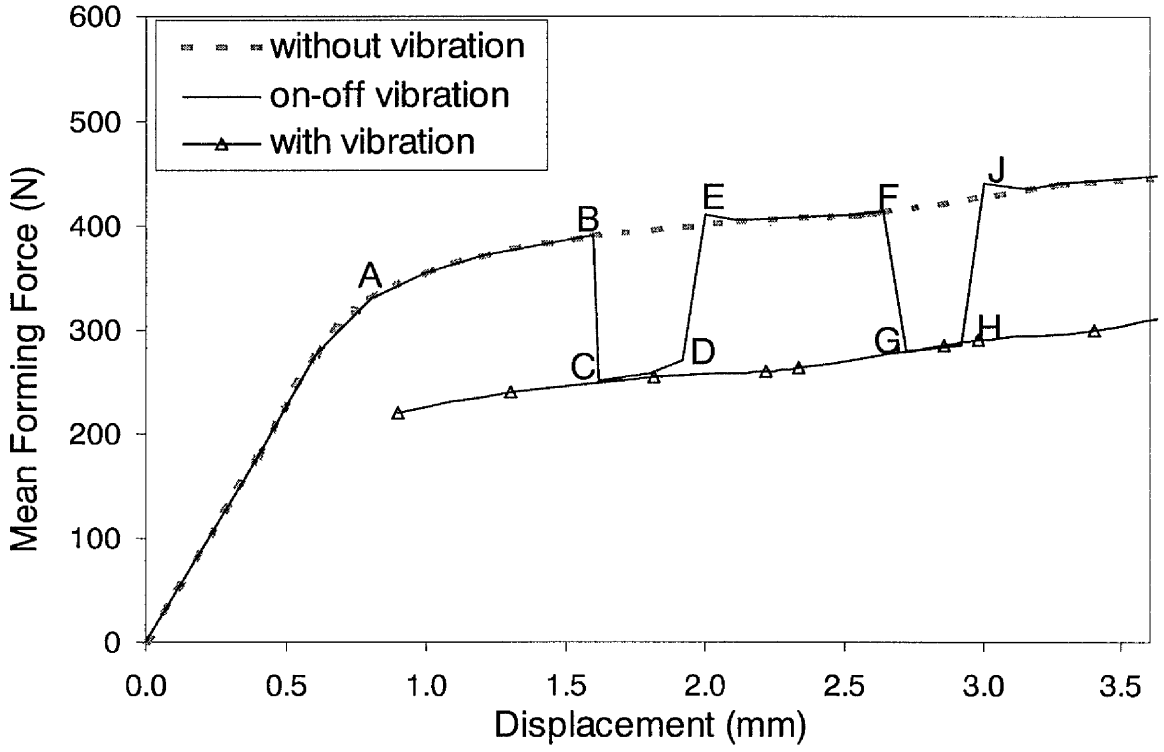

Figure 1.4 Compression test of a Plasticine specimen. In addition to the static loading with a constant speed of 2.5 mm/min, the specimen is subjected to cyclic loading at 100 Hz.

CHAPTER 2

REVIEW OF THE LITERATURE

2.1 Review of the Application of Oscillation in Metal Forming Processes

2.1.1 Fundamental Effects of Oscillation on Metal Plasticity and Surface Friction

Since the early nineteen-fifties, the application of oscillatory energy to a metal undergoing plastic deformation has been studied by a large number of investigators [11-16,20-22,24-39] and several reviews [17-19,38] have been published. Claims were made that, with superimposed oscillatory stress, which in some studies was at ultrasonic frequencies and in others at sonic frequencies, deformation may be achieved with significantly reduced forces and improved metallurgical properties and surface conditions of the finished workpiece [19].

Generally, oscillatory metalworking is said to occur when cyclic motion, or stress, is applied to the tools or the workpiece during deformation. It appears that the extent to which oscillation may be advantageous depends on the speed of processing, the type of process, the lubricant used, the mode of oscillation and the material being deformed. The cyclic variation of stress may be the feature which benefits the process of deformation, or alternatively, an improvement may arise independently of the variation of stress and result from the motion of the tools.

The first investigation into the mechanics of oscillatory metalworking was conducted by Blaha and Langenecker [11,12], who reported a yield strength reduction due to superimposed ultrasonic vibration in tensile testing of pure zinc single crystals. A comparison of oscillatory with non-oscillatory results is shown in experimental shear stress-strain curves (figure 2.1). Reductions equal to and considerably larger than the stress amplitude of vibration were reported. Similar results were also obtained by other researchers in testing a variety of metals and alloys [13-16,25].

Initially, researchers found that when a high frequency vibration was applied to a metal it softened and sometimes melted [11-13,25]. They believed that the vibration energy was preferentially absorbed at the dislocation sites enabling deformation to proceed with very much reduced forces. The effect of adding the vibration was believed to be a reduction in the rate of work hardening and an increase in the strain to fracture [15]. These effects came to be known as the volume effect. It was quickly appreciated that if these results really were achieved, then they were of significant importance to the metal deformation industry. Consequently, without a thorough understanding of the mechanics, many research workers applied vibrations, within the sonic to ultrasonic frequency range, to metal deformation processes, such as wire-drawing, tube-drawing, tube-sinking, forging, extrusion, coining, cutting and rolling [16,26]. In many cases observations of reduced deformation forces led to the belief that the volume effect did not account for all the reduction of process forces obtained and indeed that process forces could be reduced without a change in the metallurgical properties of the metal. Thus, it was proposed that the frictional conditions between the tool and the workpiece were changed in such a way as to reduce the process forces [14,27]. This effect came to be known as the surface effect.

The following investigations, undertaken by researchers having different objectives have led to a much clearer understanding of the mechanics of oscillation propagation in a yield metal. It was stated that in the absence of a rise in

temperature in the workpiece and at vibration frequencies up to about 25 kHz there is no volume effect as originally conceived, except when the intensity of vibration is sufficient to bring about a rise in temperature which changes the properties of the metal [23]. Thus, the superposition mechanism was deemed responsible for the major part of the volume effect. The superposition effect in ideal oscillatory plastic deformation of metals is said to occur when a calculable cyclic stress is superimposed on the non-oscillatory stress, the peak of each cyclic stress variation being coincident with the corresponding steady state or non-oscillatory stress, the reduction in mean force being equal to the periodic force amplitude [14].

The superposition mechanism does explain how forces can be reduced in a metal deformation process in the absence of both a change in the yield characteristics of the metal and a reduction in the coefficient of friction. However, the superposition mechanism does not account for reductions in hardness, rate of working hardening, residual stress and the large-scale reductions in stress observed when intensive ultrasound is imparted to the test piece [13,15]. Fortunately, the superposition mechanism rarely occurs in isolation and so the oscillatory metal deformation may benefit from other mechanisms, which occur simultaneously with, but independently of it.

Research and development attention has been directed towards the surface effect. Most of the fundamental research was concerned with demonstrating that vibrations can reduce friction forces. Pohlman and Lehfeldt [27] applied ultrasonic oscillations to a slider, both normal and tangential to the plane of motion, in the latter case normal and parallel to the sliding direction. In all cases an apparent reduction in friction forces was observed, the most effective configuration being motion parallel to the direction of sliding. The reduction in friction was found to be less marked at the higher sliding velocities. Similar conclusions were reached by Godfrey [35]. Reductions in sliding friction were observed by application of low-frequency normal oscillations of a plane at 20, 100 and 1000 Hz. In this case, friction was only reduced when separation of the mating surfaces occurred, i.e.

when there was a reduction in the period during which the friction forces acted (figure 2.2). Oscillations in the sliding direction have been observed to reduce static and sliding friction by Lenkiewicz [36]. At frequencies of 20-120 Hz reductions in friction of up to 80 % were observed, the effect being most marked at the high amplitudes and frequencies, and the low sliding speeds. The phenomenon of stick-slip was eliminated by oscillations.

A theoretical analysis of friction vector effects was first provided by Mitskevich [7] who showed that the friction force was periodically reversed, due to the periodic motion of one body relative to the other. The analysis showed the resulting reduction in friction to be an increasing function of the ratio of oscillatory velocity to sliding velocity only, thus agreeing with the experimental work of Lenkiewicz [36], and Pohlman and Lehfeldt [27].

A fuller explanation was given by Sansome [38], that the coefficient of friction μ may be reduced as a result of (a) pumping of the lubricant, (b) softening or melting of the asperities, (c) chemical activation of the lubricant and (d) separation of the surfaces. The extent to which any or all of these mechanisms affect a particular process has not been made clear and work still remains to be done to complete an understanding of the reasons for the frequent reduction of μ.

Consequently, in oscillatory metalworking the swaging effect may occur [38] when an increase in the lateral stresses (often compression) produces a consequential reduction in axial stress. Consideration of either of the yield criteria, applicable to ductile metals, leads to the conclusion that since the yield stress of a metal remains constant, if either of the lateral principal stresses is increased, the remaining principal stress must be reduced.

Pertinent references are to be found in the review papers by Eaves *et al.* [17] and Dawson *et al.* [18,19] which conclude that:

- the superposition mechanism occurs in almost all examples of oscillatory deformation;
- it may be useful to drawing processes and possibly other industrial metal forming processes when or if the tools can be oscillated in anti-phase;
- the reduction in friction could arise as a result of the swaging effect, changes in the coefficient of friction and the friction vector effect;
- changes in metallurgical properties arise from an increase in temperature which may occur locally at dislocations, shear planes, or discontinuities or which may occur generally;
- the use of oscillatory energy to change the metallurgical structure may be an efficient use of power since the vibration energy is dissipated at local sites where deformation is occurring.

However, none of these mechanisms were sufficiently validated. A more recent study relevant to workpiece fixture problem by Hurtodo and Melkote [24] attempts to relate friction trends to the behaviour of asperities and offers possible explanations of the frictional changes measured under oscillatory loading but these explanation remain to be validated.

2.1.2 Applications of Oscillation in Metalworking Processes

Research has been concerned not only with the fundamental effects of oscillation on metal plasticity and surface friction, but also with applications to many industrial metal-forming processes with a view to obtaining the widest commercial exploitation, such as forging [16,20,28,39], drawing [21,29-31], cutting [32,33], welding [34] and rolling [22]. In this field, the activity was shifted from theory to practice. Emphasis was placed on forming force reduction, improved formability, productivity and quality. In most cases a varying amount of force reduction was found which was attributed either to one of the superposition theories or to the reduction of friction. Formability of the materials was sometimes increased [21,29-31], other times reduced [15], but the surface finish in most cases improved. In

industrial metal-forming process, it is usual for frequency to be of the order of 13-20 kHz. The frequency chosen is the lowest which is environmentally acceptable and the resonator dimensions are manageable.

A considerable number of investigations into the application of oscillations to compressive deformation of metals have been carried out [13,16,19,20,39]. An initial series of experiments was conducted with low-frequency axial oscillation applied to forging tools. Various materials were forged, hot and cold, with and without lubrication, in both open and closed dies. The general observations were that the average pressures, hardness, degree of barrelling, and residual stresses were reduced, greater reductions were possible for the same static load, and the hardness, strain and residual stress distributions were more uniform. Reductions in the average pressures and increases in the degree of deformation were observed. The greatest benefits were obtained when separation between the tool and work-piece occurred [19]. To investigate the possibility of reducing friction forces by periodic off loading, Lee *et al.* [20] conducted compression tests on various materials with a periodic release of stress at 1-5 cycles/min. They demonstrated that under cyclic loading, peak pressures could only be reduced if a reactive lubricant was used, because the specimen may be effectively re-lubricated once every cycle.

Forging has also been attempted with ultrasonically oscillated platens. Kristoffy [16] and Kirchner *et al.* [39] succeeded in measuring the alternating component of stress during forging of aluminium with ultrasonic oscillations applied to the tooling. For low intensities both investigators found the drop in mean force to be equal to the alternating force amplitude. However, at high intensities, Balamuth [28] observed that the drop in the mean load was in excess of that predicted by a superposition mechanism. This was attributed to heating of the test-piece and its subsequent softening. Kristoffy also pointed out that when the velocity of the tool exceeds the maximum oscillatory velocity, no stress variation will be induced, and therefore there will be no reduction in mean force.

A research group at the University of Aston took advantage of the swaging effect on tube drawing processes [21]. This development followed from an ability to produce high acoustic power at an ultrasonic frequency and, by feeding the power to the tube-drawing die, cause a floating plug in the bore of the tube to vibrate. Thus, the necessity for a plug bar is eliminated and long lengths of tube in coil form can be drawn having the advantages normally associated with straight lengths of ultrasonically drawn tube. Continuing research [30] showed that the fundamental mechanics of the process could be exploited most effectively by radially vibrating the die at an ultrasonic frequency. Consequently, developments were initiated to use die radial vibration in industrial tube-draw machines. Further, it was soon realised that not only was this type of vibration motion of the draw die most effective, because the tube was swaged while friction was reduced, but that the equipment could be easily developed for drawing large diameter tube or thicker walled tube, or for drawing of cups and cans, or for the delicate drawing of very thin-walled tube. The advantages may be summarised as: reduced schedule length; reduced chatter; reduced pick-up; reduced annealing and pre-treatment costs; increased productivity of the draw machine and the operator; improved surface finish, especially in the bore; and an increase in the tool life [30].

2.1.3 Discussion of the Volume and Surface Effects in Metalworking Processes

Most of the early attempts to apply oscillations to metalworking processes were hampered by a lack of understanding of the nature of ultrasonic stress waves, and the inability to measure their magnitude accurately. Consequently, at ultrasonic frequencies only mean forces were measured. Hence, the universal claims of reduction in deformation forces are not reliable, since the peak instantaneous stresses in the deformation zones are not known. Any assessment of the kind of mechanisms involved in these apparent effects is further hampered in many cases by insufficient details of equipment, technique or results being presented.

In later investigations, however, where periodic stresses were measured [16,25,27], the universality of the superposition mechanism has been demonstrated, i.e. when the applied stress has a cyclic component, then the mean applied stress will be reduced by the cyclic stress amplitude. Furthermore this has been shown to be true at ultrasonic and sonic frequencies. Thus, even if other mechanisms of force reduction are active, superposition will always account for some reduction in forces, when the forming force has a cyclic component. Thus, in the absence of a heating or friction effect, it is thought that for the majority of instances where a reduction in load, increased deformation, or increased strain rate was observed, these effects were the result of superposition.

From the published data it is difficult to assess that the effects of oscillations on friction have been substantiated. It is considered that the majority of reductions in force observed and attributed to a reduction in friction, were more likely due to a combination of superposition and heating [25].

However, there are cases, which are not so readily explained by these mechanisms. Oscillations of the platens have been shown to reduce the non-uniformity of deformation in forging. Similarly, the virtual elimination of stick-slip and chatter in wire and tube drawing and the improved product in extrusion, point to ultrasonic oscillations improving friction conditions.

At present, the underlying mechanisms are not definitely known, but research reveals several possibilities. Low frequency oscillations are most effective in reducing barrelling in upsetting when the tools periodically separate from the surface due to the weldments being broken continually and the redistribution of lubricant [20,40]. The most probable mechanism for friction force reduction in drawing and extrusion is the reduction of its mean component in the axial direction by periodic variations in the direction of the friction vector. Periodic swinging of

the friction vector produced by torsional oscillations of the die has been proposed as a means of reducing friction in ironing [16].

When the level of oscillatory energy imparted to the workpiece is high, it will result in a rise in temperature. This may result in thermal softening of the material, resulting in a reduction in forming load [28]. However, the ultrasonic power required to achieve this effect is likely to be very large, particularly since the amount of heat generated is dependent upon the size of the workpiece. The reduction in process stress obtained by ultrasonic induced heating could equally well be obtained by heating the workpiece by some other external means, except that sometimes ultrasonic vibrations enable the heat to be located more readily in the deformation zone.

If the oscillations are applied in the direction normal to the applied work on the workpiece, then the applied work will be reduced. In operations such as wire and tube drawing, where the applied forces are tensile, real benefits are possible, since greater reductions in area are possible. Also, the conventional limit on the maximum reduction of area does not apply since with sufficiently powerful oscillations all the work could be transferred to the transverse direction, and the process becomes one of swaging only [29,30].

Finally, it is thought that when deforming metal through an oscillating die, the increased relative motion between tool and workpiece and hence frictional work will result in an improvement in the surface finish due to a changed friction force [29].

Whilst the mean friction force will be reduced at all frequencies by these mechanisms, it is not yet clear how the applied stress is affected. Technology associated with vibration assisted forming is severely under-utilised and is slow in being adapted to alternative or enhanced manufacturing processes. This is mainly due to the lack of understanding of how the benefits arise, an inability to quantify

or model their contribution and no real understanding of how the mechanisms interact. Also, research has been very largely concentrated in metalworking applications and the effects of applying oscillation to alternative complex materials has not been reported. It is expected that deformation will respond to the cyclic component, and thus benefits will be achieved. This possibility will be studied as part of this present investigation by using Plasticine as a model soft solid material.

2.2 Review of Soft Solid Material Forming Processes

2.2.1 Deformation and Flow of Soft Solid Material

Soft solid materials or pastes may be defined as highly concentrated dispersions of solid particles in a viscous liquid medium. The common feature is the two-phase composition of rather rigid, small particles combined with a viscous fluid. The relative proportion of the two phases, the surface area of the rigid particles, the particle interaction and the rheology of the viscous liquid phase all contribute significantly to the rheological properties of the paste. Generally paste-like properties occur when the solid fraction exceeds 40 %. Many paste materials are notably viscoplastic with a yield stress dependent on the applied strain rate. In addition, there may be a small elastic strain region where the material is referred to as viscoelastic-plastic. It may also be observed that the stresses will increase with the applied strain, this effect is known as strain hardening. Other common features among real paste materials are that their rheological responses are strongly dependent upon their microstructures and associated features, such as the solid volume fraction and the particle-particle interface. Most of the pastes used in the food industry are additionally biomaterials, with properties which vary with time and the incumbent variable of process history.

There has been a substantial number of reviews and studies devoted to the subject of the forming of powder and paste systems. On the subject of extrusion flow of ceramic pastes and powders, the studies have investigated the interface

phenomenon and the intrinsic flow characteristics of the systems. Adams *et al.* [5] considered orifice and capillary flow of a model paste material for estimating the rheological flow properties of the material. Benbow *et al.* [2] presented a review on the subject of the prediction of ceramic paste extrusion pressures based on the data produced from a simple laboratory-scale ram extruder. Influences of the liquid phase rheology on particulate paste extrusion [3] and the paste formulation on the extruded structure [4] have also been investigated, where each response of the system is governed by the boundary condition and the intrinsic rheology of the material. These authors have also concluded that the particle size distribution of powders not only alters the texture and the structure of the extrudant, but it may also provide certain significant advantages in forming processes.

Frictional forces between the paste and the rigid walls, usually a metal, during forming operations also play an important role in the mechanisms of compaction and motion. The frictional force is the force which acts to restrict the relative motion of the particulate in the continuous phase. Benbow and Bridgwater [41] have examined the role of frictional forces in paste extrusion. From their study it was concluded that the liquid phase, present in the paste, contributes to the presence of low interparticle and wall boundary frictional conditions. However, pastes will readily stick to the walls. This is because, unlike coherent solids, pastes may conform to the interfacial asperities of the walls.

Extruders are complex deformation configurations. Investigations of upsetting processes offer an alternative simple compressive deformation procedure available for characterising the intrinsic flow properties and interfacial boundary conditions between the soft solid and the rigid walls. Adams *et al.* [6,8,42] and Kamyab [9], based on the compression technique, studied the bulk rheology in paste flows from the observed response, which was greatly dominated by the action of the boundary conditions. In their experiments, the usual mechanical behaviour of pastes was described by an elastic deformation at very low strain followed by failure at some critical stress (the yield stress) and further flow as a non-Newtonian fluid. Previous

work [6] has established that the bulk flow behaviour may be reasonably described by the Herschel-Bulkley relationship [43]. This model is the most general form for viscoplastic materials where the viscous component is given by a power law term. The constitutive information used in this model has been obtained for pastes from tensile, compressive, orifice and indentation measurements.

Other types of deformation configurations have been examined for soft solid material including the compression of rings [8], indentation hardness with wedges [44], cones and spheres [45] and ram extrusion [8]. All these methods have virtues and limitations and should, in principle, produce consistent results. Some are more useful for sensing the wall boundary conditions (ring compression). Others provide bulk data at low strains (indentation) and high strains (upsetting).

The process parameters such as load, stress and strain distribution greatly depend on the bulk flow behaviour of the paste and the boundary condition between the deformed material and the rigid walls of the processing equipment. During the upsetting process, the frictional forces at the wall interface may contribute substantially to an enhancement of the overall load necessary to induce plastic flow during the deformation process. The effects of the surface friction have been studied by many authors, but a good example of the influence of friction at a tool-material interface is given by Rooyen and Backofen [46]. They investigated the compression of aluminium, copper and iron cylinders with various tools of different surface roughness. Their work showed a marked reduction in the applied load necessary to induce flow when the compression tests were conducted with the aid of a good lubricant, and these results are therefore of direct relevance to studies of surface friction in soft solids processes [1,9,47].

The level of wall friction also effects the way in which a material is deformed. Low frictional stresses at the walls may facilitate a near homogeneous deformation condition during the upsetting process. High frictional stresses may however, lead

to a no-slip boundary condition with substantial barrelling of the sides of the specimen [42].

2.2.2 Idealised Material Governing Equations

The description of the mechanical properties of materials by the use of mathematical or constitutive relations invariably involves certain physical idealisations about deformation or flow [1]. The characteristics of some of the most common descriptions are shown schematically in figure 2.3. A perfect solid deformation characteristic (figure 2.3a) is considered to be the one where the stress-strain interrelationship is independent of the rate of deformation or strain rate. In contrast, the perfect flow of liquids is where the stress-strain rate interrelationship becomes independent of the imposed strain (figure 2.3b). The commonly adopted constitutive relationships for shear induced deformations and flows are given in table 2.1.

As shown in figure 2.3, the deformation of a perfect elastic Hookean solid (curve 1) results in a reversible distortion and the development of an opposing elastic force or stress which, if infinitely large, is characteristic of a rigid response. For elasto-plastic solids (curve 2), permanent distortion occurs at a critical stress known as the yield value. When high strains are involved it is common to neglect the accompanying elastic strains and to employ a rigid-plastic approximation (curve 3). If the stress remains constant at strains greater than the yield value then this case is known as perfectly plastic deformation. However, some plastic solids may strain harden or soften (e.g. curve 4). Isothermal and isobaric viscous flow is characterised by the imposed stress being only a function of the resulting strain rate. If these two parameters are directly proportional then the fluid is described as being Newtonian (curve 5 where the gradient is equal to the viscosity). For the power law fluids (curve 6), the corresponding stress is proportional to the strain rate raised to a power index n ($0<n<1$). Curves 7 and 8 show two cases where a

finite stress (the yield value) is required to initiate flow. When the resulting plastic flow stress is a linear function of the imposed strain rate (curve 7), the fluid is described as a Bingham material. A non-linear stress-strain rate response in plastic flow is described as a Herschel-Bulkley characteristic (curve 8). Since the plastic flow is implicitly assumed to be initiated at a near zero value of the imposed strain, these relationships are described as rigid-viscous approximations.

The above constitutive relationships apply to coherent materials that are a nominally fixed density because of their relatively small volumetric compressibilities.

2.2.3 Evaluation of the Interfacial Friction

In metalworking theory two types of slip boundary conditions are generally considered. These are referred to as Coulombic and the Tresca criteria.

For the case of a Coulombic boundary condition, it is assumed that the wall tangential stress τ is directly proportional to the normal wall stress, p, in the presence of a lubricant. That is to say

$$\tau = \mu p \tag{2.1}$$

where μ is the conventional coefficient of friction. In the case of uniaxial deformation, both the values of τ and p would generally be functions of the radial co-ordinate, r, that has its origin at the axis of the cylindrical shaped specimen.

The Tresca boundary condition, in contrast, defines the wall traction as being some function of bulk shear stress, τ_0, thus

$$\tau = m\tau_0 \tag{2.2}$$

where m is known as the interface shear or the friction factor. As an approximation, the coefficient of friction, μ, is given as $\mu = m/\sqrt{3}$ by Von Mises criteria.

The least value in the fully lubricated case where the normal wall stress will induce plastic flow is given as σ_0 or σ (the uniaxial yield or the flow stress). Then, the maximum value of the coefficient of friction is given by a ratio of the shear yield stress, k, to the flow stress, σ_0. Hence, using the Von Mises criterion, $\mu = \tau_0 / \sigma_0 = 1.155/2$, where $\mu_{max} = 0.57$ or $m = 1.0$. For the Tresca criterion, $\mu = \tau_0 / \sigma_0 = 1/2$, where $\mu_{max} = 0.5$. Thus the estimated maximum value of the coefficient of friction for a slip boundary condition will be equal to 0.577 or 0.5 depending on the yield criterion used. It may be assumed for the practical estimations of the coefficient of friction, that under a sufficiently lubricated wall boundary condition, the wall shear stress, τ, is given by $\tau = \mu p$. This is only valid provided the value of $\tau < \tau_0$, otherwise, there is a sticking boundary friction condition i.e. $\tau \geq \tau_0$. It is, however, quite difficult to achieve a perfectly lubricated condition during the deformation process. This may be simply due to the deterioration of the lubricant as a result of the thinning of the film when the deformation proceeds. The deterioration of the lubricant exposes fresh and unlubricated material to the tool surfaces, which may lead to a sticking rather than a sliding boundary at the interfaces. In soft solid processing operations sticking is a predominant feature of the interface between the material and the processing tools. This behaviour may result in the effective value of the coefficient of friction exceeding the value of 0.577 [9].

Among the methods to measure the magnitude of the friction coefficient encounted in large deformation during metal forming processes, the ring compression test has been widely used [8,9,48-54]. Male and Cockcroft [52] introduced the classical experimental ring geometry of 6:3:2 (outer diameter:inner diameter:height). This technique utilises the dimensional changes of a test specimen to arrive at the magnitude of the friction coefficient. For a given percentage of height reduction

during compression tests, the corresponding measurement of the internal diameter of the test specimen provides a quantitative measure of the magnitude of the friction coefficient at the die/specimen interface. If the specimen's internal diameter increases during deformation, friction is low; if the specimen's internal diameter decreases during deformation, friction is high. Using this relationship, specific curves (later called friction calibration curves) were generated by Male and Cockcroft [52]. It was stated that the friction calibration curves do not depend on material properties. Barrelling and strain hardening effects have been assumed to be negligible. Many further studies have attempted to investigate the effects of different factors on friction calibration curves for Plasticine [8,9,49,50,53], including material properties, strain-rate sensitivity, deformation speed and barrelling. These studies included experimental investigations, upper bound solutions and finite element analysis. Adams *et al.* [8] and Kamyab [9] found that the friction calibration curves are not in good quantitative agreement with experimental data, but only provide some approximate estimate of trends. Sofuoglu and Rasty [50,53], Carter and Lee [49] all conclude that friction calibration curves are indeed affected by the material properties and test conditions and every material has its own distinctive friction calibration curve. For Plasticine, they reported that friction calibration curve was unique for each colour.

2.2.4 Plasticine as a Model Material

Plasticine, the well known modelling material, is a concentrated dispersion of clay particles in mineral oil which, as its name implies, is a very plastic soft solid material, obviously exhibiting an apparent yield stress. It offers some advantages in that it is readily available, reasonably stable and non-drying in the short term [7]. It has the added advantage that it can be layered in different colours, reassembled before experimentation, and cut after working to show the extent of deformation within each of the coloured layers. Where it is in contact with solid surfaces, it can be lubricated if necessary. Table 2.2 shows the chemical composition of a typical Plasticine batch (Yagishita [55]).

In the simulation of metal forming processes, physical modelling technique offers an alternative and relatively inexpensive method to simulate the actual metal forming process by utilising a model material and process geometry that closely resemble those in the actual metal process. Typical model materials for modelling workpiece are Plasticine, wax and lead [56]. Choosing a model material requires of similarity and practicality to be addressed. It generally impractical to select a model material that satisfies similarity of geometry, mechanical properties, friction conditions and thermal conditions. Thus partial similarity was accepted if the necessary similarity conditions are selected carefully. Plasticine has been the most widely used plastic material (especially in simulating hot steels) in fundamental studies of forging [57], rolling [58] and extrusion [59] as well as many other metal component forming processes [60,61]. The rheological characteristics of Plasticine, in terms of the effects of strain-rate on its flow stresses and the stress-strain behaviour, is very similar to that of steel at elevated temperature [55]. A review of the study of simulative model tests in metal forming using Plasticine has been presented by Yagishita *et al.* [55]. The authors examined the plastic characteristics of white Plasticine, especially with respect to its similarity to the deformation behaviour of hot steel. It was confirmed that the flow characteristics of the material were similar to those encountered in the hot working of steels. The boundary condition exhibited during the deformation of the material, however, offers a complex phenomenon compared to those exhibited by hot steel. The rheology of Plasticine is also found to be very temperature sensitive. The yield stress and compressive stresses may decrease with rising specimen temperature in the region of 3.5 % per degree [9]. However, the major problem faced in using Plasticine is the different properties exhibited from batch to batch. Careful control of the initial properties must therefore be performed for each batch that is acquired.

In more recent years, Professor Wannheim and co-workers at the Technical University of Denmark [62] have developed expertise in the use of microcrystalline wax as a model material and enabled considerable insight to be

gained into many metal forming processes under laboratory conditions [56,62-64]. However, it is impossible to define a wax as a real material. It has been reported that such model materials are not realistic in the simulation of thermal effects, which can be vitally important in hot and warm forming, nor can they reproduce the interface friction conditions to which some aspects of metal flow and tool wear are sensitive [56,63,65].

The rheology of Plasticine is also very similar to that of other soft solids such as concentrated particulate suspensions, which exhibit plasticity [7,9]. Such substances include food products and ceramic particles combined with fluids [44]. It has thus been extensively used as a yield-stress soft solid in squeeze-film deformation (known as upsetting in metal forming processes) [6], indentation [45], scratch hardness and friction tests [44], as well as in the study of interface constraints and general flows such as extrusion through orifices and through tubes [5]. The post-yield behaviour of Plasticine is well characterised [6] using the Herschel-Bulkley equation [43]. Plasticine was chosen as the generic soft solid material in this study in order to investigate the effect of application of oscillation on the interface mechanics.

2.3 Simulation of Process Operations

More recently, a rapid increase in the use and application of FE modelling has occurred due to the increase in capability of computers. The flexibility of the commercial packages available allows the input of numerous material parameters in complex calculations. Numerical computational packages also operate with differential equations describing the mass, momentum and energy balances. The effective application of these procedures depends upon the availability of a set of governing equations which provide the inputs for this type of simulation. These governing equations comprise the wall boundary conditions and bulk constitutive relationships that represent the interaction of the feed material with the equipment walls and the intrinsic bulk response respectively.

Bulk metal forming process simulation allows a realistic prediction of the workpiece response during the forming process. Therefore, the process development engineer can gain a better understanding of material flow within the die and can optimise tooling to eliminate tears, laps, and other defects. In addition, the prediction of tool-workpiece interface forces is useful for estimating press loads and die wear. Simulations have contributed to a reduction in process development time and could potentially eliminate the need for costly trial-and-error tooling prototypes.

Finite element (FE) modelling has been usefully employed in a number of commercial areas and has become a normal part of the design and improvement of many industrial processes. Examples include hot rolling [66], upsetting [48,67] and extrusions [68]. The analysis has proved to be flexible and easy to adapt for a particular process. The results obtained from such methods have proven to be in agreement with those obtained in experimental studies and the theoretical analysis.

Among different testing methods that have been examined, solid cylindrical upsetting was studied extensively by researchers to better understand the influence of friction on barrelling, working hardening and contact pressure distribution. A comprehensive discussion on the experimental aspects and finite element simulation of rate-dependent metal upsetting was given by Shih and Yang [67]. Complete sticking friction was assumed in the simulation, such that the billet adhered to the die. Simulations conducted by Adams *et al.* [47] featured the squeeze flow of a paste material under no-slip and lubricated boundary conditions and led to the development of an elasto-viscoplastic formulation for the deformation and flow of such fluids. The approach used the Coulombic friction contact model, where the workpiece was permitted to slide along the tool to approximate lubricated forming conditions. This work is extended in this thesis, where finite element simulations provide a basis for gaining insight into the deformation of the model material under static and oscillatory loads.

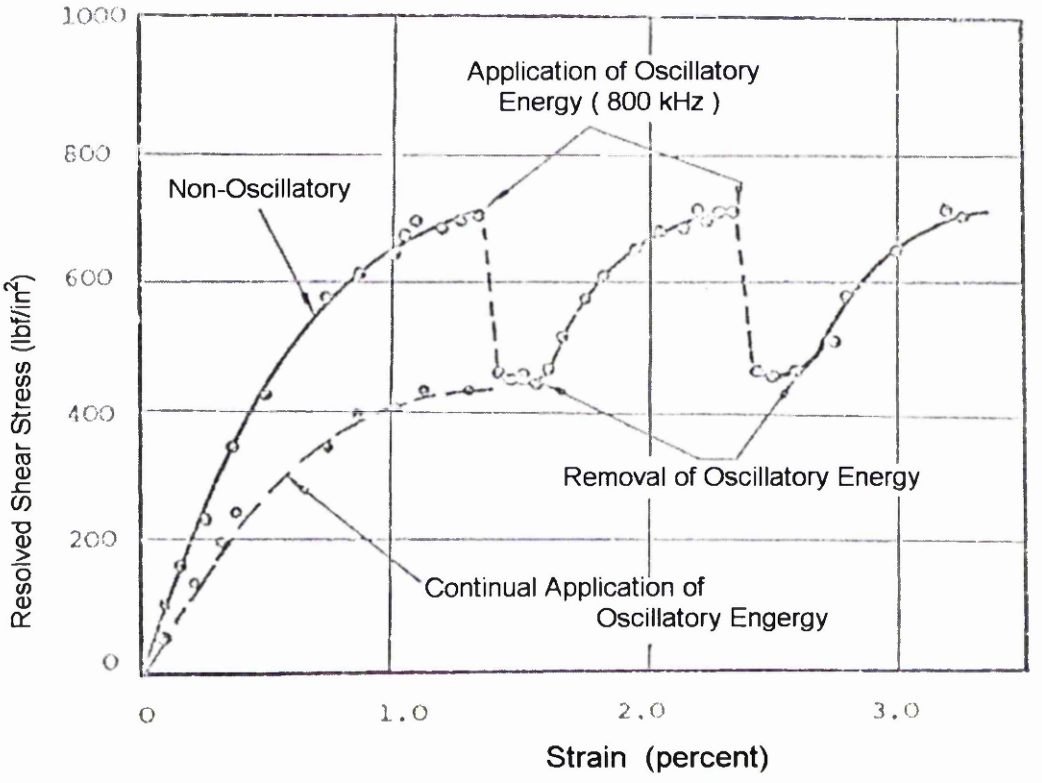

Figure 2.1 Shear stress-strain curve for a single crystal of zinc (Blaha and Langenecker [11]).

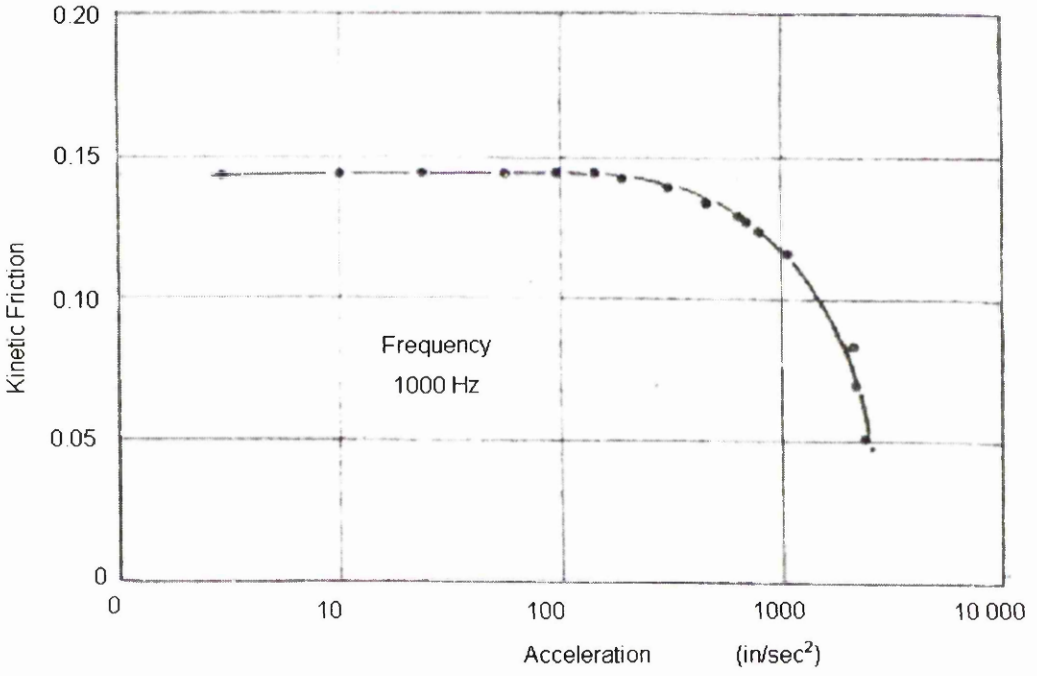

Figure 2.2 Effect of vibration on coefficient of kinetic friction; lubricated steel sliding on steel (Godfrey [35]).

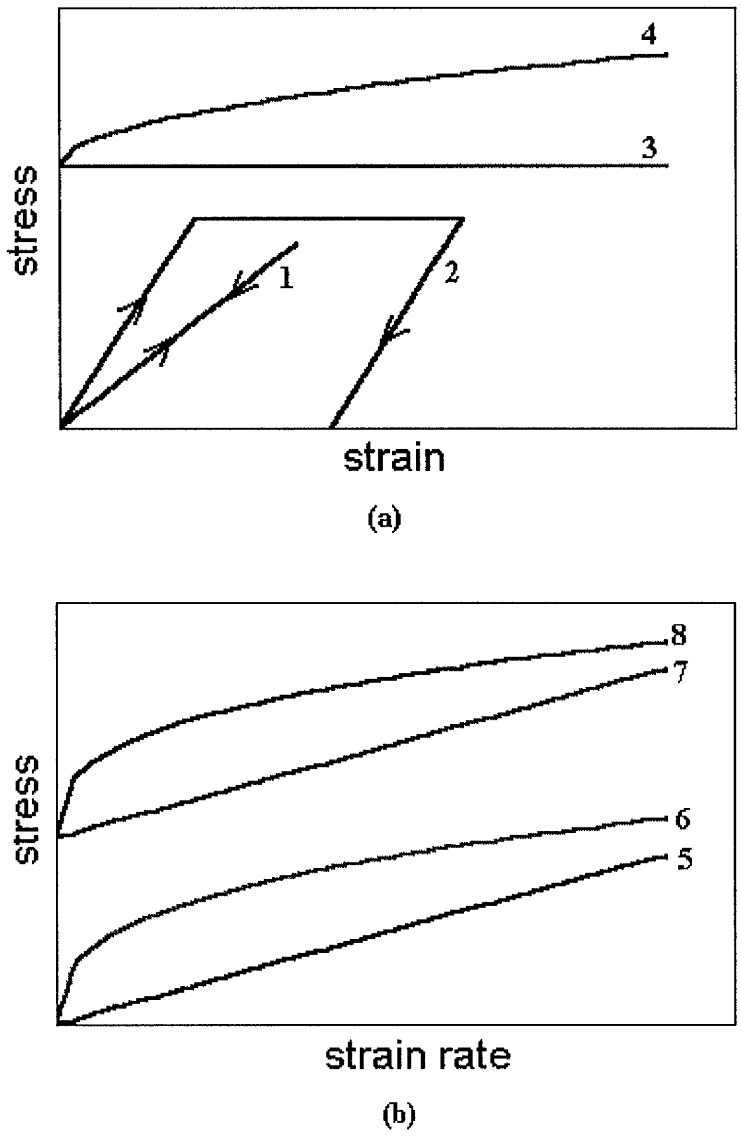

Figure 2.3 (a) Some idealised stress-strain curves for solid deformation and (b) stress-strain rate curves for fluid flow: (1) linear perfectly elastic, (2) elasto-plastic, (3) rigid-plastic, (4) rigid-plastic with non-linear strain hardening, (5) Newtonian, (6) Power law, (7) Bingham and (8) Herschel-Bulkley.

Table 2.1: Idealised shear constitutive relationships for the curves shown in figure 2.3 where the shear parameters are as follows: τ, stress; τ_0, yield stress; γ, strain; $\dot{\gamma}$, strain rate; G, shear elastic modulus; η, viscosity; η_p, plastic viscosity; k, flow consistency; k_p, plastic flow consistency; n, flow index; z, strain exponent and a, material constant.

Curve	*Constitutive relationship*	*Type*
1	$\tau = G\gamma$	Hookean
2	$\tau = \begin{bmatrix} G\gamma : \gamma < \tau_0 / G \\ \tau_0 : \gamma \geq \tau_0 / G \end{bmatrix}$	Elasto-plastic
3	$\tau = \tau_0 : \gamma > 0$	Rigid-plastic
4	$\tau = \tau_0 (1 + a\gamma^z) : \gamma > 0$	Plastic strain hardening
5	$\tau = \eta\dot{\gamma}$	Newtonian
6	$\tau = k\dot{\gamma}^n$	Power law
7	$\begin{cases} \tau = \tau_0 + \eta\dot{\gamma} : \tau \geq \tau_0 \\ \dot{\gamma} = 0 : \tau < \tau_0 \end{cases}$	Bingham
8	$\begin{cases} \tau = \tau_0 + k\dot{\gamma}^n : \tau \geq \tau_0 \\ \dot{\gamma} = 0 : \tau < \tau_0 \end{cases}$	Herschel-Bulkley

Table 2.2 Chemical composition of Plasticine (Yagishita *et al.* [55]).

Item	Measured Values		Remark
Chemical Composition	SiO_3	10.7 %	Main component is $CaCO_3$
	Al_2O_3	19.8 %	
	$CaCO_3$	58.2 %	
	MgO	0.4 %	
	Ma_2O	0.5 %	
	TiO_2	10.4 %	
Specific gravity	1.9 g/cm^3		

CHAPTER 3

STATIC UPSETTING OF A MODEL SOFT PLASTIC SOLID MATERIAL

A finite element simulation was performed for the upsetting of a cylindrical specimen of a model material between two parallel rigid dies. A series of experiments was conducted to determine the material properties and then to validate the finite element model for the model material, Plasticine. Initially, sets of uniaxial compression measurements allowed the material properties to be obtained, and these were used to establish suitable material model parameters for the finite element simulation.

The results of the finite element simulation provide a detailed knowledge of the distributions of deformed configurations at any instant during the forming process. Comparisons between the experimental and finite element simulation results are made for the relationship between forming force and die displacement, distributions of the wall pressure and deformed configurations. Advantages in finite element predictions for squeeze flow are reported and the confidence in the modelling technique has allowed new studies of vibration assisted processing to be initiated.

3.1 Introduction

Soft solid forming processes, which include rolling, forging, extrusion and drawing, are common in food industry processes. Improving the quality of formed components in such processes requires a detailed knowledge of the flow behaviour

of the forming material. Traditionally, model based tests of these processes, using an alternative material such as Plasticine, gave some insight into the material flow, stress-strain and temperature history of a particular process [5,8], but the explicit deformation history remained to a large extent unknown, appropriate experimental strategies being costly and time consuming [1].

Computer simulation offers the possibility of a better understanding of a forming process and the capability to predict the detailed material deformation history. With the development of finite element methods, a more accurate determination of the field variables governing flow in forming processes, involving complex boundaries and realistic material constitutive models, becomes feasible. These all contribute to the successful analysis of the deformation behaviour of materials.

Since the contact surface between a feed material and a tool governs the boundary conditions of the deforming workpiece, a successful analysis of the problem is dependent on a capability to model the interfacial phenomena accurately. Many authors have examined the tool-workpiece interface under plastically deforming conditions [8,42,46]. Adams *et al.* [8] described a number of potentially viable experimental configurations, which involved pipe flow, constriction flows and, in particular, compressive (squeeze film or upsetting) deformation of a model material between parallel platens. The resulting velocity fields associated with the deformation and flow are characteristically sensitive to the wall boundary conditions.

The axisymmetric upsetting process was selected for study because it is of industrial importance and a wealth of published experimental and analytical data is available for validation. Solid cylinder upsetting has been extensively studied by researchers to better understand the influence of friction on barrelling, work hardening and contact pressure distribution [69]. A comprehensive discussion on the experimental aspects of ductile material upsetting was given by Hsu [70] and an elastic-plastic finite element analysis of the upsetting process has been reported

by Vertin and Majlessi [48] using the plasticity deformation theory. Further, Carter and Lee [49] used the Coulomb friction contact algorithm from the incremental finite element code ADINA to analyse both ring and solid cylinder upsetting processes.

The present study investigates a process of unconfined uniaxial deformation of a cylindrical specimen between parallel rigid platens to gain insight into interface mechanics. The technique is usually called 'upsetting' and is commonly used to characterise the intrinsic flow properties and interfacial boundary conditions between a soft plastic solid and rigid walls during deformation processes. Plasticine (a commercially available concentrated dispersion of clay particles in a mineral oil), which has been used in previous studies [5,6,8,9,47] to mimic the behaviour of soft plastic solid material, is used as the material model. Upsetting experiments were conducted to compare with the FE simulation results. The experimental variables include the surface roughness, lubricant viscosity and mechanical properties of the workpiece. For the finite element model, an axisymmetric solid finite element, with four nodes, eight degrees of freedom and quadrilateral cross-section, has been used to simulate the model material, which includes the effects of elasticity, viscoplasticity, strain rate, large strains and friction boundary conditions. Numerical results using the ABAQUS code are compared with the measured geometry of the deformed workpiece. The predictions of the model are further compared with experimental measurements of the distribution of the local wall normal stresses between the workpiece and tooling, as reported by Adams *et al.* [47].

3.2 Mechanical Properties of Plasticine

Plasticine, the model elasto-viscoplastic material, is usually formulated from a mixture of fine, hard solid particles (in the range of 4-40 μm) and a low viscosity non-Newtonian liquid (typically about 400 cs). It may have solid fractions

approaching 40-80 % by volume. Thus the mechanics of Plasticine depends on the properties of both solid and liquid components.

As discussed previously, work by Adams *et al.* [6] has established that the post-yield constitutive behaviour of Plasticine is reasonably described by the Herschel-Bulkley relationship [43], which can be written in the following form for the case of uniaxial deformation:

$$\bar{\sigma} = \sigma_0 + k(\dot{\bar{\varepsilon}}^{vp})^n \tag{3.1}$$

where $\bar{\sigma}$ and $\dot{\bar{\varepsilon}}^{vp}$ are the effective stress and strain rate respectively. The material parameters σ_0, k and n are the uniaxial yield stress, the uniaxial plastic flow consistency and the flow index respectively. Provided that a Von Mises yield criterion exists, then this relationship is adequate to describe the viscoplastic behaviour.

The experimental results in figure 3.1 show the compressive true stress-strain curves for Plasticine at three different velocities of loading, which were found by compressing cylindrical specimens, initially 20 mm high and 60 mm diameter, between parallel platens on a LLOYD test machine. The three different velocities of loading are 0.5, 5 and 100 mm/min, which are presented as three different mean values of strain rate of 4.8×10^{-4}, 4.7×10^{-3} and 9.2×10^{-2} 1/s respectively. The natural strain $ln(H/h)$ is employed where H and h are initial and current heights of the specimen respectively. During compression, linear elastic deformation occurs prior to yield. Subsequently, for the same value of strain, the stress is greater for a higher compression rate due to the viscous effect during plastic deformation. These over-stresses are strain rate dependent, thus the flow is treated as elasto-viscoplastic.

The general formulation of elasto-viscoplasticity, contains two key assumptions: that there is no irreversible flow if the yield criterion is not satisfied and also that the elastic and viscoplastic strain rates are additive. Thus,

$$\dot{\varepsilon}_{ij} = \dot{\varepsilon}_{ij}^{el} + \dot{\varepsilon}_{ij}^{vp} \tag{3.2}$$

where $\dot{\varepsilon}_{ij}^{el}$ and $\dot{\varepsilon}_{ij}^{vp}$ are the elastic and viscoplastic components of the strain rate tensor respectively. Furthermore, it is assumed that $\dot{\varepsilon}_{ij}^{el}$ may be obtained from the constitutive relationship for a linear elastic solid and that the magnitudes of the elastic strains are small compared with the inelastic components. The viscoplastic strain rates are derived from the application of the associated flow rule [71] which refers to the condition of co-axiality of the stress and strain rate vectors. The viscoplastic component may be transformed to the generalised Herschel-Bulkley relationship using equation (3.1), such that a linear elastic relationship is used to specify the pre-yield deformation and the plastic strain rate is

$$\bar{\dot{\varepsilon}}^{vp} = D(\frac{\bar{\sigma}}{\sigma_0} - 1)^p \tag{3.3}$$

where D and p are the material property parameters. The mathematical details of this transformation are given in Appendix A [47].

Measurements of the rheological flow properties of Plasticine have been presented by Adams *et al.* [5], who describe the characterisation of the bulk rheological properties and the boundary conditions using the extrusion flow geometry which involves shear flow. For a material that obeys the Von Mises yield criterion, the shear stress, τ, and the shear strain, γ, are transformed to the corresponding uniaxial quantities by the relationships $\tau = \sigma/\sqrt{3}$ and $\gamma = \sqrt{3}\varepsilon$ respectively where ε is the extensional strain. Thus, the shear component of equation (3.1) may be written in the following form:

$$\tau = \tau_0 + \frac{k}{\left(\sqrt{3}\right)^{1+n}}\left(\dot{\gamma}^{vp}\right)^n \tag{3.4}$$

where $\dot{\gamma}^{vp}$ is the viscoplastic shear strain rate and τ_0 is the shear yield stress. It follows that the shear plastic flow consistency, k_{sc}, is given by the following relationship:

$$k_{sc} = \frac{k}{\left(\sqrt{3}\right)^{1+n}} \tag{3.5}$$

which reduces to the Trouton ratio for Newtonian fluids for which $n = 1$ and $\tau_0 = 0$. In deriving equation (3.4), it has been assumed that the flow index n in extensional flow is equal to that in shear flow, there is some evidence that this is a reasonable approximation for Plasticine [6].

The flow parameters for Plasticine used here are: uniaxial plastic flow consistency, k_{sc}, 0.039 MPaS^n, and flow index, n, 0.34. Thus the material property parameters, D = 30.41 1/s and p = 2.94, were obtained. A maximum constant value of 0.49 was used for Poisson's ratio. The density of 1878 kg/m^3 was determined as the ratio of the mass and volume of a sample. The Young's modulus, E, 17.8 MPa, and the uniaxial yield stress, σ_0, 0.26 MPa, were determined from simple compression measurements involving cylindrical specimens on a LLOYD test machine, which are described in the next section.

3.3 Experimental Procedure

In many experimental studies of material forming processes, Plasticine has been used as a favoured model plastic material, especially in simulating hot metal and soft solid material [6,8,9,42,45,55,60]. The aim of the experimental work described here was to obtain selected data as a basis for validating the numerical simulation. Upsetting tests were conducted with Plasticine (obtained from Bluebird Toys Ltd, UK) on a LLOYD test machine. Uniaxial compression tests were performed to obtain the yield material properties for Plasticine.

3.3.1 Specimen Preparation and Experiments

Plasticine was homogenised in a Z-blade mixer. The required specimen thickness was achieved by compression between parallel platens using a LLOYD test machine. The Plasticine was contained between waxed paper for easy removal. Then a special circular cutter was used to cut cylindrical shaped specimens into the chosen dimensions. The specimens were allowed to thermally equilibrate for 24 hours at 21°C. The equilibrium period of 24 hours was maintained constant throughout the experiments since the values of compressive stresses were found to fluctuate with age. The specimens used in this study were all 20 mm in height and 40, 60 or 80 mm in diameter.

The experiments were performed on a LLOYD test machine with a maximum capacity of 5 kN. Two stainless steel parallel platens were used as dies for the upsetting tests. The movement of the upper platen was controlled by the constant velocity of the machine crosshead, with a range of 0.5-100 mm/min, while the lower platen was fixed to the base. The load required to compress a specimen was recorded by a load cell attached to the crosshead.

Effects of changes in the surface condition of the tools on the resistive compressive force of cylindrical specimens during upsetting has been studied. For this purpose, various substrates were inserted between the specimen and the platens so that the insertions completely covered the specimen during the upsetting process. The substrates chosen for these experiments were, dry talcum powder, silicon oil and silicon grease used as lubricants, while the no-slip boundary condition was achieved by placing abrasive paper between the specimen and dies. The forming force-displacement data was recorded using dedicated computer software assuming a homogeneous deformation condition prevailing during the upsetting tests.

3.3.2 Material Properties Measurements using an Upsetting Technique

Initially, uniaxial compression tests were performed between two parallel platens to establish the material properties. As the speed of compressive displacement was slow, the temperature effects were neglected.

Two compression tests were performed. First, compression tests with constant velocities of 0.5, 5, 25 and 100 mm/min and a set of different sized specimens allowed measurement of the quasi-static yield stress. The die displacement was increased to a set value with constant velocity, as shown in figure 3.2a. A second compression test with unloading, as shown in figure 3.2b, allowed measurement of the elastic modulus. In this test the die displacement was linearly increased and then decreased with constant velocity.

Under no-slip wall boundary conditions, a lubrication solution for the mean squeeze flow pressure, $\overline{p}$, that takes into account the finite specimen edge pressure is given by [6]

$$\overline{p} = \sigma_0 \left[1 + \frac{2}{3\sqrt{3}} \frac{R}{h} \right] + \left(\frac{2}{n+3} \right) \left(\frac{2n+1}{n} \right)^n \left(\frac{R}{h} \right)^{n+1} \left(\frac{\dot{h}}{h} \right)^n k_{sc} \tag{3.6}$$

where n is material flow index, R and h are the plastically deformed specimen's radius and height respectively.

The above expression, which is consistent with the analysis of Sherwood and Durban [10] and confirmed by Adams *et al.* [47], suggests that the mean compressive stress is the sum of a plastic and a viscous component. The first term is the lower bound solution for a rigid perfectly-plastic solid [69] and the second is the lubrication solution for a power law fluid. As with all rigid-viscoplastic relationships, such as the bi-viscosity equation, the elastic component is neglected

although an elastic response has been clearly demonstrated in the current work. However, for large deformations its contribution is relatively small.

The material parameters obtained using equation (3.6), where the flow index, n, was determined independently using spherical and conical indentation procedures as indicated in Chapter 5, agreed well with previously published experimental work [6] which involved a wide range of imposed velocities and specimen heights obtained for Plasticine. This current work also provides a more rigorous assessment of the relationship for the finite element simulation, since the material parameters were obtained from independent measurement procedures.

3.3.3 Cylindrical Upsetting

Specimens of 20 mm in height and 40, 60 and 80 mm in diameter were prepared to show the effect of the wall boundary conditions on the force-displacement behaviour. The experiments involved compression at a constant speed of 0.5, 5, 25 and 100 mm/min under no-slip and lubricated conditions by using abrasive paper and silicon grease respectively between the specimen and platen. The forming force-displacement data were recorded using a dedicated computer and software.

3.3.4 Flow Visualisation

Specimens of 20 mm in height and 60 mm in diameter were prepared with horizontal layers of different colours of Plasticine, to allow a flow visualisation study to be conducted. After compression to a specified strain, the specimens were sectioned and photographed.

Quantitative measurements of radial surface displacements were made by creating a specimen from its two halves through the major axis. The inner surfaces of the two halves were grid marked using a special grid before joining. Dry powder was used to prevent the two halves from sticking together and, after deformation, they

were easily separated. The specimen was cleaned and photographed and the positions of the grid marks were measured.

3.4 Finite Element Method

Theoretical models of most metal forming operations are concerned with the prediction of the stresses acting during the deformation process and, subsequently, of the forces which must be applied to induce plastic flow. These forces are known as the working loads and determine the power requirement necessary to perform a particular operation.

In order to study the upsetting forming of Plasticine thoroughly, a finite element analysis was carried out using the commercial codes MSC/Patran 8.0 (MacNeal-Schwendler Corporation) and ABAQUS 5.8 (Hibbitt, Karlsson & Sorensen, INC), which allows a stress-displacement analysis. It is able to deal with the non-linearities arising from large displacement effects as well as material non-linearities and boundary non-linearities such as contact and friction.

Figure 3.3 shows a schematic diagram of the axisymmetric finite element model for the simulation of upsetting the model material, Plasticine. The following assumptions were made in the numerical analysis:

- The model is axisymmetric and symmetric about the central plane, so it allows only the right half specimen to be modelled by axisymmetric solid quadrilateral cross-section elements. Each finite element features four integration points and two translational degrees of freedom per node.
- The material is initially isotropic, homogeneous and incompressible such that the volume of each element of the model remains constant.
- The behaviour of Plasticine is treated as elasto-viscoplastic with material properties defined previously.
- The two parallel platens were modelled as analytical rigid surfaces.

- Steady state deformation at room temperature was considered and no temperature effects were included.

In the analysis, displacement boundary conditions were imposed in the axial direction along the symmetry plane. The relative motion of the upper and lower platens is controlled during upsetting. The tool movement is specified and used to enforce the total axial displacement at the contact surface. Then the outer wall of the workpiece is displaced radially outward such that volume constancy is preserved.

A slave and a master surface, representing the deforming specimen and rigid dies respectively, are defined in terms of nodal points. During each equilibrium iteration, a check is made to determine if contact between the master and slave occurs. Contact is defined in the following way. When the surfaces are in contact at a point, any positive pressure can be transmitted, when the clearance between the surfaces is positive, there is no contact. When contact occurs, friction models are generally formulated to represent a dry friction interface condition. For modelling an upsetting process, a standard Coulombic friction model is considered and it is assumed that no relative motion occurs if the equivalent frictional stress τ_{eq} is less than the critical stress, τ_{crit}, which is proportional to the contact pressure, p, in the form

$$\tau_{crit} = \mu p \tag{3.3}$$

where μ is the coefficient of friction. If the equivalent stress is at the critical stress ($\tau_{eq} = \tau_{crit}$), slip can occur. If the friction is isotropic, the direction of the slip and the frictional stress coincide. For solid cylinder upsetting simulations, all nodal frictional forces are directed radially inwards to oppose the outward flow of material. Hence, using the Von Mises criterion, the maximum numerical friction coefficient value $\mu_{max} = 0.577$. When contact occurs, a sticking (or no-slip) wall boundary condition was given by the maximum numerical friction coefficient

value of 0.577. For the lubricated case, a Coulombic coefficient of friction equal to 0.05 for silicon grease, or 0.2 for dry powder with silicon oil, was used. These values were selected on the basis of ring compression test results (details are presented in Appendix C). The static and kinematic values of the coefficient of friction were assumed to be equal.

The analysis was implemented using a stress-displacement procedure with explicit solution. A large number of very small time-steps and a fine mesh model was used to preserve accuracy. At each time step, a displacement increment of about 0.5 % of the original height of the specimen was applied until approximately 50 % reduction in height was achieved. A Lagrangian formulation for geometric and material non-linearity was used. At each time step, the stiffness matrix was updated and equilibrium was re-established.

3.5 Comparison of FE and Experimental Results

During an upsetting process, the frictional forces at the wall interface may contribute substantially to an enhancement of the overall load necessary to induce plastic flow. Many authors [46,49] have studied the effect of surface friction during metal processes. Their work showed a marked influence of the frictional conditions at a tool-material interface.

The level of wall friction also affects the way in which a material is deformed. Low frictional stresses at the walls may facilitate a near homogeneous deformation condition during the upsetting process. A homogeneous deformation condition conveys the notion that the elements at the interface, at a particular axial co-ordinate, are being displaced with the same radial velocity as those in the bulk of the specimen with the same axial co-ordinate. For this condition to prevail, the wall frictional stresses must be sufficiently small to allow interfacial slip between the wall and the elements at the interface, as shown schematically in figure 3.7a. However, if the frictional stresses are sufficiently large, non-homogeneous

deformation conditions will prevail, resulting in a non-uniform distribution of the radial velocity. This effect may cause barrelling and folding of the specimen, as shown in figure 3.4. Barrelling is a process where the bulk of the specimen is moving at a higher velocity than the surface, causing the sides of the specimen to deform in a concave manner. Folding is a process where the barrelled faces eventually becoming part of the plane surface of the specimen.

The predictions of overall shape changes of the specimen at an 8.3 mm height reduction under no-slip boundary conditions were compared with the experimental results and are presented in figure 3.4. The figure clearly shows that the side of the sample has folded onto the platen and the barrelling effect on the edge of the sample is also correctly predicted. The same outer diameter of 86.42 mm is both calculated and measured. In figure 3.5, the predicted displacement field is compared with data measured in the flow visualisation study and is presented for a cylindrical specimen with an initial 60 mm diameter and 20 mm height, at 40 % deformation under a no-slip boundary condition. The predicted internal deformed profiles show close agreement with the experimental results.

The results of the finite element simulation also provide a detailed knowledge of distributions of the effective stress, plastic strain, the axial stress and shear stresses. These are shown in figure 3.6 for a 42 % reduction in the height of the specimen. The figure 3.6a also shows that there are regions in the workpiece with relatively greater values of effective stress, plastic strain, axial stress and shear stresses, due to the no-slip wall boundary condition. The region is near the two right hand corners of the model (the two edge circumferences of the workpiece). These are regions with relatively more severe deformation and where damage is more likely to occur. The contour of plastic strain clearly shows the central un-yielded static region and also similar zones at the periphery of the specimen (shown as shaded areas in the figure). Material in the mid-plane is less restricted and hence the flow is greater leading to the barrelling effect described previously.

In most cases minimising friction is beneficial since it reduces the force and energy required for a given operation. This will reduce the stresses imposed on tooling and contribute to longer tooling life and better quality control. In practice, barrelling is prevented by lubricating the interface of the rigid dies. The application of surface lubrication brings about a general reduction in the magnitude of the interfacial friction and results in a more homogenous deformation process, as shown in figure 3.6 curves b and c. It also can be seen from the material flow patterns presented in figure 3.7 curves b and c. However, it is difficult to achieve a perfect lubricating condition during the deformation process in practice because bollarding rather than barrelling can occur, where excessive radial stresses at the platens cause the diameter of the specimen faces, which are in contact with the platens, to deform more than the diameter at the centre. This is shown in figure 3.8. This may simply be due to the deterioration of the lubricant as a result of the thinning of the film as the deformation proceeds. The deterioration of the lubricant film exposes fresh, un-lubricated material to the tool surfaces, which may lead to a sticking rather than a sliding boundary at the interfaces. To minimise barrelling and bollarding, an optimal interfacial friction condition is needed.

In the finite element simulation, the forming force is obtained from the contact deformation between the deformed workpiece and the rigid dies. The load-displacement curves offer another comparison of analytical and experimental results. These results are summarised in figures 3.9, 3.10 and 3.11 for different specimen diameters, cross-head velocities and friction coefficients, respectively. The computed load-displacement data show close agreement with the measured values. As seen in figure 3.9 curve a, the computed curve exhibits a few discontinuities in the upsetting force at some die displacements. At each of these die displacements, an additional nodal circle at the circumference of the workpiece along the vertical boundary comes in contact with the die. The magnitude of these discontinuities has been reduced and the curves smoothed out in curves b and c by refining the mesh or rezoning in the vicinity of the right corners of the workpiece model.

The complexity of the die-specimen interfacial phenomenon may be further illustrated by the predicted distribution of normal contact pressure at the die-specimen interface as a function of radial distance to the initial outer radius (r/R_0). The finite element models were deformed to 10 %, 20 %, 30 % and 40 % reduction in height for specimens with an initial diameter of 60 mm under a no-slip boundary condition. The results are summarised in figure 3.12a together with experimental results reported by Adams *et al.* [47]. By using the same specimen geometries, a comparison of the force-displacement relationship in figure 3.12b shows that the material properties used in this thesis closely match the material properties of the Plasticine specimens used in the experiments reported by Adams *et al.* [47]. For deformations in all the ranges of 10-40 %, the normal contact pressure variation agrees very closely with the experimental results. For both data sets, the pressure is a maximum in the central region and decays towards a value that is approximately equal to the uniaxial yield stress at the edge (this value is shown as the horizontal chain line in the figure). The FE predictions correctly show increases in the edge region arising from the formation of the un-yielded regions which cause a local constraint on the flow near the platens. This effect was not apparent for the measured data which is probably due to the general unreliability of the stress measurement in the small stress range. Also, compared with the finite element simulation reported in [47], which is shown in figure 3.13, the pressure predictions in this thesis show better agreement with the experimental results.

Figure 3.14 shows the corresponding wall shear stress distributions. The agreement between the measured and the computed data sets is relatively poor. However, for both sets of figures, predicted and measured, the shear stress appears to be rather independent of the applied normal load. The shapes of the distributions are quite different from those reported experimental results for the shear pressure at the centre of the specimen. The computed values approach zero, which is reasonable, since the material will be static at this location. The wall shear stresses gradually increase towards the edge of the specimen reaching an asymptotic value of *ca.* 0.26

MPa. Under a no-slip wall boundary condition the maximum value will be equal to the dynamic shear yield stress ($\tau > \tau_0 = 0.16\,\text{MPa}$). The poor agreement is an indication of the difficulty associated with measuring the shear stresses using the technique described in [47], which is based on measurements using a pin load cell transducer located at 45° to the surface of the platen. These issues are recognised and reported in the paper [47].

Wall normal contact pressure distributions predicted using a coefficient of friction value of 0.45, which represented a lubricted specimen with a high value of friction, are shown in figure 3.15 together with the measured values obtained by Adams *et al.* [47] for un-lubricated specimens. For deformations in the range of 10-40 %, the agreements are even closer than the finite element predictions using a no-slip boundary condition (shown in figure 3.12). This would indicate that the measurements in [47] were, in fact, under a lightly lubricated condition, rather than the no-slip boundary condition reported. Figure 3.16a shows the corresponding wall shear stress distributions. At first sight, there appears to be little agreement between the data sets of figure 3.16a and b. However, several trends shown in this figure are consistent with experimental results, which are shown in figure 3.16b. The higher shear contact pressure occurred at the outer edge of the specimen and was lower at the centre. The greater the deformation, the greater the shear stress because of a higher friction contribution. High stresses at outer diameters, evident in figure 3.16a and b, cause barrelling at the outer edge of the specimen. A reduced coefficient of friction in the finite element analysis causes lower stresses (in the r/R_0 = 0.6~0.9 region) than predicted by the fully no-slip friction boundary condition (compare with figure 3.14). Lower stresses are also measured and are evident in the experimental results in figure 3.16b. A significant difference between the finite element analysis and the experimental results is apparent at the centre of the specimen, where the finite element values approach zero. The explanation for this discrepancy is given in the previous paragraph.

These results suggest that the measurements reported in [47] may not be under a fully no-slip boundary condition but under a lightly lubricated wall boundary condition due to the limit of the experimental set-up, and in fact, complete no-slip friction did not exist in the interface. In the present analysis, the finite element model allowed relative motion at the interface, and thus the results show better agreement with the experimental findings.

3.6 Conclusions

A large strain finite element simulation, which includes the effects of elasticity, viscoplasticity, strain rate and boundary condition, was developed for the model material, Plasticine. The upsetting of a cylindrical specimen between two parallel platens was simulated and tested under similar conditions and results were obtained for the upsetting force-displacement and profile field for static loading controlled by a constant velocity. Simulations were implemented for different specimen sizes and wall boundary conditions.

Uniaxial compression tests were conducted to establish the material flow parameters, and the elastic modulus and quasi-static yield stress were generated.

Agreement was obtained when the predictions of forming force-displacement behaviour and overall shape changes of the workpiece were compared with the experimental results. The versatility of the finite element simulation allows detailed information during the forming process to be obtained. This was demonstrated by displaying the effective stress, plastic strain, the axial stress and shear stresses. The high and low strain regions were correctly predicted and the influence of variations in process conditions was predicted with high precision, such as local wall friction conditions. The resulting wall normal contact pressure distributions correlated well with the published experimental observations. The corresponding wall shear stress distributions allowed trends to be correlated but there was poor agreement in values due to measurement difficulties. In addition,

the finite element predictions of contact stresses agreed much more closely with the reported measurement data than the corresponding simulations reported in [47].

The high level of confidence gained from the demonstrated accuracy obtained from the finite element models has resulted in further analytical studies being initiated to improve the forming process by vibration assistance.

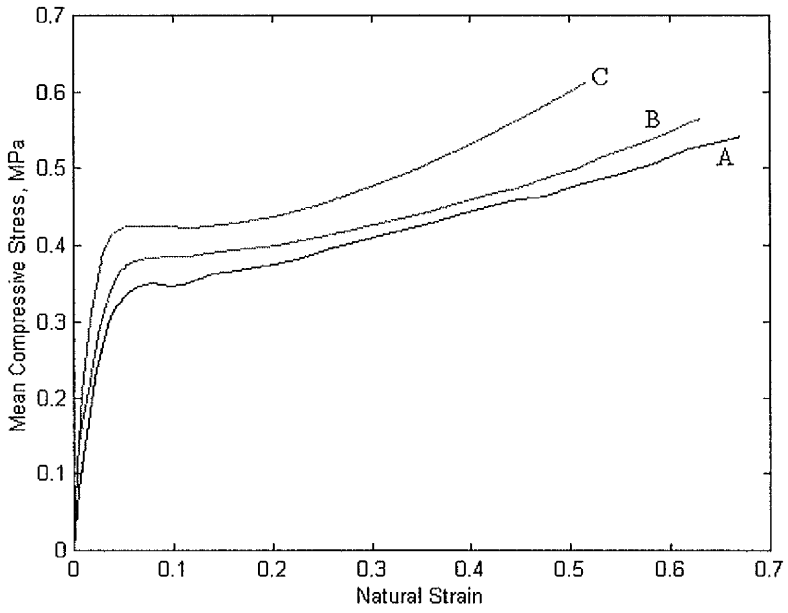

Figure 3.1 True stress-strain curves for Plasticine under uniaxial compression at the following mean strain rates: curve A, 4.8×10^{-4} 1/s; curve B, 4.7×10^{-3} 1/s; curve C, 9.2×10^{-2} 1/s, for cylindrical specimen with an initial 60 mm diameter and 20 mm height.

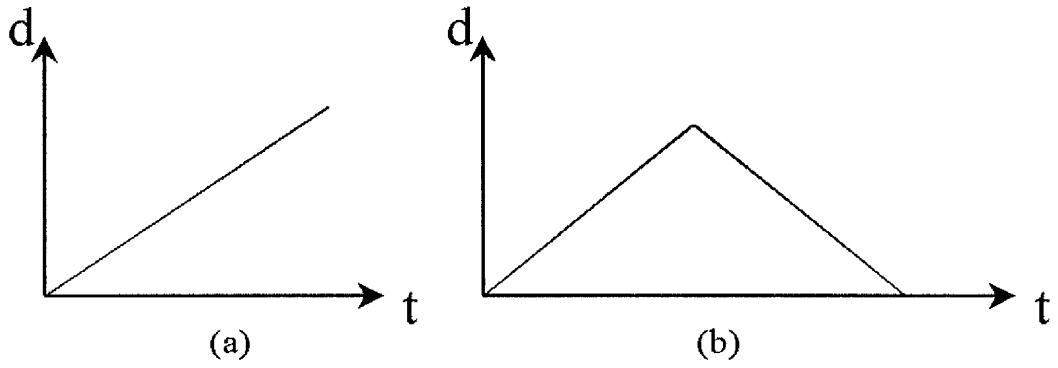

Figure 3.2 Uniaxial compression tests of Plasticine between two parallel platens with two die displacement-time functions, d-t, for (a) quasi-static yield stress and (b) elastic modulus measurements.

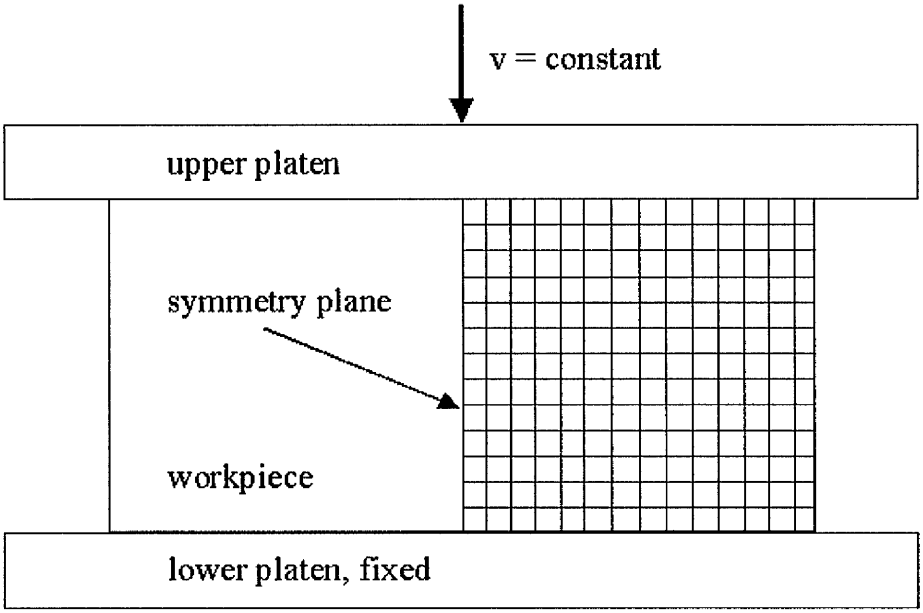

Figure 3.3 Axisymmetric finite element model for the simulation of upsetting of a model specimen.

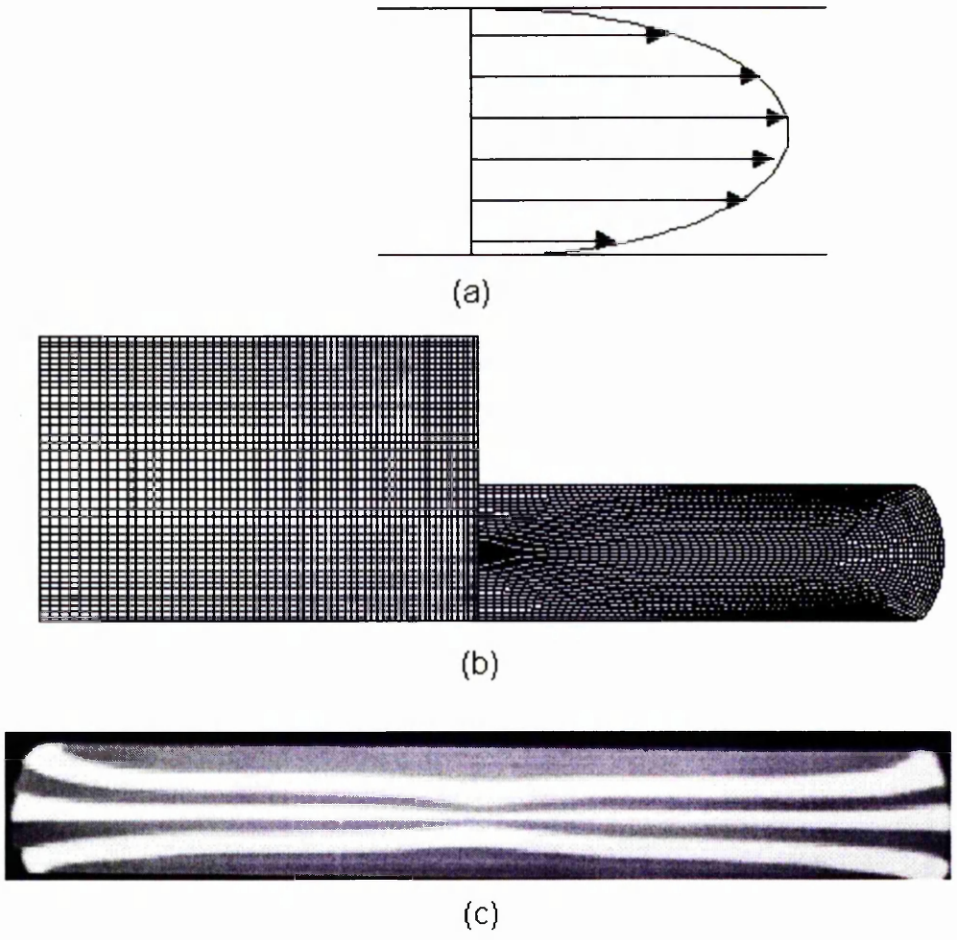

Figure 3.4 (a) Schematic diagram of material flow pattern; material flow pattern obtained from (b) computed and (c) experimental results for a cylindrical Plasticine specimen, after 8.3 mm reduction in height under a no-slip boundary condition.

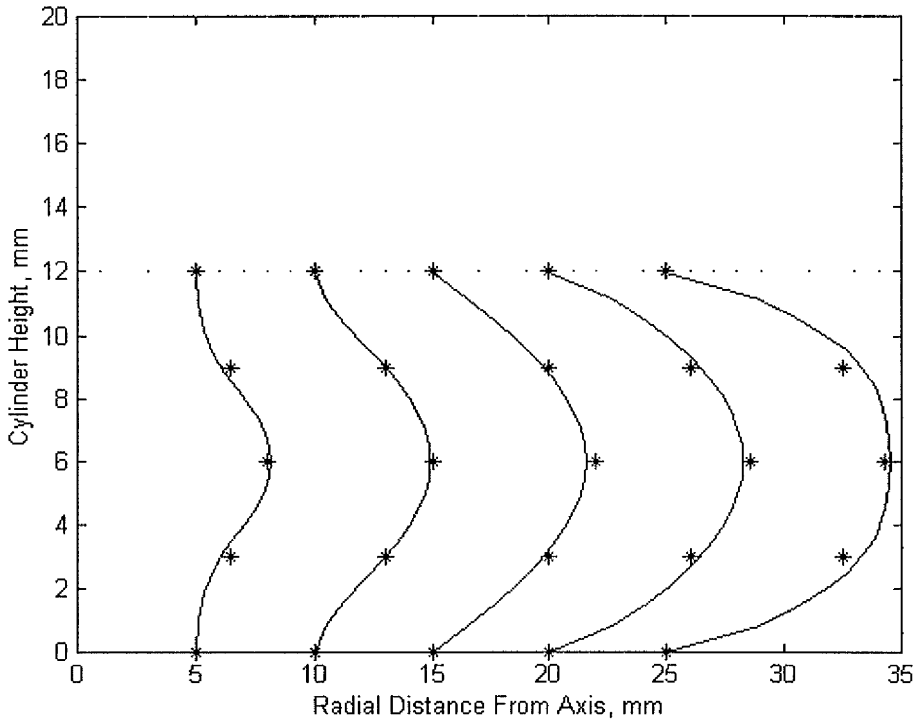

Figure 3.5 Experimental (*) and computed (—) displacement profiles at 40 % deformation under a no-slip boundary condition.

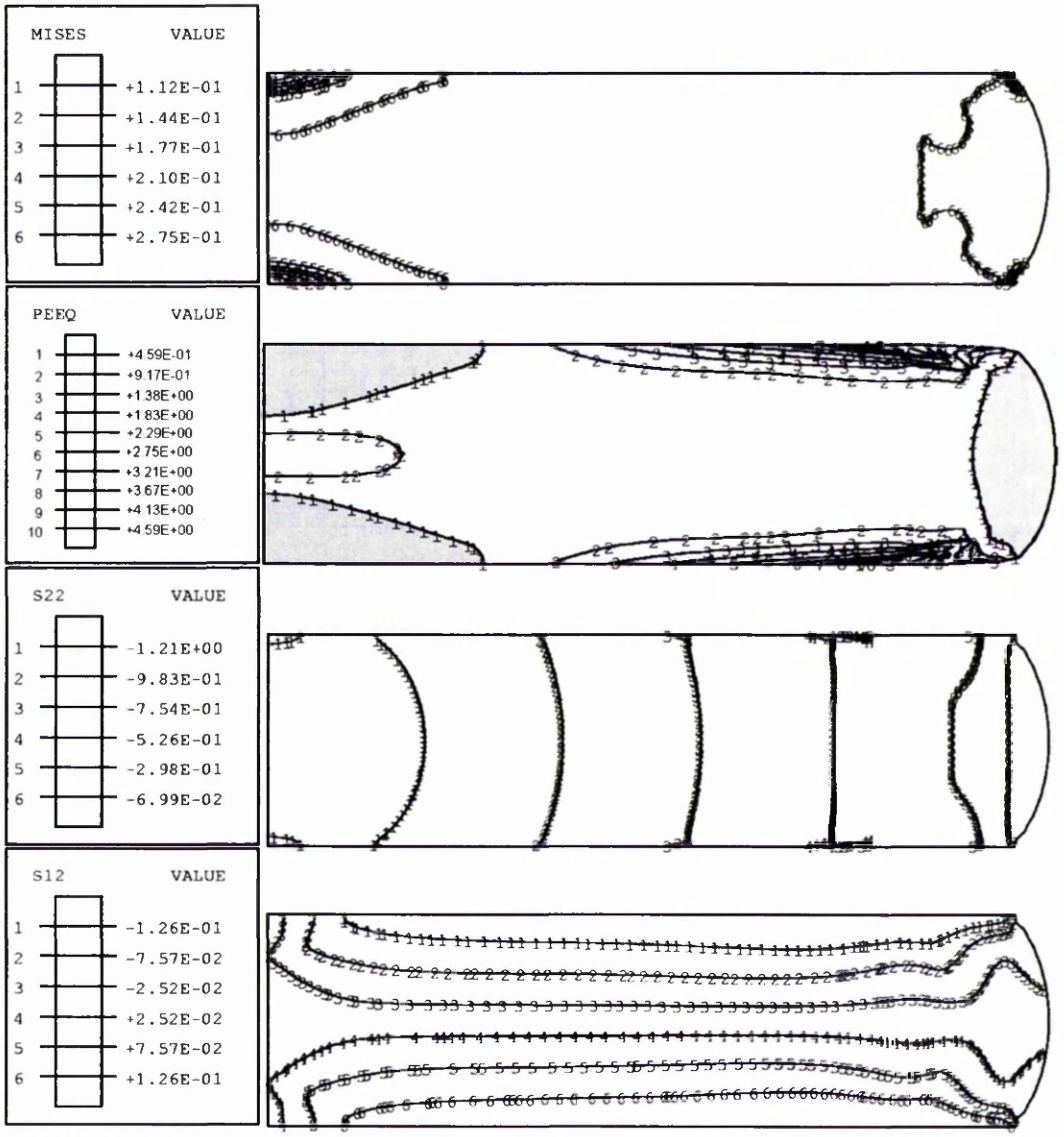
MISES
VALUE
1 +1.12E-01
2 +1.44E-01
3 +1.77E-01
4 +2.10E-01
5 +2.42E-01
6 +2.75E-01
PEEQ
VALUE
1 +4.59E-01
2 +9.17E-01
3 +1.38E+00
4 +1.83E+00
5 +2.29E+00
6 +2.75E+00
7 +3.21E+00
8 +3.67E+00
9 +4.13E+00
10 +4.59E+00
S22
VALUE
1 -1.21E+00
2 -9.83E-01
3 -7.54E-01
4 -5.26E-01
5 -2.98E-01
6 -6.99E-02
S12
VALUE
1 -1.26E-01
2 -7.57E-02
3 -2.52E-02
4 +2.52E-02
5 +7.57E-02
6 +1.26E-01

3.6(a)

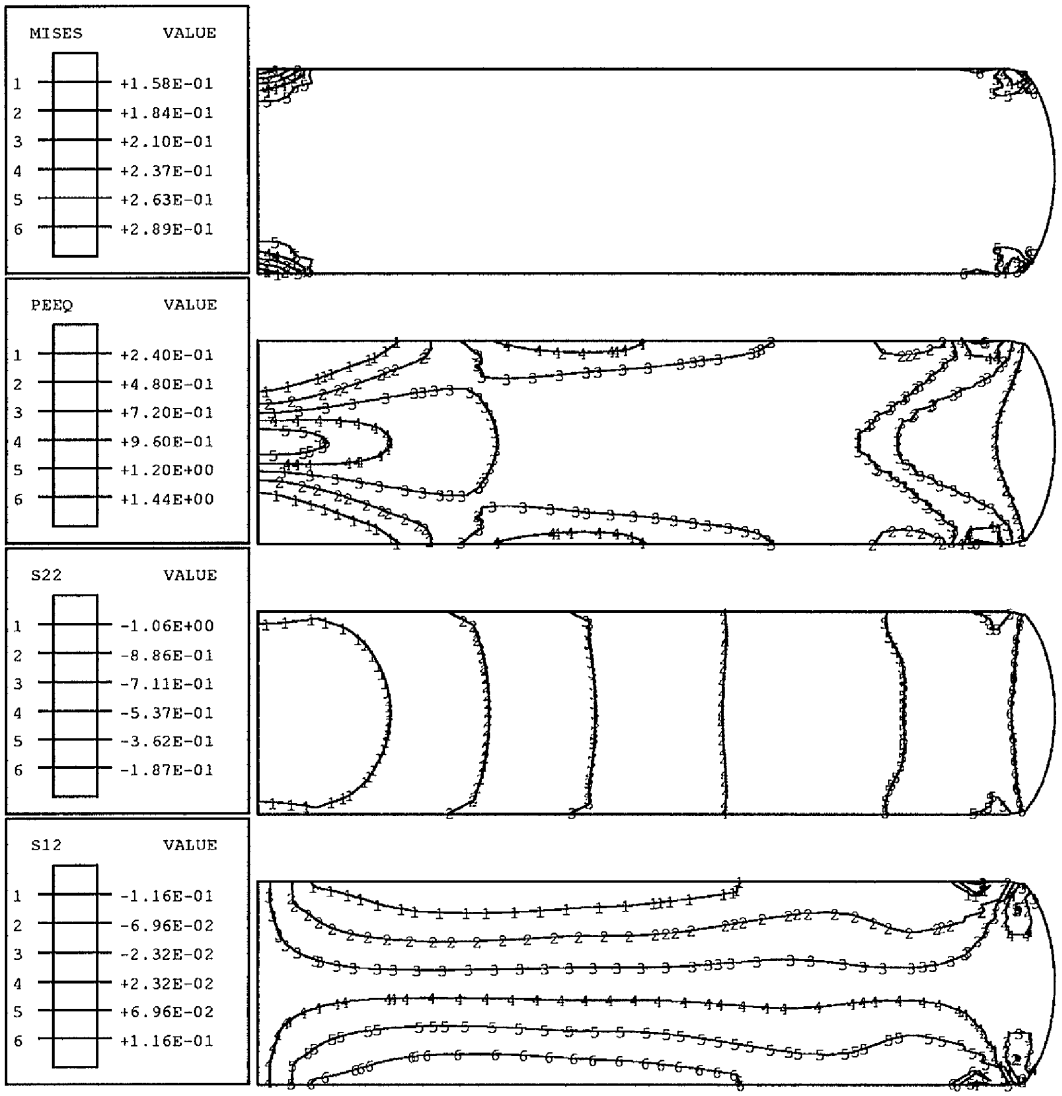
MISES
VALUE
1 +1.58E-01
2 +1.84E-01
3 +2.10E-01
4 +2.37E-01
5 +2.63E-01
6 +2.89E-01
PEEQ
VALUE
1 +2.40E-01
2 +4.80E-01
3 +7.20E-01
4 +9.60E-01
5 +1.20E+00
6 +1.44E+00
S22
VALUE
1 -1.06E+00
2 -8.86E-01
3 -7.11E-01
4 -5.37E-01
5 -3.62E-01
6 -1.87E-01
S12
VALUE
1 -1.16E-01
2 -6.96E-02
3 -2.32E-02
4 +2.32E-02
5 +6.96E-02
6 +1.16E-01

3.6(b)

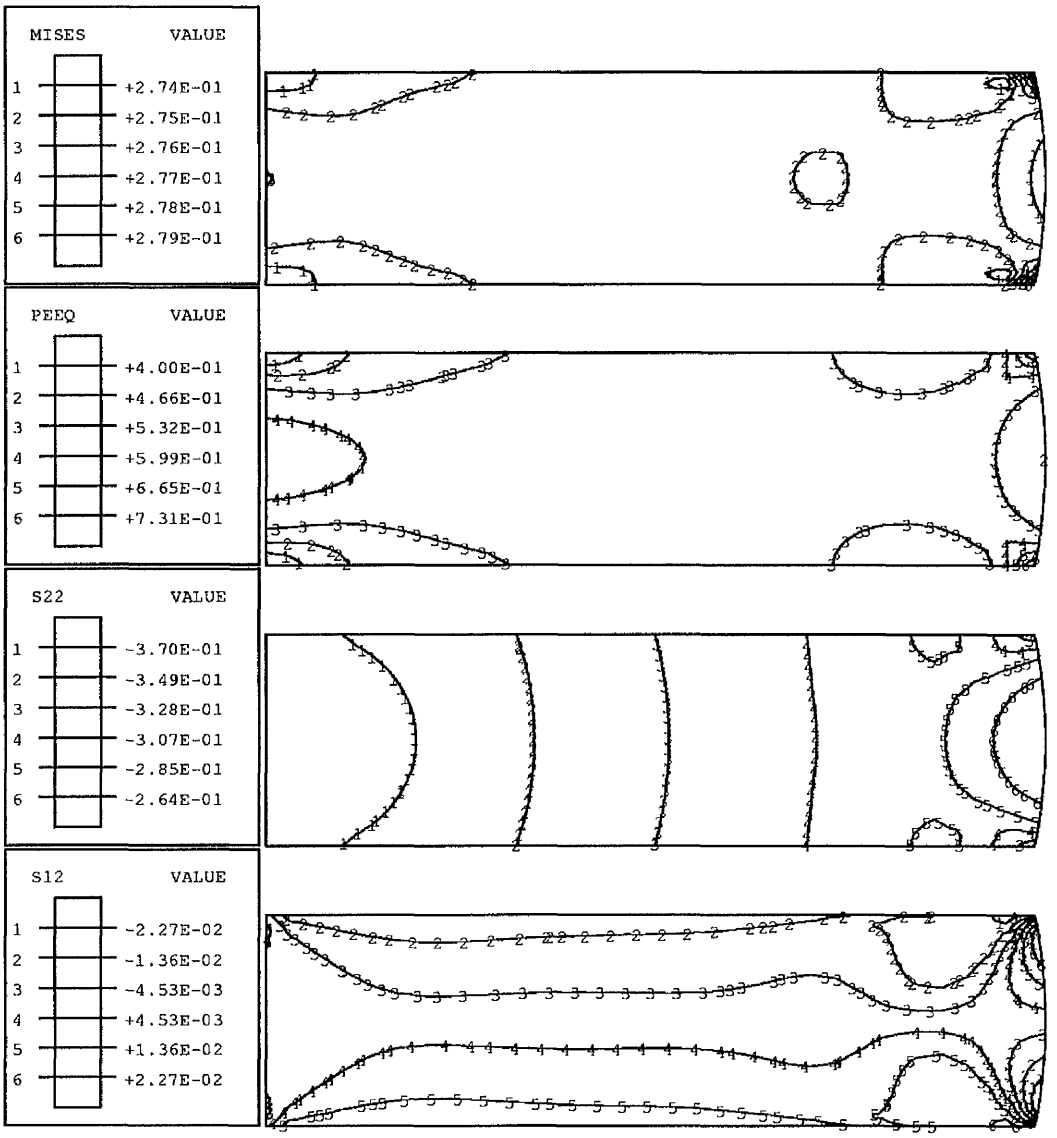

3.6(c)

Figure 3.6 Contours of the effective stress, plastic strain, the axial stress and shear stresses at 42 % reduction in the height of the specimen, (a) under a no-slip boundary condition, (b) under a lubricated boundary condition of μ = 0.3 and (c) under a lubricated boundary condition of μ = 0.05.

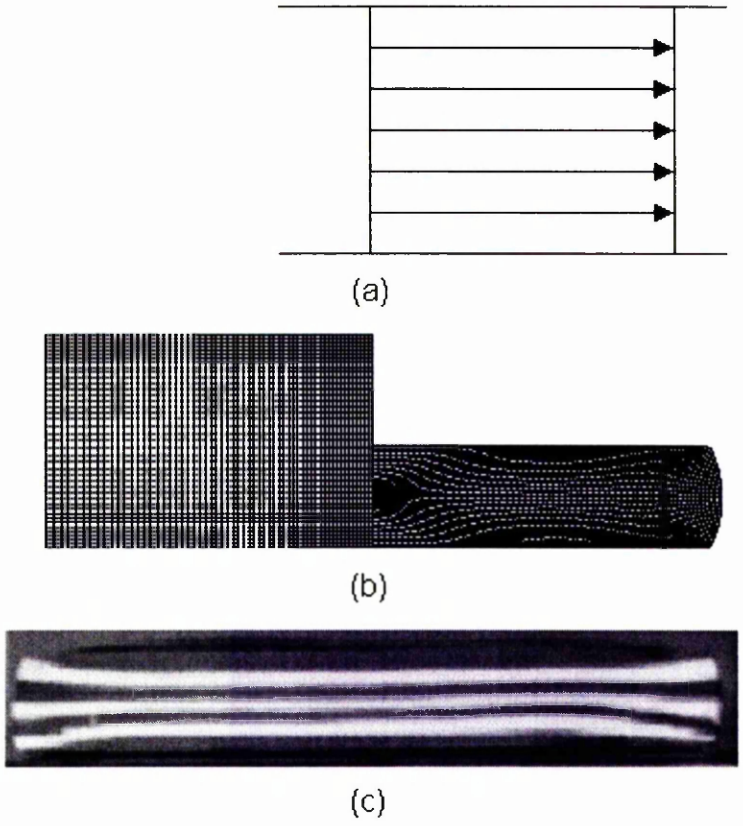

Figure 3.7 (a) Schematic diagram of material flow pattern; material flow pattern obtained from (b) computed and (c) experimental results for a cylindrical Plasticine specimen, after 8.3 mm reduction in height under a lubricated boundary condition.

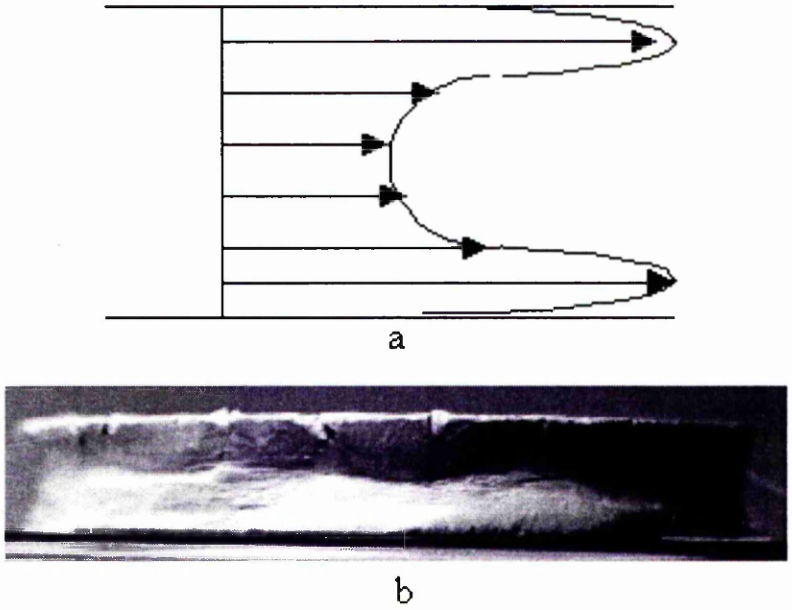

Figure 3.8 (a) Schematic diagram of material flow pattern; material flow pattern obtained from (b) experimental results, for a cylindrical Plasticine specimen, after 8.3 mm reduction in height under an over-lubricated boundary condition.

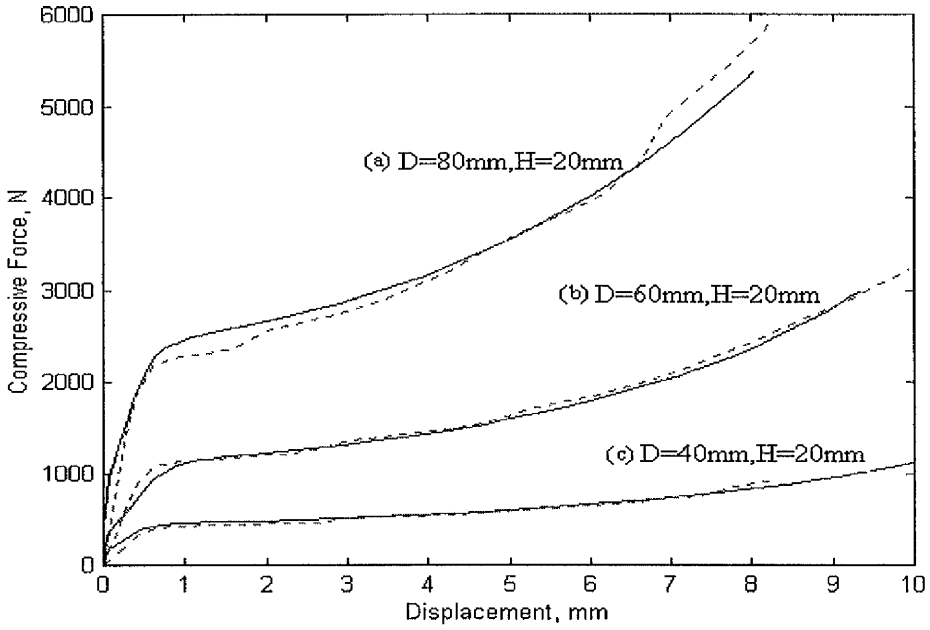

Figure 3.9 Analytical (---) and experimental (—) load-displacement results for different sizes of specimen under a no-slip boundary condition.

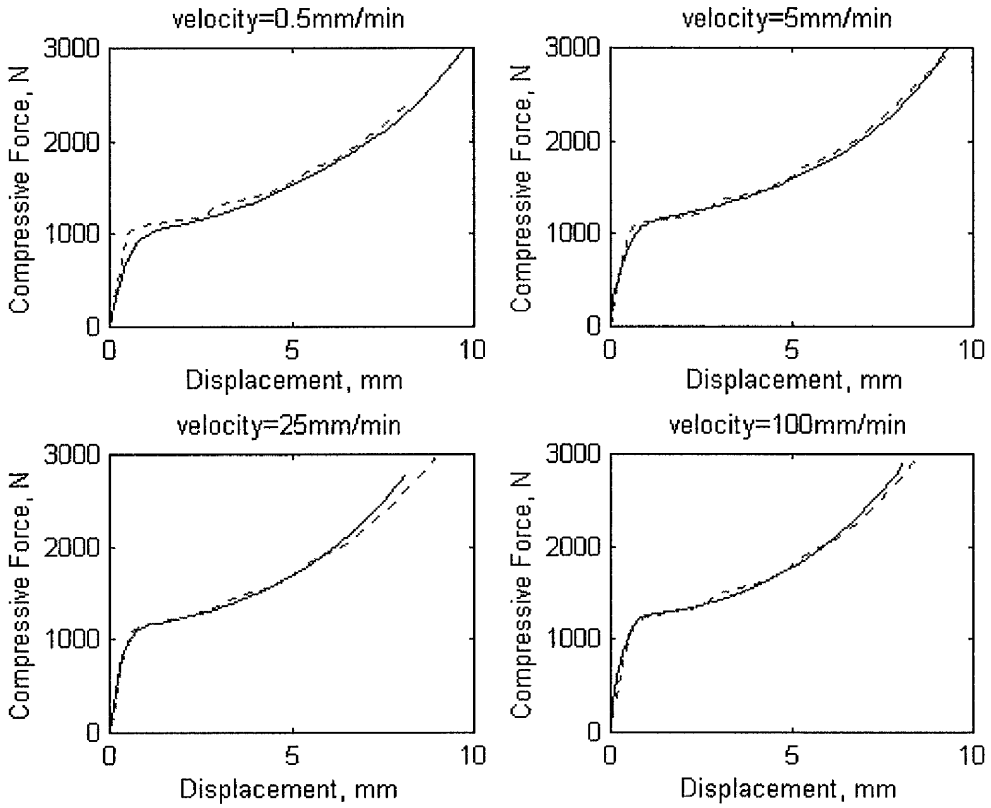

Figure 3.10 Analytical (---) and experimental (—) load-displacement results for different loading velocities under a no-slip boundary condition, for cylindrical specimen with an initial 60 mm diameter and 20 mm height.

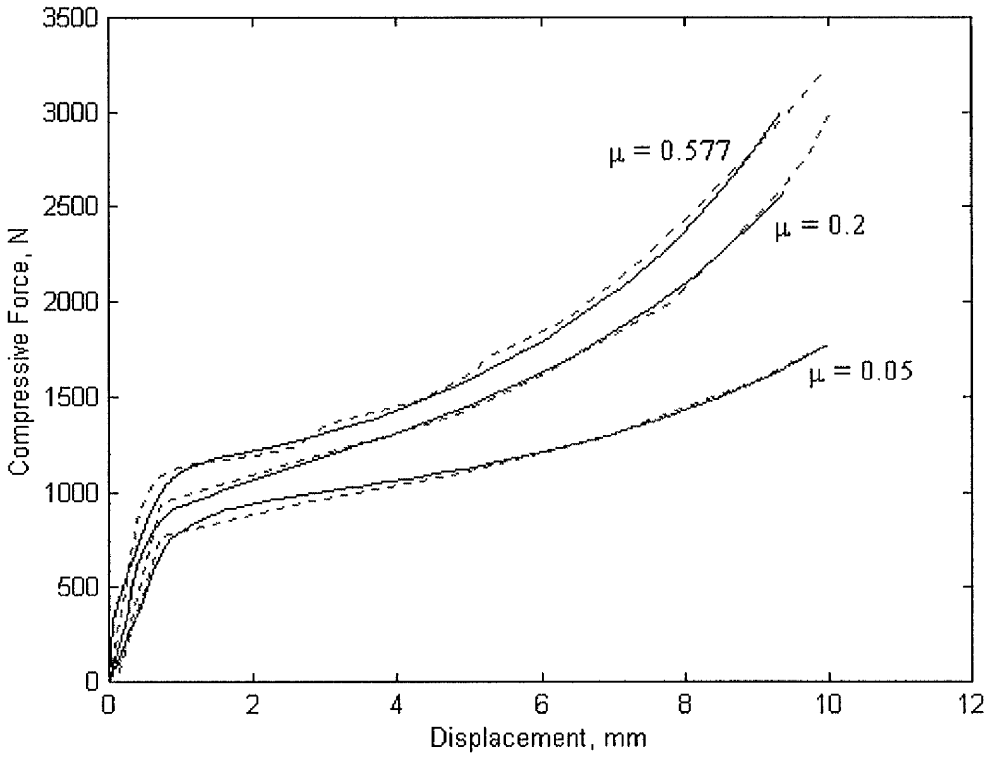

Figure 3.11 Analytical (---) and experimental (—) load-displacement results for different friction coefficients, for cylindrical specimen with an initial 60 mm diameter and 20 mm height.

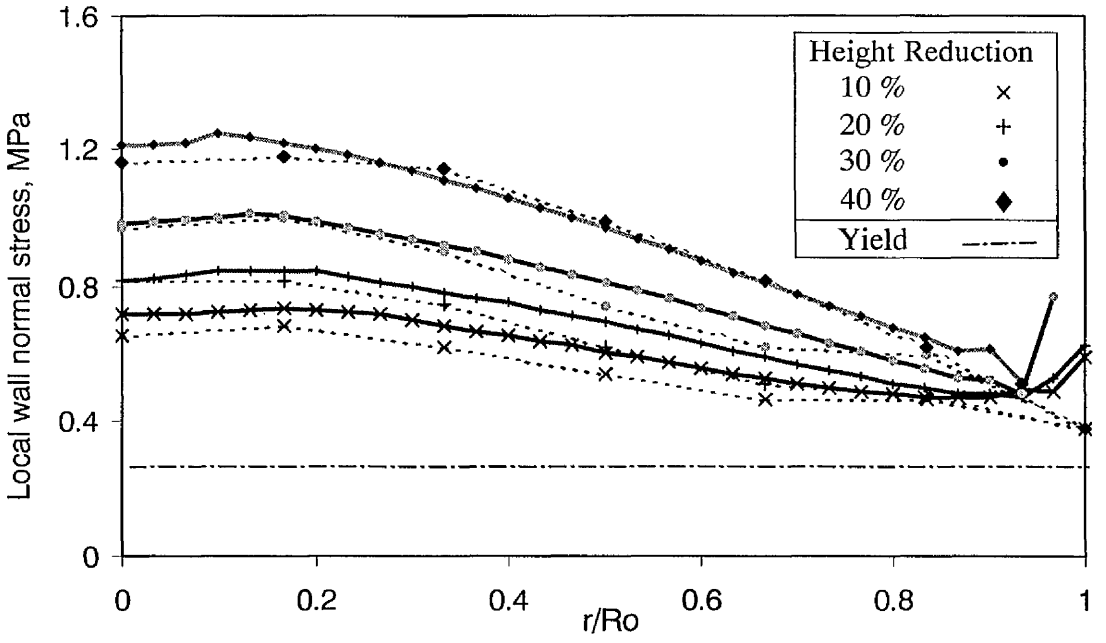

(a)

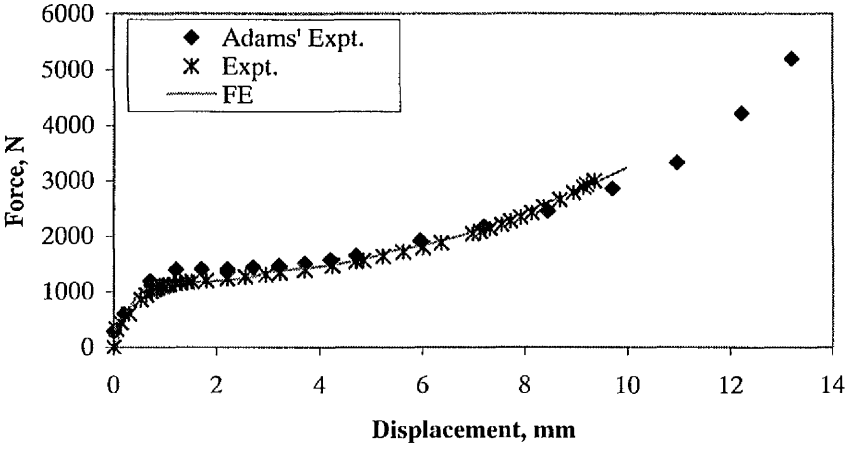

(b)

Figure 3.12 (a) Predicted (—) and measured (---) by Adams *et al.* [47] contact normal stress distributions, (b) predicted and experimental force-displacement results compared with measured data by Adams *et al.* [47], for cylindrical specimen with an initial 60 mm diameter and 20mm height.

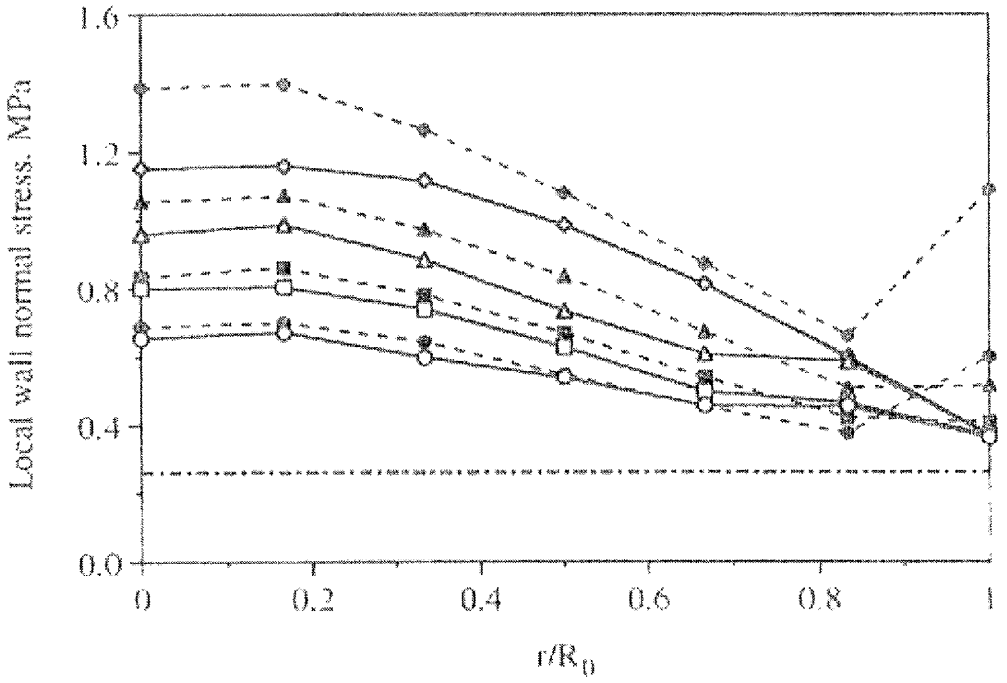

Figure 3.13 The radial wall normal stress distributions under a no-slip wall boundary condition for a range of compressive deformations. The open and corresponding filled symbols, connected with the solid and dashed lines respectively, represent the measured and computed values respectively for the following deformation ranges: ○, 10 %; □, 20 %; △, 30 % and ◇, 40 %. (reprinted from Adams *et al.* [47])

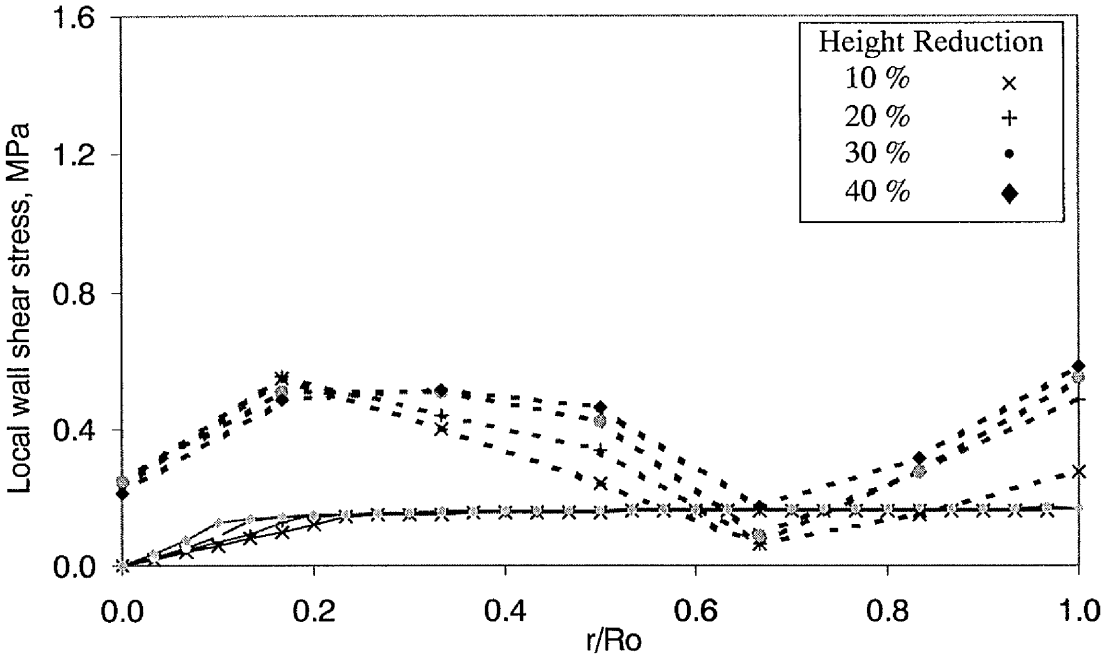

(a)

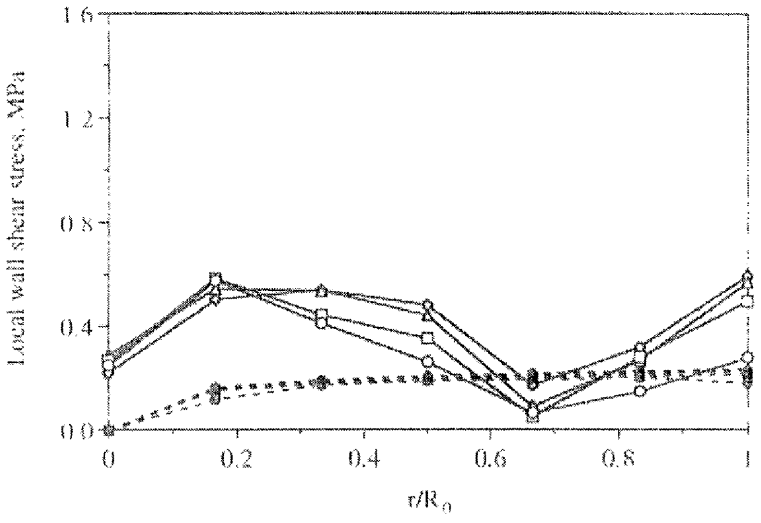

(b)

Figure 3.14 (a) Predicted (—) and measured (---) by Adams *et al.* [47] contact shear stress distributions, (b) the measured (---) and computed (—) values of the radial wall shear stress distributions under a no-slip wall boundary condition for a range of compressive deformations of ○, 10 %; □, 20 %; △, 30 % and ◇, 40 %. (reprinted from Adams *et al.* [47])

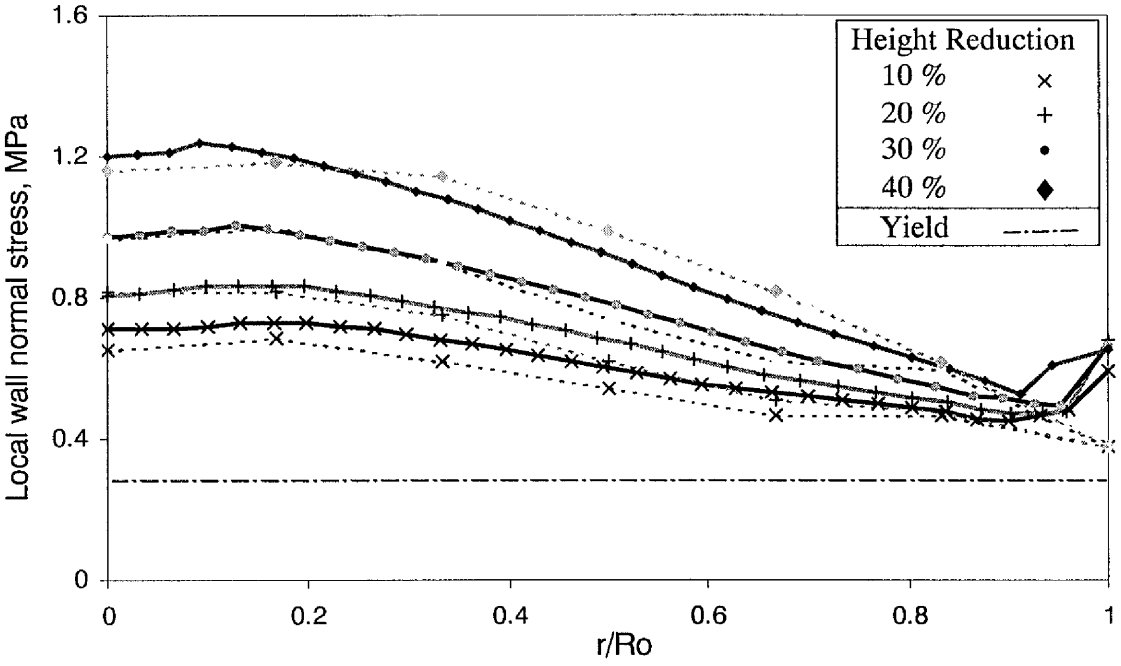

Figure 3.15 Contact normal stress distributions predicted with a wall boundary condition of μ = 0.45 (—) and measured (---) by Adams *et al.* [47], for no-slip upsetting of a cylindrical Plasticine specimen.

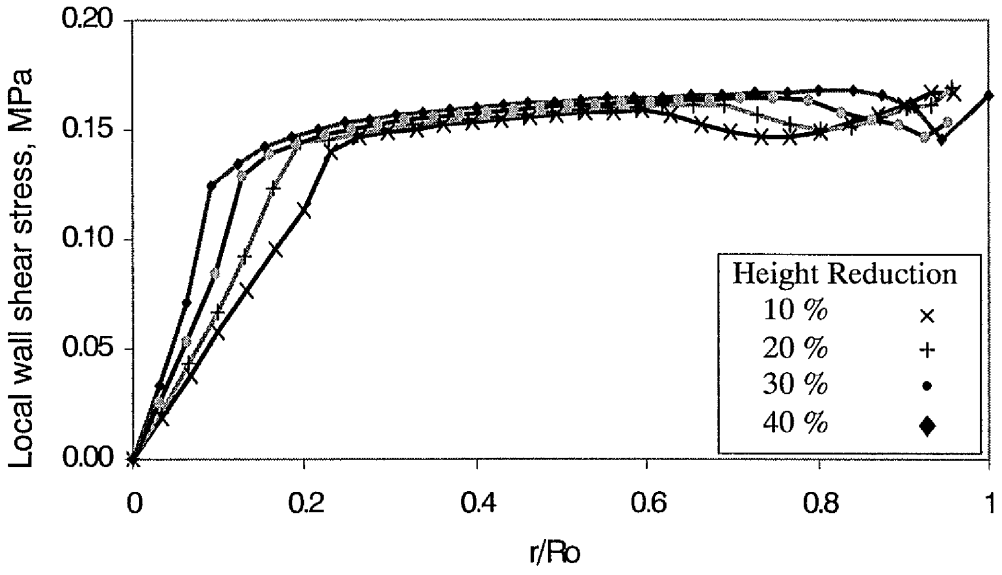

(a)

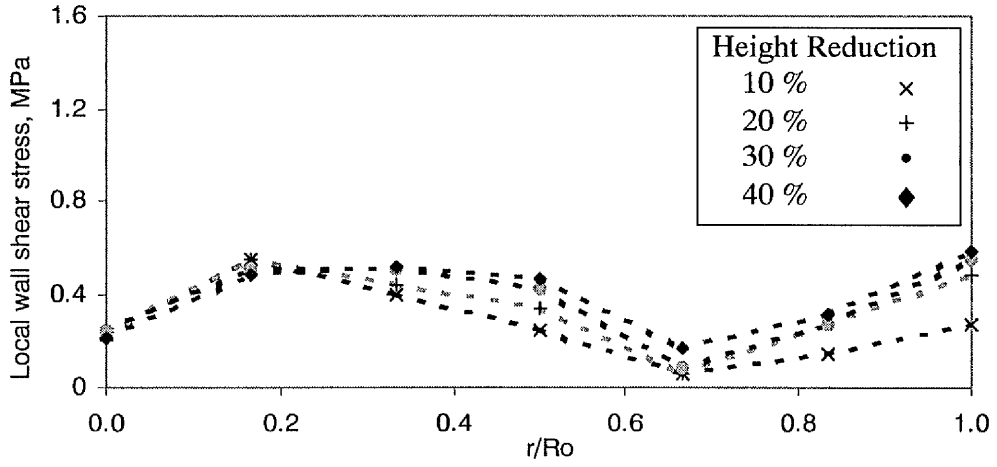

(b)

Figure 3.16 (a) Contact shear stress distributions predicted with a wall boundary condition of μ = 0.45 (—) and (b) measured (---), by Adams *et al.* [47], for no-slip upsetting of a cylindrical Plasticine specimen.

CHAPTER 4

APPLICATION OF OSCILLATION TO THE UPSETTING PROCESS

This chapter describes a study of the effects of applying vibration to the forming tools of an upsetting process. A detailed finite element analysis is described involving the compression of a model soft plastic solid material, where the workpiece is exposed to kinematic and sinusoidal vibration loading conditions. An oscillatory forming system is designed and used to investigate the potential benefits of vibration assistance for the cylindrical upsetting of a model material in a low frequency range. In this study, both finite element simulations and experiments have been performed for specimens with a range of sizes under different frictional boundary conditions. The results show that whenever vibration loading is superimposed on kinematic loading, there is an apparent decrease in the mean force. Force-displacement data is presented to illustrate the effect of vibration loading on upsetting deformation. It is demonstrated that when vibration is applied to the die, there is a reduction in the mean force, which recovers to the original elastic curve when the vibration is discontinued. These results are discussed in terms of friction reduction at the die wall in addition to a stress superposition mechanism.

4.1 Introduction

Due to rapid advances in processing technology, the design of optimised upsetting schedules has become increasingly important in terms of time and cost in a

competitive environment. This is due to factors which include the introduction of more speciality products with complex microstructures, the general need for shorter process development time-scales, the demand for increased production efficiencies and reliability and the requirement for improvements in product quality.

The benefits of oscillatory metalworking processes have been studied for several decades [17]. Such processes involve the application of a cyclic motion or stress to the tools or the workpiece during deformation. It appears that the extent to which an oscillation may be advantageous depends on the speed of processing, the type of process, the lubricant used, the mode of oscillation and the material being deformed [38]. Experimental studies of the machining mechanism of metal forming processes show that oscillatory metalworking operations have the capacity to achieve improved surface qualities, a reduction of the working loads and also a reduction of the friction between the die and workpiece. Several studies have clearly demonstrated the advantages of the application of ultrasonic vibration in a range of forming processes [30]. Also, developments in vibration measurement and modelling techniques [33] offer an opportunity to enhance the design of the excitation system. Due to the growing interest in vibration assisted manufacturing operations, efforts to examine the effects of the application of vibration to complex material forming processes is timely.

Decreasing the deformation load and improving the evenness of strain distributions in upsetting is a topic of interest to engineers. It is known that interface friction is an important factor in metal forming processes because of its effects on deformation load, surface quality, internal structure of product and die wear. The main purpose of the present study is to investigate the possible advantages of vibration assistance for upsetting of a model soft plastic solid material and to study the kinematics and geometric wall boundary conditions, in order to improve the operation.

Although much of the previously reported work in metal forming has incorporated ultrasonic excitation, in practice, a uniform, controllable oscillation amplitude is difficult to achieve at ultrasonic frequencies unless a vibration system comprising highly tuned transmission elements and dies is used. There is also a requirement for high power frequency generation and complex resonance tracking equipment. Moreover, as a starting point for this current research, and to provide effective experimental validations of the finite element models, the application of low frequency oscillations has been adopted. Low frequency oscillations may be generated by simple mechanical means, with relatively large amplitudes which are readily controlled for all loading conditions. In view of these considerations, this initial research has relied on the study of the fundamental benefits of vibration assistance in upsetting of a model material, in a low frequency range of 0-120Hz.

In this chapter, a finite element model is described for the analysis of upsetting of a cylindrical specimen of a model material assisted by vibration of the die within the selected frequency range. A uniform, controllable oscillation amplitude was achieved by the excitation system. Plasticine is used as the model material. The finite element model accounts for both the elasto-viscoplastic properties of the model material being processed and the frictional forces acting on the tool-workpiece interface. Numerical results are presented to show the effects of a variation in several parameters on the die-specimen interface for Plasticine. Friction conditions, and the amplitude and frequency effects of vibration loading in the specified frequency range are investigated.

4.2 Excitation System Design for Vibration Assisted Upsetting

This section concentrates on the design of the oscillating die in a vibration assisted upsetting process. Predicting natural frequencies and mode shapes of the die is achieved by validating finite element models with experimental modal analysis, using a non-contact laser vibrometer and the LMS data processing software. A design modification procedure was established to achieve efficient vibration

transmission and uniformity of vibration amplitude on the working surface of the oscillating die. A compromise in the design is reached to accommodate the requirement of supporting the high compression loads and the need to achieve vibration amplitude constancy and uniformity throughout the process. Measurements during the upsetting process confirm the success of the designed tools in maintaining the critical vibration conditions required to perform the vibration assisted upsetting investigations, which are necessary to characterise such vibration assisted processes.

The study of oscillation performance of forming dies is of great importance to industry and it has attracted many researchers [21,72,73]. However, poor reliability of such operations has often hampered exploitation of the technology and is the result of a lack of understanding of the fundamental mechanisms affecting such processes. Reliable operations can only be achieved by successful characterisation of the process and optimisation of the oscillatory characteristics of the forming equipment [73].

The upsetting equipment consists of a compression press, generator, transducer, amplifier and dies. The force required for the upsetting process is produced by the compression press. The key factors in obtaining reproducible vibration assisted process quality are, the right choice of compression equipment, the design of the die and the ability to transmit a uniform constant amplitude vibration to the working surface of the die under varying compression loading and specimen deformation. The oscillating die is particularly important, as consistent process results can be ensured if it is properly designed and manufactured. A better understanding and modelling of such oscillating die motions essentially relies on the accurate computation of the dynamic characteristics of the system eigenvalues (natural frequencies and damping ratios) and corresponding eigenvectors (mode shapes) [74].

The mathematical eigenvalue problem is a classical field of study, and much work has been devoted to providing eigenvalue extraction methods. A general equilibrium equation for eigenvalue problems is given by

$$(\varphi^2[M]+\varphi[C]-[K])\{\phi\}=0 \tag{4.1}$$

where *[M]* is the mass matrix, which is symmetric and positive definite; *[C]* is the damping matrix; *[K]* is the stiffness matrix; φ is the eigenvalue and $\{\phi\}$ is the eigenvector – the mode of vibration. Assuming *[K]* is symmetric and positive definite and neglecting *[C]* during eigenvalue extraction, then the eigenvalue problem can be written as

$$(-\omega^2[M]+[K])\{\phi\}=0 \tag{4.2}$$

where ω is the circular frequency.

However, during the compression process, the oscillatory die is attached to the specimen with distributed loads from the upper die, and these loads greatly complicate the analysis of the die motions. Therefore, numerical methods have been used in the investigation of die motion under a varying load, in particular in finding the die natural frequencies and vibration mode shapes.

A three dimensional model has been developed to describe the dynamic motion of the die. The model was established and the natural frequencies and vibration mode shapes obtained using ABAQUS. It has been found that the change of static equilibrium state of the die due to load, alters the die's natural frequencies and mode shapes. The design of the die therefore concentrates on delivering the required vibration amplitude and achieving amplitude uniformity on the working surface to ensure reliable operation. Typically, a minimum of 80 % uniformity is a design target [72]. The uniformity is defined as the ratio of the minimum divided by the maximum amplitude of vibration on the die working surface (U_{min}/U_{max}). An

oscillatory die has been designed by using an effective finite element model in conjunction with experimental modal analysis. The die is used in a laboratory compression test to evaluate the capabilities and accuracy of the designed system.

4.2.1 The Excitation System

The apparatus for incorporating vibration excitation into the compression test is shown in figure 4.1. The vibration system is set up between the upper die and the base of the Instron universal hydraulic testing machine, which is capable of controlling the loading speed and has a maximum load capacity of 5 kN. The upper die is attached to the crosshead of the Instron and the oscillation is provided by the lower die, under which is suspended the vibration exciter. The lower die and vibration exciter are supported on rubber mounts by a series of rigid cylinders attached to the base of the Instron. The rubber mounts allow the lower die to vibrate essentially in a free-free arrangement and prevent vibration transmission to the support structure. The primary performance indicator for such an oscillating die is the uniformity of amplitude distribution along the working surface. In this case the die is required to deliver a vibration amplitude of 40 μm during the test.

The mechanical vibration is generated by a signal from a frequency generator and is amplified before being fed to the vibration exciter, which is suspended under the lower die and attached via a rigid stinger. The static compressive force from the Instron testing machine is simultaneously applied to the upper die. The vibration force from the excitation system is therefore superimposed on the static compressive force from the Instron machine.

The magneto-vibrator used in this experiment is a Ling Dynamic Systems (LDS) V406, with dimensions of 165 mm in diameter and 198 mm in height. The static magnetostriction is capable of producing a sine vector force of 196 N. A maximum amplitude of about 40 μm at the top surface of the oscillatory die is required for the upsetting test, in which the maximum static force may be up to 1 kN. The

frequency of the oscillator is to be varied for the experiments in a range between 0 and 120 Hz.

The aim is to maintain a constant, uniform vibration amplitude across the working surface of the lower die throughout each compression test. To achieve this, a laser Doppler vibrometer (LDV) measures the displacement amplitude of the die response during the test. The vibrometer measurement is monitored and used as a feedback signal to control the driving power to the exciter, which is adjusted during compression to maintain the required die vibration amplitude.

4.2.2 Measurement System

The experimental set-up used for measurement, as shown in figure 4.2, consists of three major items: (1) an excitation signal, provided by LMS CADA-X system and LDS power amplifier and exciter, (2) a laser Doppler vibrometer, used to measure the die response and a piezoelectric force transducer used for measuring the excitation and (3) data analysis, provided by the LMS CADA-X system for processing of the response data collected by the laser vibrometer and force transducer.

A laser Doppler Vibrometer consists of an optical head that emits a laser beam and a converter that processes the Doppler frequency of the reflected laser beam. The laser beam is directed onto a vibrating test structure using an aiming device and with the aid of an optical mirror, it is possible to measure vibration at constrained locations that are usually difficult to measure. The back-reflected beam is recombined with the internal reference beam. When the test structure moves, the frequency of the signal beam reflected from the structure ($f_0 + f_D$) is shifted from the original frequency of the emitted laser beam (f_0) due to the Doppler effect. The change in frequency (referred to as the Doppler frequency, f_D) is given by $f_D = 2v/\lambda$, where v is the velocity of the moving structure and λ is the wavelength of the emitted laser beam, λ = 0.633 μm. The voltage signal converted from the

recombined beam is proportional to the velocity at which the structure under measurement moves. This signal is then converted into a displacement signal.

Vibration testing using LDV offers advantages over conventional accelerometers because accelerometers mass load the test structure causing the frequency response to be distorted and altered by the measurement location. LDVs do not affect the structure under measurement due to the non-contact measurement method. The sensor head can be placed at a reasonable distance from the structure providing ease of use in a laboratory. Consequently, the laser beam spot on a test structure is minutely small, measuring only several tens to several hundreds of microns. Hence the LDV provides better point resolution than accelerometers and the vibration of a small structure can be readily measured.

LMS CADA-X is a HP-Unix-based suite of software for structural dynamics engineering. The system provides an integrated vibration excitation, test and analysis facility via sophisticated data acquisition, involving high speed on-line multi-channel data reduction and integrated analysis software. LMS provides a total solution for structural modal analysis which is used in this study. The extracted modal parameters, of modal frequency and mode shape, are used to formulate a mathematical dynamic model of the test structure.

4.2.3 Finite Element Analysis in Oscillating Die Design

Following the design strategy set out in the last two sections, the first stage of the analysis involved measurement of the performance of the designed system, in order to satisfy the requirement of supporting high compression loads and to achieve the vibration amplitude uniformity and constancy throughout the compression process. A modal analysis was performed by a finite element simulation and experimental validation procedure. Modal analysis is a process of determining the modal parameters of a structure for all modes in a frequency range of interest. A mode may be longitudinal, flexural or torsional.

A rectangular carbon steel solid plate 340 x 340 mm and 10 mm in thickness was initially selected as the oscillatory die to satisfy the requirement of supporting the high compression load whilst accommodating the dimensions of the vibration exciter. A new configuration (shown in figure 4.3) was designed to reduce the mass of the plate and increase the attainable vibration.

The finite element model was developed using ABAQUS code with 8 node 3D solid fine mesh elements, as shown in figure 4.4, to predict the eigenvalues (modal frequencies) and eigenvectors (mode shapes) of the die. The oscillating die material, carbon steel, is assumed to be homogeneous with elastic material parameters of Young's modulus 193 GPa, Poison's ratio 0.33 and density 7832 Kg/m^3.

It was anticipated that dimensional changes to the Plasticine specimens due to plastic deformation and static loading of the tools would result in variations in the performance of the oscillating die. Therefore, the changes in the vibration response of the oscillatory die were predicted as affected by the increasing static load. The plate was preloaded in an initial step for a static stress analysis and the eigenvalues of the preloaded plate were then obtained.

4.2.4 Experimental Validation

The oscillating die was manufactured from carbon steel. Experimental modal analysis was carried out using the LDV and LMS system for measuring the dynamic response to a known excitation force at an array of points on the surface of the die. The ratio of response to force in the frequency domain is known as the frequency response function (FRF). When the FRF measurements were completed, the LMS system was used to extract modal parameters through curve fitting. The requirements of the test are accurate estimates of natural frequencies and

descriptions of the mode shapes using sufficient measurement points to permit their identification and correlation with those from the finite element model.

In the 5-1000 Hz range, the modes of vibration were detected and recorded for use as validatory data for the FE model. The natural frequencies and the corresponding modes obtained experimentally and numerically, based on free-free vibration conditions, are shown in figure 4.5. Agreement is obtained between the numerical predictions and the experiment results. One flexural vibration mode of the plate was detected within the working frequency range of 5-120 Hz by both experiment and FE simulation. However, a uniform response is obtained on the working surface at the centre of the plate, as illustrated in figure 4.6. A surface uniformity of 96 % was calculated from the experimental data, while 94 % uniformity was predicted by the FE simulation. The results show that the designed die has achieved the target uniformity of 80 % on its working surface. Therefore, the operation of the die is enhanced by this mode (less force to excite the working amplitude).

These findings indicate that the working surface of the oscillating die operates in an effective rigid body vibration during the oscillatory upsetting test in a frequency range of 5-120 Hz. A uniform vibration amplitude can be achieved by this designed die.

Simulations were also performed by initially applying external loads of 0-2000 N at the centre of the plate. The eigenvalues of the preloaded structure were then obtained. The first natural frequency varied with pre-loading as shown in figure 4.7. The result shows that, within the working frequency range of 5-120 Hz, the designed die is able to produce a uniform vibration amplitude throughout all loading condition during an upsetting test.

Figure 4.8a illustrates finite element simulation results of the plate producing a uniform amplitude of 43 μm on its working surface with surface uniformity of 99

% during a compression operation under a maximum load of 1000 N and superimposed oscillation frequency of 120 Hz. The surface performance was also measured using LDV and LMS systems. The measured response of 41 μm amplitude at the centre of the working surface, and 99 % surface uniformity, is shown in figure 4.8b. The result compares well with the numerical predictions. The measurement of displacement on the working surface during the oscillatory upsetting process, which is shown in figure 4.9, confirmed the success of the die in maintaining the vibration conditions required to perform the vibration assisted upsetting investigations.

4.3 Oscillatory Upsetting Experiments

The specimens used in this study were all 20 mm in height, 40 mm and 60 mm in diameter. Specimens were prepared as described previously in section 3.3.1.

Compression tests were performed at constant speeds of 1-5 mm/min under no-slip and lubricated conditions by using abrasive and wax paper respectively between the specimen and platens. The forming force-displacement data were recorded using a dedicated computer and software. For conducting oscillatory upsetting, a minimum static load, which is dependent on the peak-to-peak vibration force ($2F_A$) and a constant value c, ($2F_A + c$), is required before onset of vibration. Lower static loads are not sufficient to prevent movement of the specimen's position between the platens and therefore, initially, an appropriate value of c was determined experimentally by observing movement of the specimen under various static loads at the onset of vibration. After the onset of plastic flow and once the minimum required static load has been reached, vibration excitations of various frequencies and amplitudes were superimposed on the static load. During and between the intervals of vibration loading, static deformation was continued. Specimens were therefore subjected to a strain history given by:

$$\varepsilon(t) = \dot{\varepsilon}_0 t + \varepsilon_A \cos(\omega t) \tag{4.3}$$

where $\dot{\varepsilon}_0$ and ε_A are the constant static strain rate and vibration strain amplitude respectively. The corresponding strain rate history is given by:

$$\dot{\varepsilon}(t) = \dot{\varepsilon}_0 + \omega\varepsilon_A \sin(\omega t) \tag{4.4}$$

It was assumed that there was no increase in the surface or bulk temperatures of the specimens, which is consistent with the small amplitude (≤ 40 μm) and low frequency range (≤ 120 Hz) of the imposed vibration.

The mean compressive flow stress is considerably reduced by superimposing oscillation on the static load. Figure 4.10 illustrates this consistent result of compression tests where vibration is superimposed on the static loading. The measured mean force–displacement data shown in the figure are presented for compressing a specimen with an initial diameter of 40 mm under a no-slip boundary condition. During the four intervals of superimposed vibration, constant die vibration amplitude of 40 μm and frequency of 100 Hz were maintained. The static loading compression test results and a compressive test where the vibration load was applied continuously are also shown in the figure. In general, the onset of vibration results in an immediate drop in the mean forming load. During the interval of superimposed vibration loading, the mean force follows the curve associated with continuous vibration loading. After each interval of vibration, a new elastic line starts at the mean reduced level, finally reaching and following the curve associated with the static loading.

Figure 4.10 also shows that if the amplitude of oscillation remains constant throughout the compression, the reduction in load is constant. The factors that cause the reduction in mean flow stress may be attributed to oscillatory effects of stress and velocity due to vibration. These factors are dependent on the amplitude of vibration. Figure 4.11 shows the measured compressive load–displacement relationship and the corresponding mean true stress-strain relationship for a

specimen with an initial diameter of 60 mm under a no-slip boundary condition and a compressive velocity of 5 mm/min (compared with finite element predictions which are discussed later). The amplitude of vibration is varied in the range of 0-40 μm for successive intervals of vibration loading. As the vibration amplitude is increased, the mean load decreases (figure 4.11a) and stress (figure 4.11b) markedly. Within the measured amplitude range, the mean flow stress was observed to decrease in proportion to the vibration amplitude as shown in figure 4.12.

The relationship between the flow stress and that generated by the superimposed vibration, $\overline{\sigma}_v$, can be expressed as follows (shown in figure 4.13):

$$\overline{\sigma}_v = \sigma_s - \hat{\sigma} \tag{4.5}$$

where σ_s is the flow stress without vibration and $\hat{\sigma}$ is the maximum oscillatory stress amplitude due to vibration.

Consider the case where a specimen is compressed by two parallel dies such that the velocity of the upper die is V_T and the lower die is oscillating with displacement amplitude A as represented in figure 4.14. The position of the upper die at A represents the furthest position of the upper die from the lower die. After time t_1 at point B, the upper die and the lower die are travelling in the same direction at the same speed so that at this instant compression ceases. Subsequently, assuming the vibration velocity is greater than the velocity of the upper platen, two scenarios can occur: (1) the vibration velocity is low enough to result in elastic unloading of the specimens but no separation of the specimen and die surfaces occurs or (2) the vibration velocity is high enough to result in elastic unloading followed by separation of surfaces. As a result of the elastic extension in the specimen, after time t_1 has elapsed, the specimen at point B″ follows the lower die movement to where the specimen elastically relaxes. At the same time, the upper die unloads the specimen at a constant speed, as represented by the broken

line B″C″D″. When the lower die velocity again equals the mean velocity of the upper die at point C, an elastic extension has been released in the specimen that is equal in magnitude to C′C″. This extension is then taken up partly by the upper die and partly by the lower die on its return cycle, until at point D″ compression commences again. At C, the relative velocity between the platens is zero and the relative displacement is therefore a maximum. The length C′C″ therefore represents the peak-to-peak amplitude of movement in the compressed specimen and the corresponding time t_2 is when the maximum reduction in compression force is reached. This analysis can be described in mathematical terms as follows:

The velocity of the lower die is given by $V_L = A\omega sin(\omega t)$. It is assumed that compression ceases when the constant velocity of the upper die $V_T = V_L = A\omega \sin(\omega t)$ at time

$$t_1 = \frac{1}{\omega}\arcsin\left(\frac{V_T}{A\omega}\right) \tag{4.6}$$

If the periodic time $T = 2\pi/\omega$, then after $t_2 = \pi/\omega - t_1$ has elapsed, the displacement of the specimen is at a maximum for its cycle. During the interval $t_2 - t_1$, the lower die will have displacement D_L:

$$\begin{aligned} |D_L| &= \left|A\cos(\omega t_1)\right| + \left|A\cos\left[\omega\left(\frac{\pi}{\omega} - t_1\right)\right]\right| \\ &= \left|2A\cos(\omega t_1)\right| \end{aligned} \tag{4.7}$$

And the upper die will have displacement D_T:

$$|D_T| = V_T\left|\frac{\pi}{\omega} - 2t_1\right| = \frac{V_T}{\omega}|\pi - 2\omega t_1| \tag{4.8}$$

The oscillatory elastic displacement D_{max} induced in the specimen is then obtained by subtracting equation (4.8) from equation (4.7).

$$|D_{\max}| = |2A\cos(\omega t_1)| - \frac{V_T}{\omega}|(\pi - 2\omega t_1)|$$
$$|D_{\max}| = |2A\cos(\omega t_1)| - \frac{v_T}{\omega}|(\pi - 2\omega t_1)| \qquad (4.9)$$

Now the maximum acoustic stress amplitude in a standing wave is related to $|D_{\max}|$ by the equation (5):

$$\hat{\sigma} = \frac{\omega|D_{\max}|E}{2C} \qquad (4.10)$$

where E and C are the elastic modulus and sound velocity of the sample material. Therefore, the cyclic stress amplitude may be computed. Within the limits of experimental accuracy, it agrees with the measured mean changes in stress $\sigma_s - \overline{\sigma}_v$, as shown in figure 4.12. This result clearly indicates that the reduction in mean stress by oscillation may be explained by the superposition of the induced vibratory stress on the static stress.

In fact, the peak of the oscillatory force (F_{peak}) was not reduced for a no-slip boundary condition but, in fact, it exceeded the static forming force (F_{static}) in this study, as shown in figure 4.15. The amount by which the peak forming force exceeds the static forming force is small, but increases with increasing vibration amplitude, as shown in figure 4.16. For a strain rate sensitive material, such as Plasticine, this may be explained by changes in the strain rate when a vibration load is applied.

Following the strain rate sensitivity equation (3.1), the bulk flow behaviour of Plasticine may be approximately given by

$$\overline{\sigma} = 0.26 + 0.08(\dot{\overline{\varepsilon}}^{vp})^{0.34} \qquad (4.11)$$

During intervals of superimposed vibration loading, the specimen undergoes a strain rate change from $\dot{\varepsilon}_0$ to $\dot{\varepsilon}_0 + \omega\varepsilon_A$ (according to equation (4.4)). Following on from equation (4.11), the stress changes from $\bar{\sigma}(\dot{\varepsilon}_0)$ to $\bar{\sigma}(\dot{\varepsilon}_0 + \omega\varepsilon_A)$, and the resulting general stress-strain curve shown in figure 4.13 is expected for a strain rate sensitive material such as Plasticine. Hence, when increasing the vibration amplitude, the maximum stress increases due to the increase in strain rate.

However, figure 4.17 shows the reduction in forming force achieved under superimposed vibration loading when certain lubricants are applied. This is observed in the figure as a reduction in the maximum force during the interval of vibration loading rather than the increase measured under no-slip boundary conditions. The measurement of the mean reduction in compressive force was considerably larger than the vibration force amplitude, thus indicating that superposition alone could not explain the reduction in load. This reduction in force may be attributed to a reduction in the coefficient of friction, as a result of effectiveness of the lubricant. The observed reduction of barrelling in the finished specimen strongly supports the conclusion that the coefficient of friction is reduced, as shown in figure 4.18.

4.4 Numerical Analysis

4.4.1 Finite Element Model

Figure 4.19 shows the upsetting system, which is analysed numerically by a finite element method. The workpiece was deformed by controlling the upper die with a constant velocity, while the lower die was fixed during intervals of static deformation. A sinusoidal vibration was superimposed on the static motion by vibrating the lower die with displacement amplitude A and frequency ω. The displacement of the lower die is therefore described by $X_L = A\cos(\omega t)$. To minimise vibration amplitude non-uniformity across the lower die face and to

achieve an effective rigid body vibration of the lower die, stiff springs were selected to support the lower die, as shown in the figure.

Plasticine is used as the material model. The specimen model and associated material parameters have been described in Chapter 3. The two stainless steel parallel dies were modelled as rigid surfaces.

In the numerical analysis, the upsetting process was carried out using the commercial code ABAQUS, using a formulation described previously in Chapter 3. The speed of the upper platen was set to the same constant value as set in the experiments. The vibration displacement amplitudes selected for the lower platen were 5, 10, 20 and 40 μm and the frequencies were 5, 10, 25, 50, 75 and 100 Hz. Since the speed of upsetting was slow and the vibration loading was superimposed for a very short time interval at room temperature, it was assumed that the system was isothermal.

During each equilibrium iteration, a check was made to determine if contact between the master and slave surface had occurred. The contact and master and slave surfaces were defined in section 3.4, Chapter 3. To simulate the deformation with a no-slip boundary condition, the coefficient of friction was assumed to have a constant value of 0.57 throughout the process. When a lubricant was introduced, a value of 0.3 was used during the deformation. This value was selected on the basis of ring compression test data (details shown in Appendix C).

A stress-displacement analysis was implemented and the oscillating upsetting calculations were performed using the following procedure. Initially, the finite element model undergoes static loading. A displacement increment of about 0.5 % of the original height of the specimen was applied until approximately a 12.5 % reduction in height was achieved (which ensures that the model is post-yield), by controlling the velocity of the upper platen to the same constant value as set in the experiments. For the second step, vibration loading of the lower platen was

superimposed on the static load, by controlling the sinusoidal amplitude and frequency of the lower platen for 20 intervals. Subsequently, the model returns to its static loading condition. Again, a displacement increment of about 0.5 % of the original height of the specimen was applied until an approximate 2 % reduction in height was achieved, by controlling the constant velocity of the upper platen. The addition of the vibration load was repeated for two further intervals, with a return to static loading between them. The strain history and the corresponding strain rate history during the whole oscillating upsetting procedure are presented in figure 4.20. As shown in the figure, the strain rate increases for part of the vibration cycle and, for part of the cycle, which can be calculated from the vibration velocity and upper die velocity, the specimen experiences elastic recovery. Four different vibration amplitudes at four different frequencies were selected to be applied in the model.

Throughout, the static and kinematic values of the coefficient of friction, μ, were assumed equal when the interfaces were in contact.

4.4.2 FE Results

The force-displacement data in figure 4.21 show the effect of the oscillatory load on the squeeze flow deformation. Following the elastic line to the yield point A of 1092 N then the plastic part to point B corresponding to a load of 1252 N, vibration loading was applied, providing a die displacement amplitude of 20 μm at 10 Hz. This immediately results in the mean force decreasing to 1160 N (point C). When the vibration loading is discontinued at D, the specimen again follows an elastic line until it reaches E (as would have been reached in a purely static loading - shown as a broken line). At F, 1370 N, the vibration loading was superimposed again and the mean force level decreased to 1280 N (point G). At H the vibration loading is discontinued and again the specimen follows an elastic line and reaches the static curve at I. Again the curve from J to K-L-M follows the history of onset to discontinuation of vibration loading. The reason why vibration of the tooling die

has such an effect on the upsetting process can be explained as the superposition mechanism of induced oscillatory stress on the static stress.

The peak of the oscillatory force was not reduced but, in fact, it exceeded the static forming force and was correctly predicted. The amount ($\Delta F = F_{peak} - F_{static}$) by which the peak forming force (F_{peak}) exceeds the static forming force (F_{static}) was small, but increases with increasing vibration amplitude, as shown in figure 4.22. The effect of frequency on ΔF has also been plotted in figure 4.23, for a set of vibration amplitudes. It shows that there is a weak influence, compared with the influence of vibration amplitude. For a strain rate sensitive material, this is explained by changes in the strain rate when a vibration load is applied, as detailed in the previous section. For the part of the vibration cycle that the material and die are in contact, an increase in the strain rate to a power of $n = 0.34$ slightly increases the stress in the low strain rate range (from 0.004 1/s to $\leq$ 10 1/s) where strain rate varies due to low frequency oscillation. This can be clearly seen from the stress-strain rate curve for Plasticine in figure 4.24. The following decrease in strain rate which occurs for the part of the cycle when the compressive deformation ceased, relaxes the specimen elastically to a much lower stress. The mean stress and therefore the mean forming force is reduced.

The results in figure 4.25 indicate that the reduction in the mean force increases with increasing vibration amplitude. It is clear that the reduction in the mean force is dependent on vibration amplitude, but only a weak influence is observed due to the frequency variation, as shown in figure 4.26.

Figure 4.27 shows the mean forming force as a function of the vibration displacement amplitude and clearly demonstrates the decreasing forming force with increasing amplitude. It also shows that if the amplitude of oscillation remained constant at different reductions in height during deformation, the reduction in load was constant. In the figure, the horizontal lines represent the forming force without vibration superposition. It is obvious that the force

reductions during intervals of vibration are of the same magnitude for all true strains.

Computer simulation offers the possibility of a detailed investigation of a forming process and predicts in detail the material deformation history, which is almost impossible by experimental methods. A comparison of the distributions of the effective stress, plastic strain, axial stress and shear stress is shown in figure 4.28, for the same reduction in height of the specimen. It can be clearly seen that the higher values of axial and shear stress and plastic strain were reduced by the addition of vibration with amplitude of 20 μm at 10 Hz.

4.5 Comparison of FE and Experimental Results

Figure 4.29 shows the agreement obtained between the numerical and experimental results for the force-displacement relationship for Plasticine. The superposition effect is clearly demonstrated.

The experimental results show a agreement with the finite element predictions and provide a validation of the models. Thus the effect of oscillatory stress superposition is predictive and verifiable. Successful modelling of this loading regime, however, is not sufficient to explain further measurable beneficial mechanisms of force reduction under superimposed oscillating loading and lubricated boundary conditions. Comparing curve a and b in figure 4.30, some discrepancies exist between the computed and measured data for a lubricated boundary condition, due to beneficial improvements in friction under vibration loading in the upsetting experiments. Improved interface friction conditions under vibration loading have been investigated and incorporated into the finite element models by employing a reduced coefficient of friction value of 0.25. This allows a closer agreement with experimental results to be achieved, as shown by comparing figure 4.30b and c.

The predictions of force reduction as a function of the vibration amplitude are compared with the experimental results in figure 4.31, for upsetting under no-slip and lubricated conditions. For the lubricated condition the reduced coefficient of friction of 0.25 was incorporated in the FE model. It is clearly seen that a decrease in forming load and an improved friction condition can be achieved by superimposed oscillation as described previously.

The results also indicate that the reduction in mean force increases with increasing vibration amplitude, but there is only a weak influence observed due to the frequency variation, as shown in figure 4.32.

4.6 Conclusions

In this chapter, a description of the apparatus for oscillatory upsetting was presented. The feasibility of using finite element simulation to assist the design of the oscillating die was demonstrated. A compromise in the design is reached to accommodate the requirement of supporting the high compression loads and the need to achieve vibration amplitude constancy and uniformity throughout the process. A die vibration displacement amplitude ($\leq$ 40 μm) for all working frequencies (5-120 Hz) was achieved.

An experimental study of a vibration assisted upsetting process has been carried out using the designed apparatus. A large strain finite element simulation has also been generated to study the influence of vibration on the upsetting process, which includes the effects of elasticity and visco-plasticity for the material model, boundary conditions and loading. The upsetting of a cylindrical model material specimen between two parallel platens or dies under static loading was simulated and results were obtained for the forming force for a constant die velocity. Vibration loading of the lower die was initiated and the effects of vibration amplitude and frequency variations on the forming load were studied.

The results show that applying oscillation to the die reduces the static forming force during upsetting. The application of low frequency oscillations to the die in upsetting causes the specimen to be deformed intermittently once every cycle. At these instances, deformation occurs under a slightly higher load than that observed for static loading under a no-slip boundary condition. This increase in load is the result of increasing the stress by an increase in strain rate due to the strain rate dependent behaviour of Plasticine. During the remainder of the cycle, the specimen is elastically off-loaded and subsequently loaded relative to the static motion of the test machine. This results in a mean force reduction during upsetting. The reduction of the mean forming force is greater for higher vibration amplitude and there is a weak influence observed due to frequency variations.

In processes where lubricated boundary conditions are applied, then the intermittency of upsetting produced by the oscillation of the die as described above, enables real reductions in forming force to be realised. This is achieved since the deformation proceeds with a reduced value of coefficient of friction, μ. Hence, the maximum force is reduced. Together with the elastic off-loading during part of the interval, the specimen never experiences a forming force exceeding the static force level. Thus the result is a further reduction in the forming force.

Therefore, it is concluded that applying oscillation to the die reduces the forming force during upsetting. The force reduction can be explained by the superposition effect for no-slip boundary conditions and by a further reduction in the coefficient of friction for the lubricated cases.

Finally, no changes in the material properties were observed when low frequency oscillations were applied. There is evidence that the coefficient of friction μ does not change during static loading, as there is no evidence of lubricant breakdown or reduced effectiveness. Reducing μ as a result of the application of oscillation allows the experimental and finite element results to agree and supports the conclusion that μ is effectively reduced by vibration.

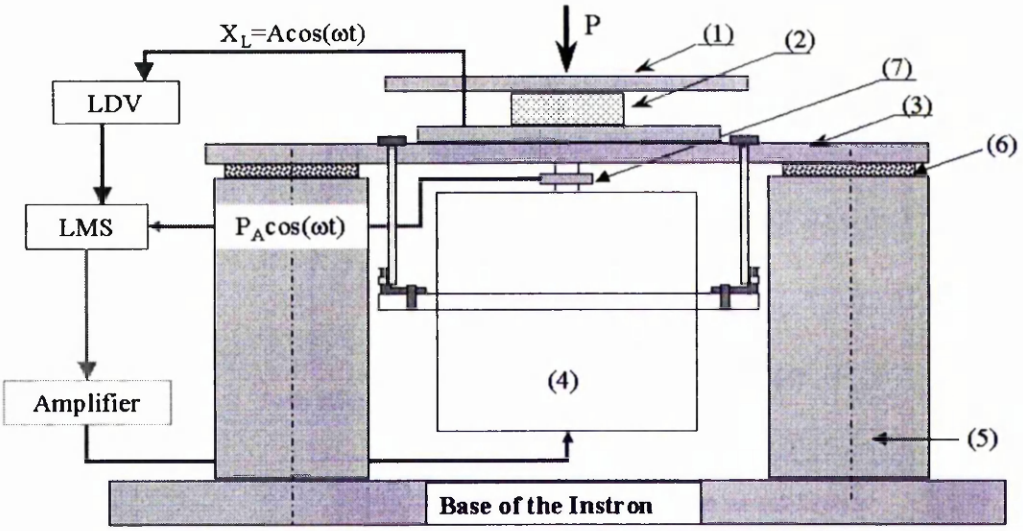

(1) upper die, (2) specimen, (3) oscillatory die, (4) exciter, (5) rigid cylinder, (6) rubber mounts, (7) force transducer.

(a)

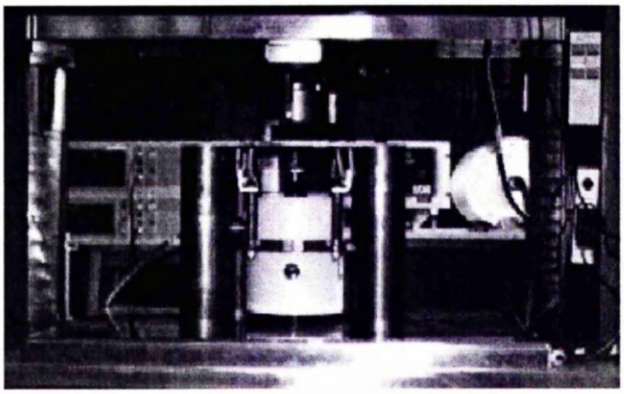

(b)

Figure 4.1 Apparatus for oscillatory upsetting study (a) schematic diagram, (b) photograph.

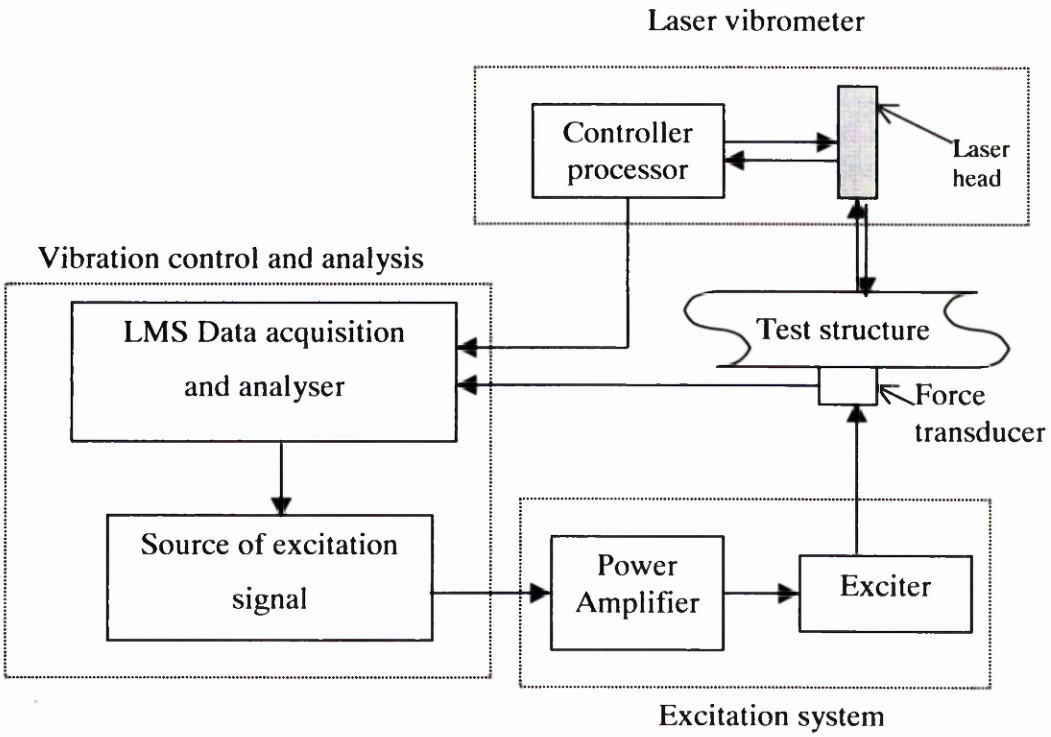

Figure 4.2 Schematic diagram of the experimental measurement system.

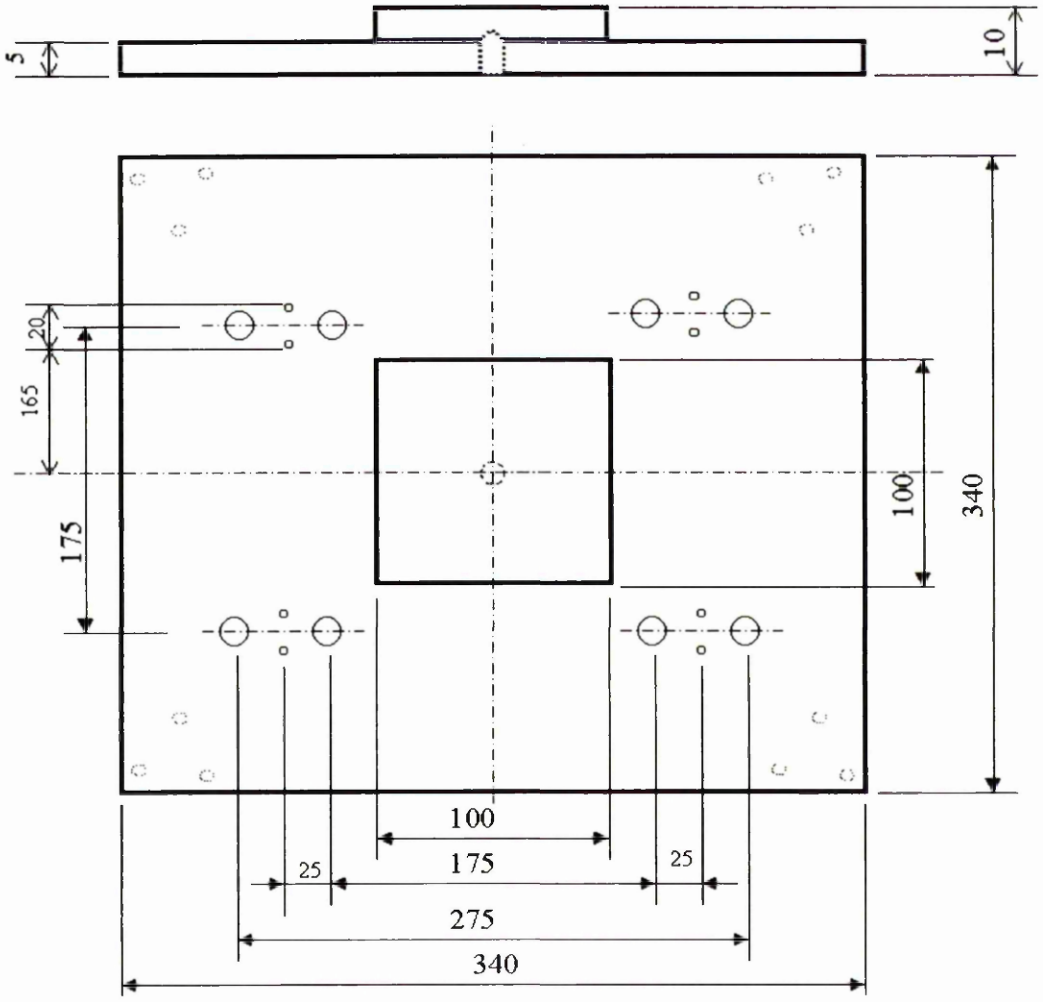

Figure 4.3 Oscillatory die, all dimensions in mm.

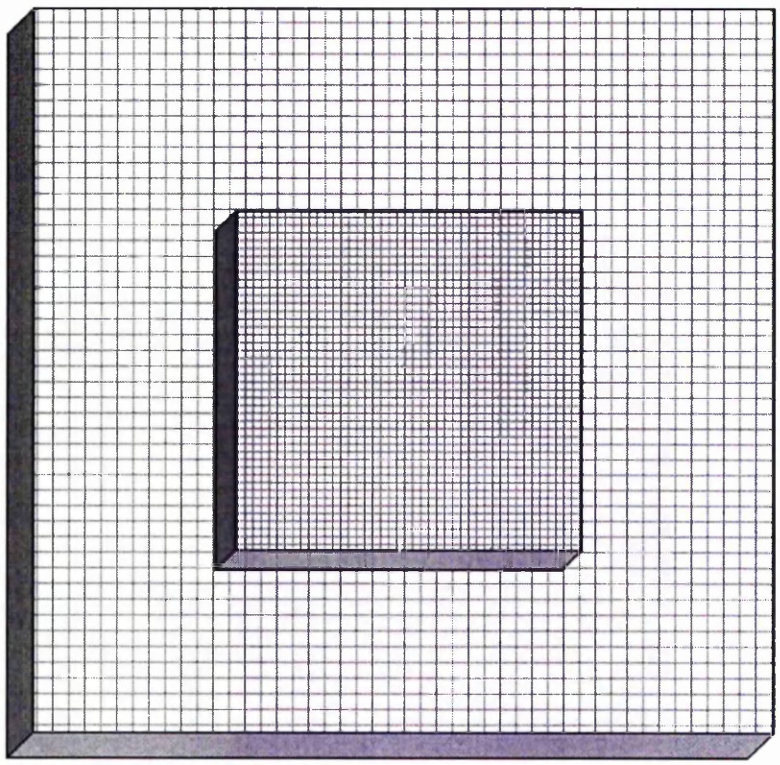

Figure 4.4 3D finite element model for the oscillatory die.

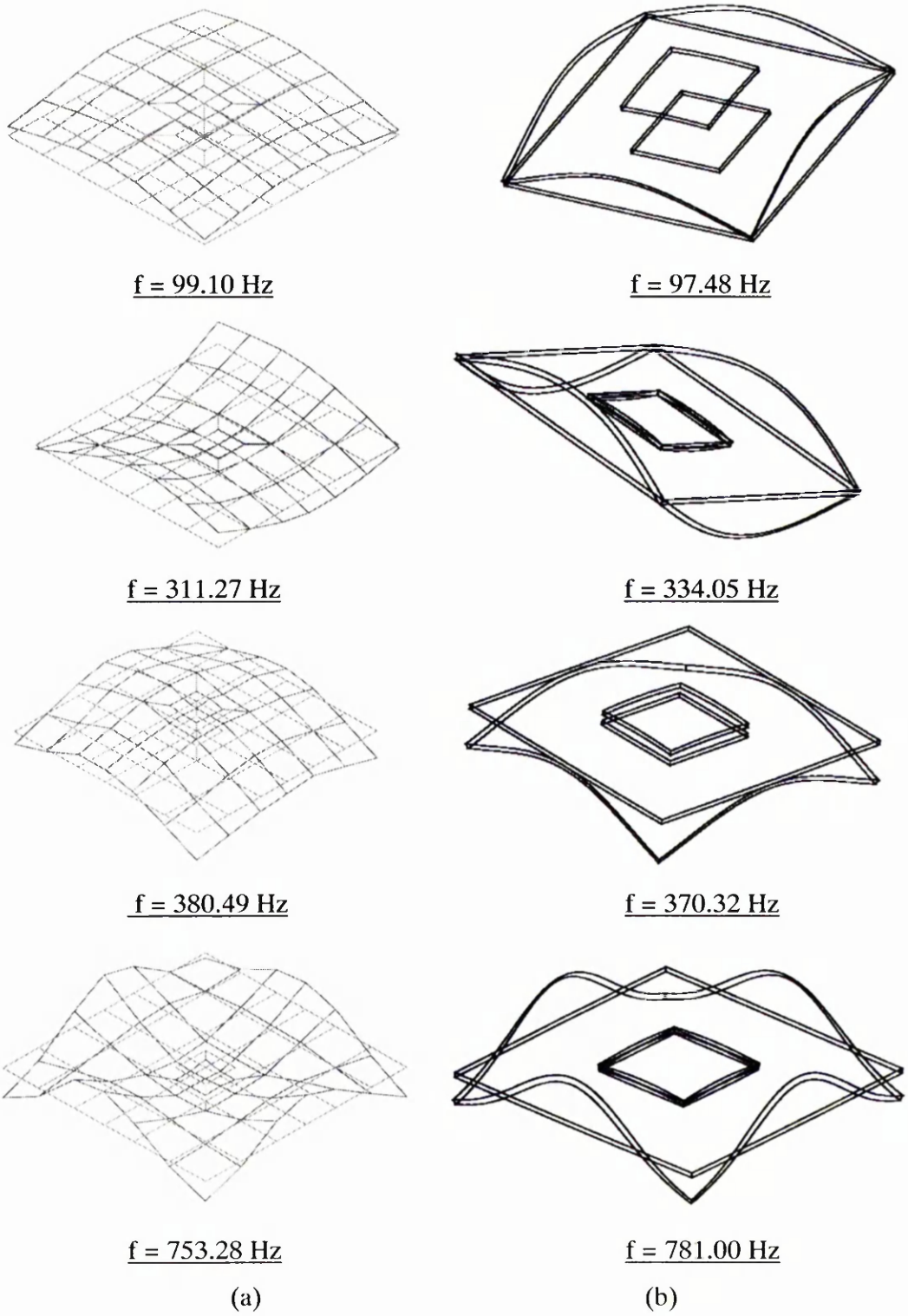

Figure 4.5 Mode shapes for the oscillating die obtained from (a) experiment and (b) FE simulation.

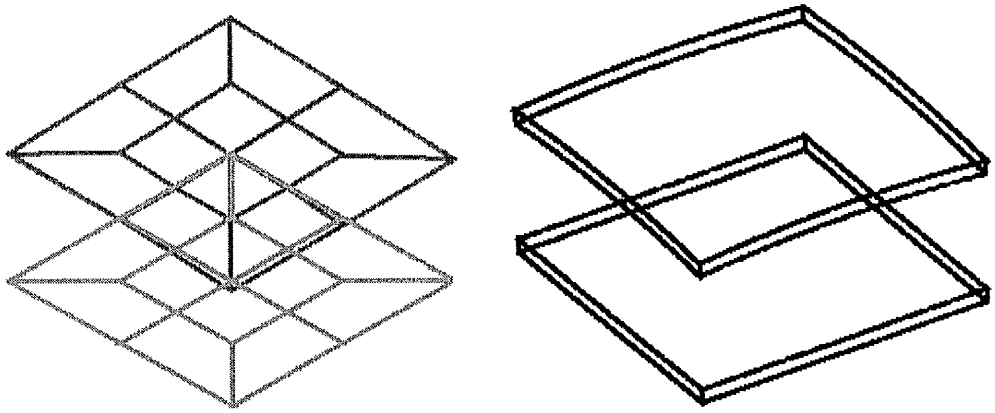

(a) (b)

Figure 4.6 Motion on the working surface of the oscillation die at first vibration mode obtained from (a) experiment and (b) FE simulation.

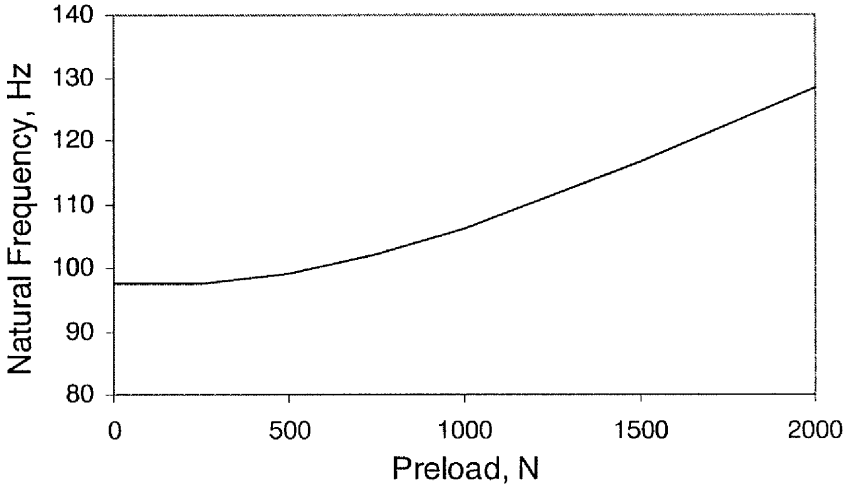

Figure 4.7 Natural frequency of the die modified by pre-load.

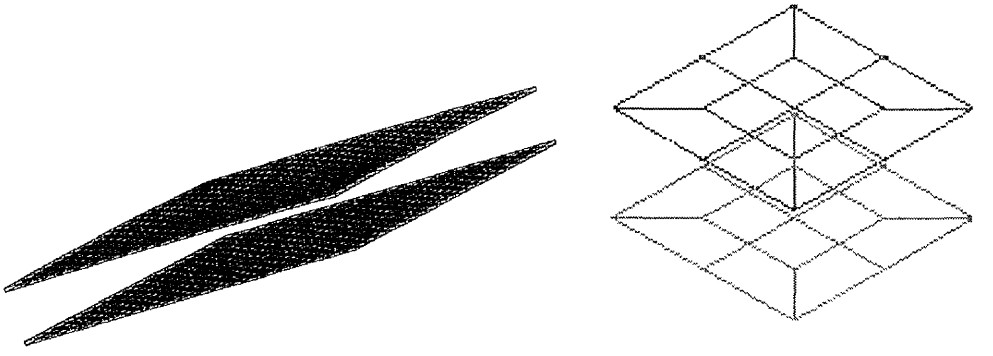

(a) (b)

Figure 4.8 Displacement configuration of the working surface of the oscillating die under dynamic load, obtained from (a) finite element simulation and (b) experimental measurements.

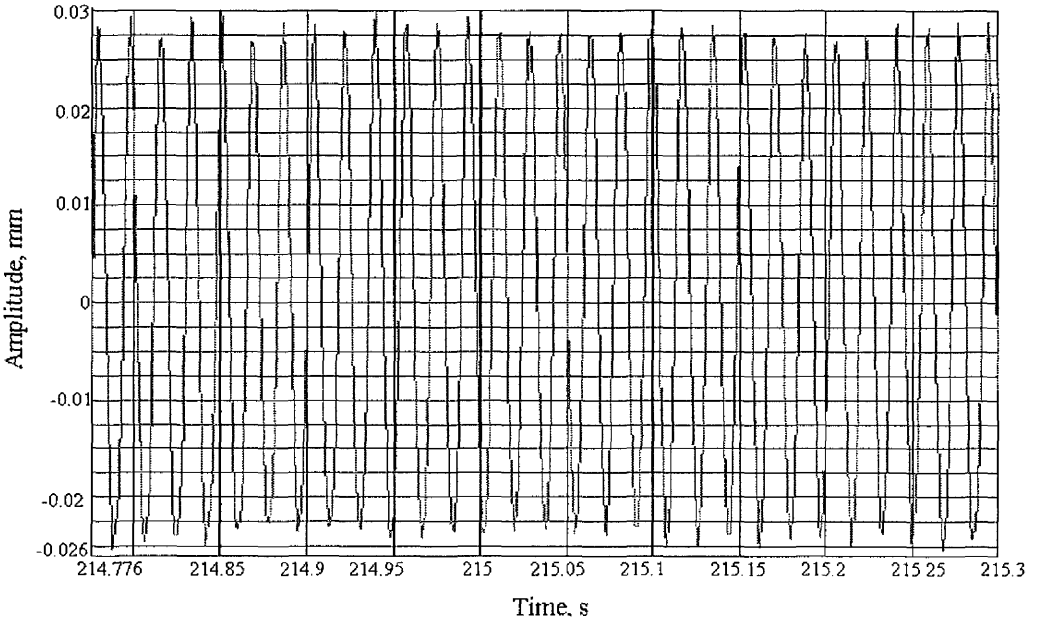

Figure 4.9 Displacement produced on the working surface during oscillatory upsetting, measured using LDV.

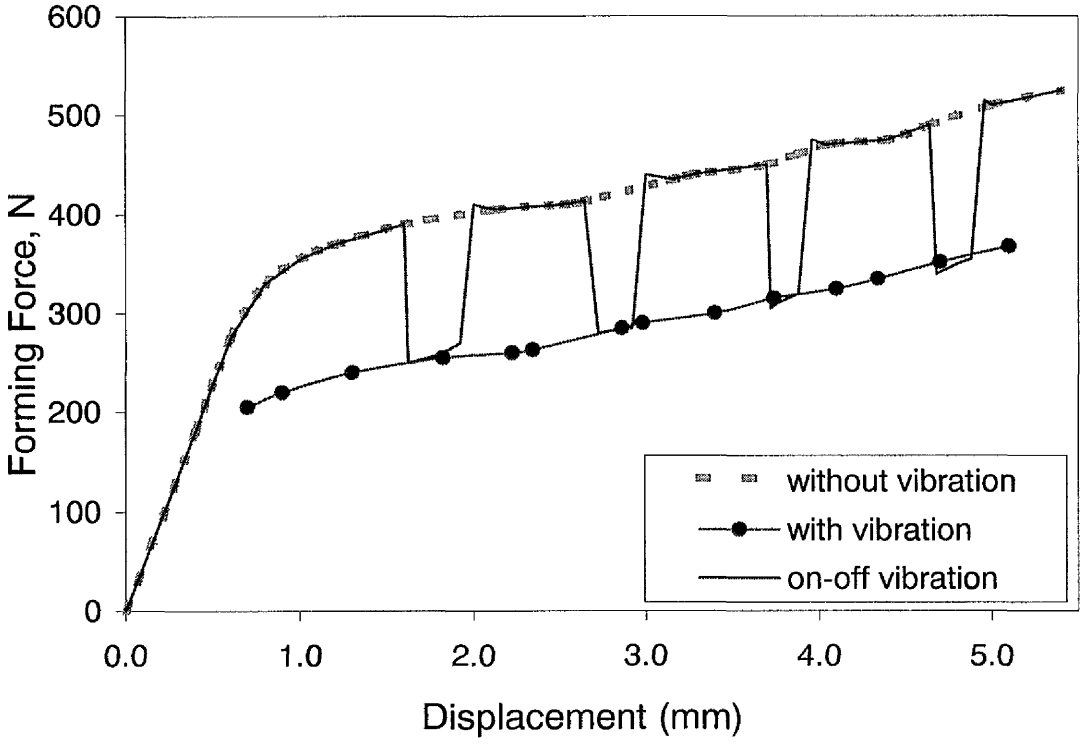

Figure 4.10 Influence of vibration at an amplitude of 40 μm and frequency of 100 Hz on the measured forming force as a function of displacement for a specimen with an initial diameter of 40 mm under a no-slip boundary condition.

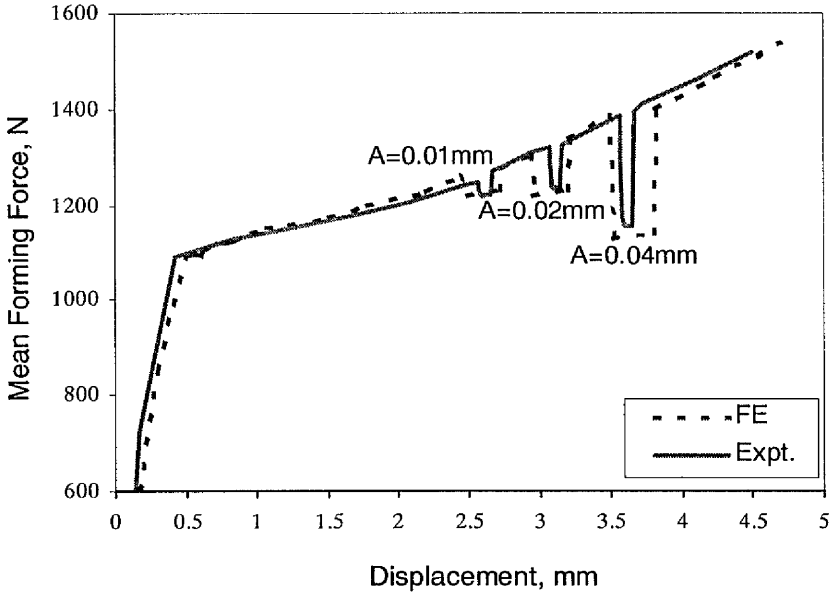

(a)

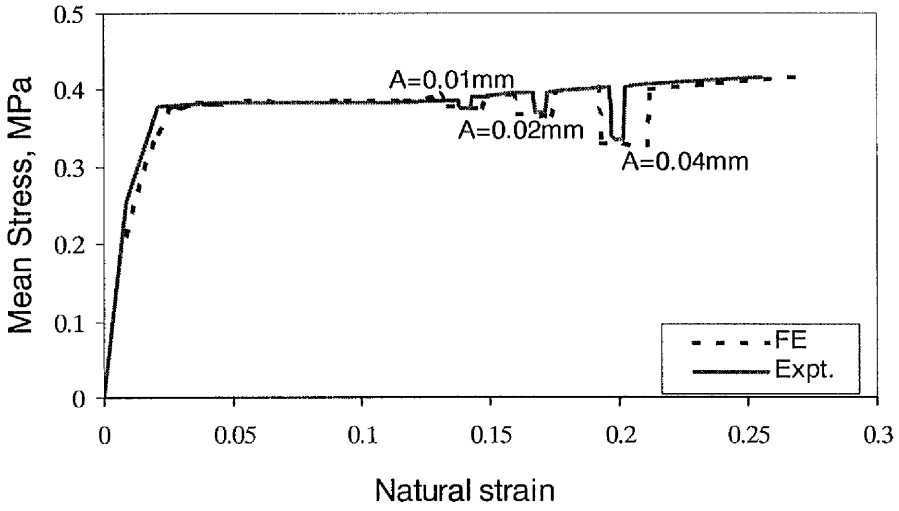

(b)

Figure 4.11 The influence of vibration amplitudes of 0.01 mm, 0.02 mm and 0.04 mm and frequency 20 Hz on the measured (a) compressive load–displacement and (b) mean true stress-strain relationships obtained by compressing a D_0 = 60 mm specimen under a no-slip boundary condition.

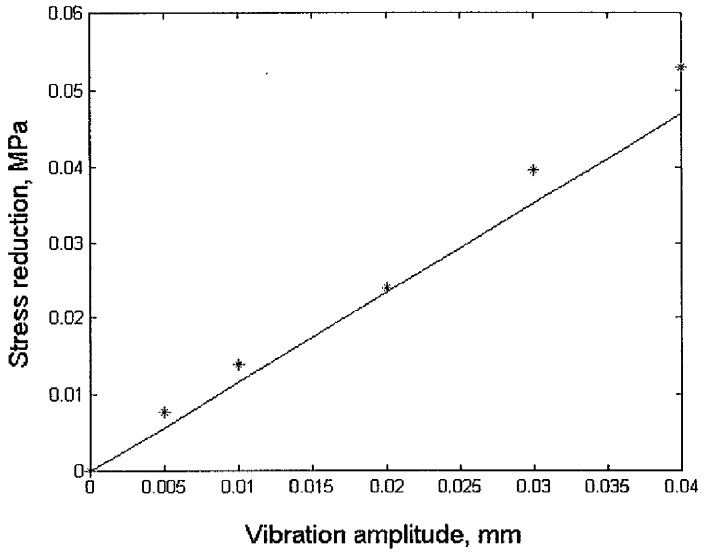

Figure 4.12 Reduction in mean stress as a function of vibration amplitude, obtained from theoretical (—) and experimental (*) data for $D_0 = 60$ mm specimens under no-slip boundary condition.

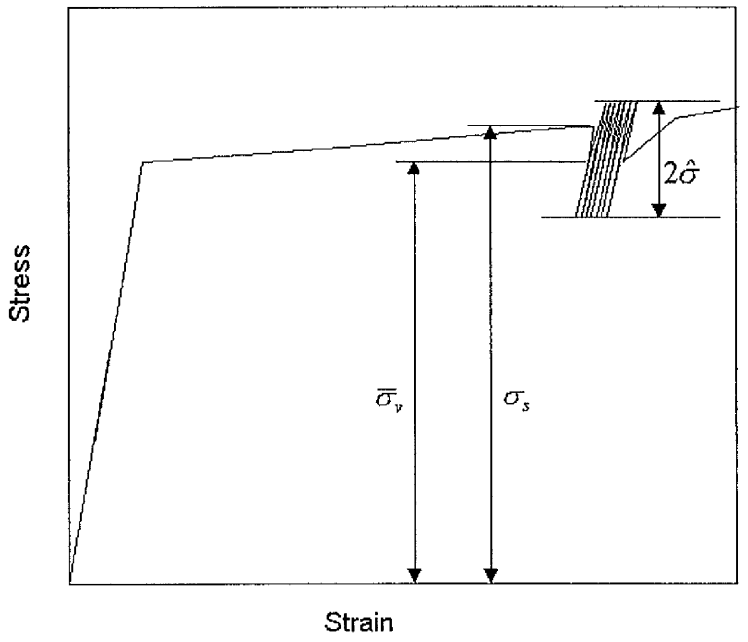

Figure 4.13 Stress-strain curve for general strain rate dependent material if an oscillatory load is superimposed on the static load.

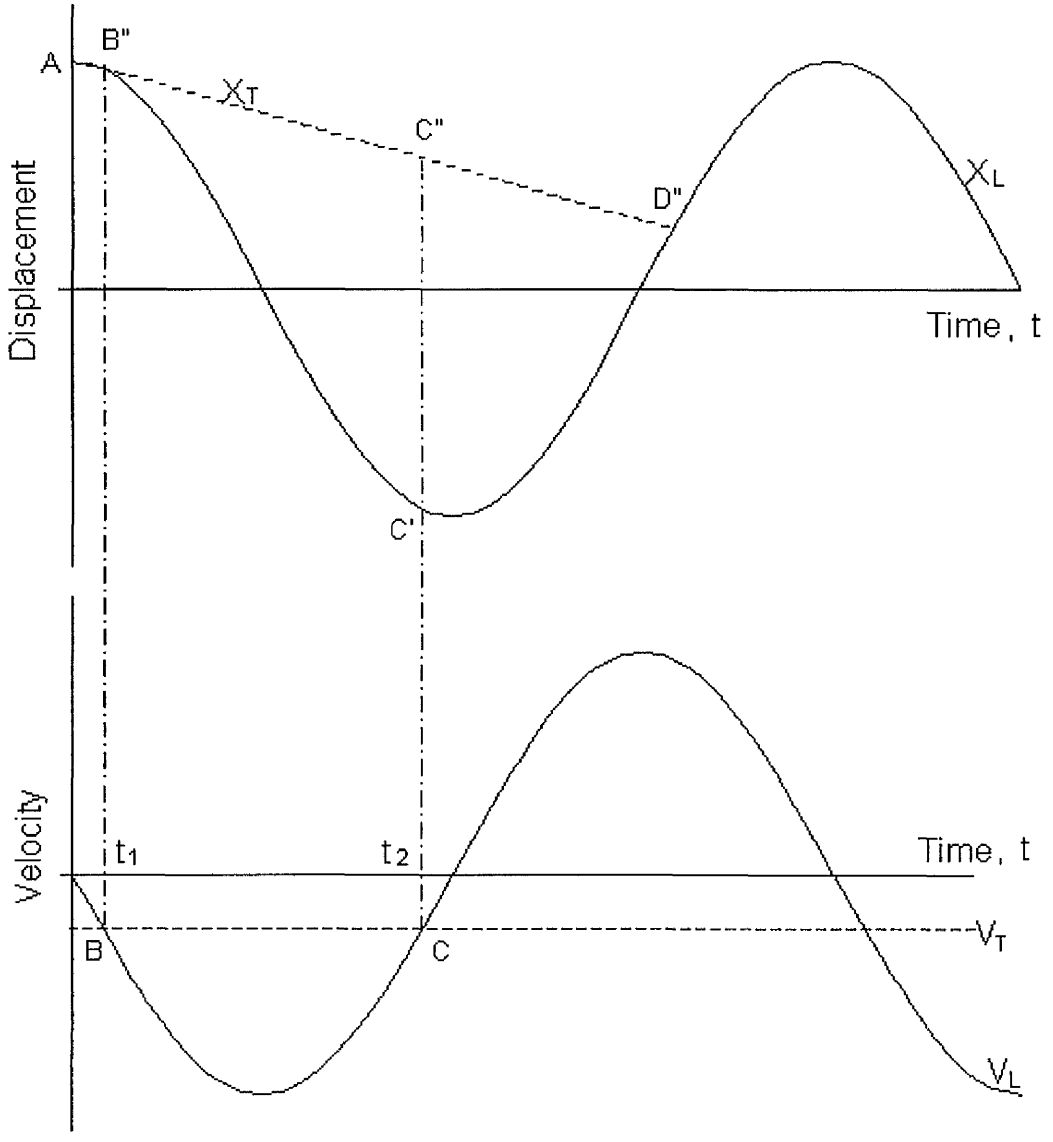

Figure 4.14 Displacement and Velocity diagrams for oscillatory upsetting.

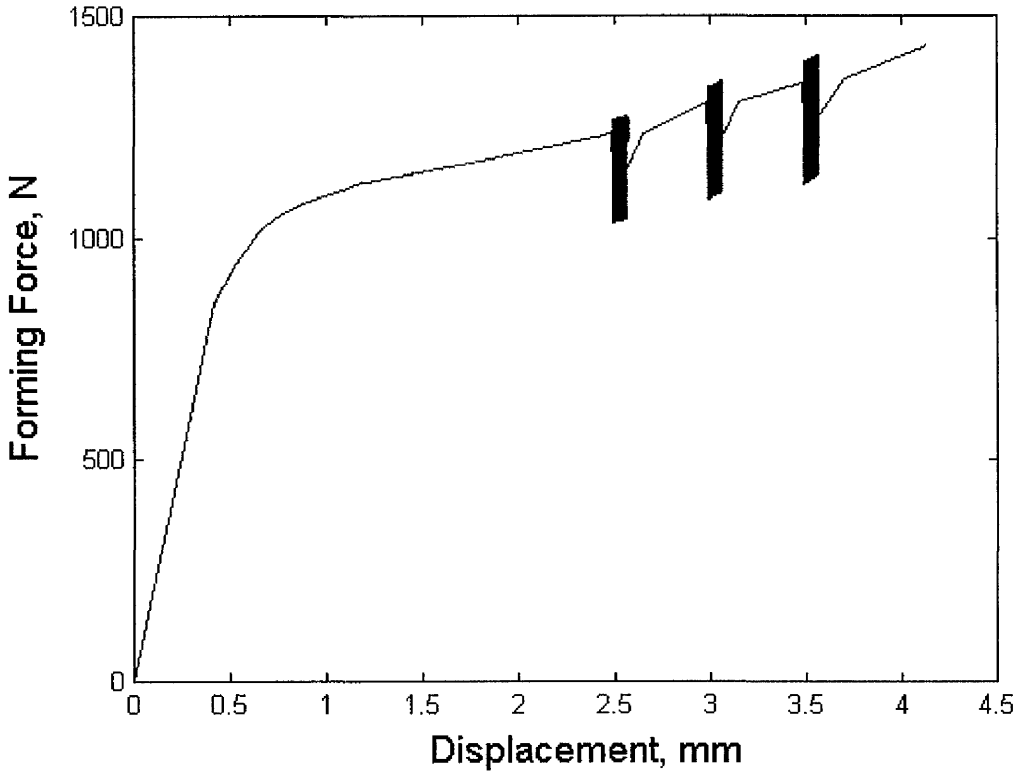

Figure 4.15 Force–displacement data for $D_0 = 60$ mm Plasticine sample obtained from experimental measurement under no-slip boundary condition.

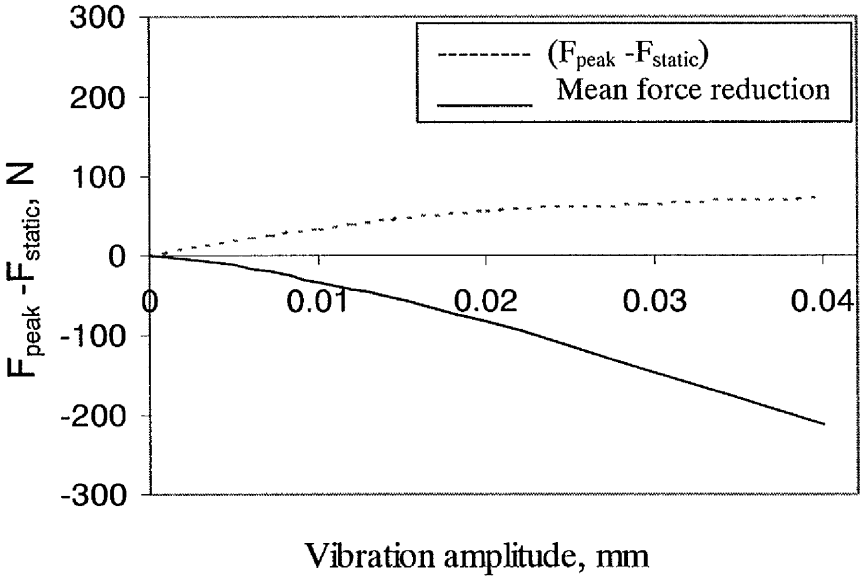

Figure 4.16 F_{peak} -F_{static} as a function of vibration amplitude during oscillatory loading at 10 Hz under a no-slip boundary condition.

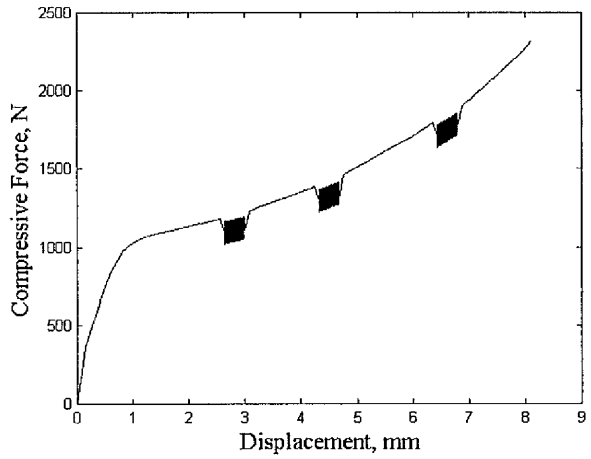

Figure 4.17 Measured force-displacement for upsetting a D_0 = 60 mm specimen under static-oscillatory loading with a lubricated boundary condition.

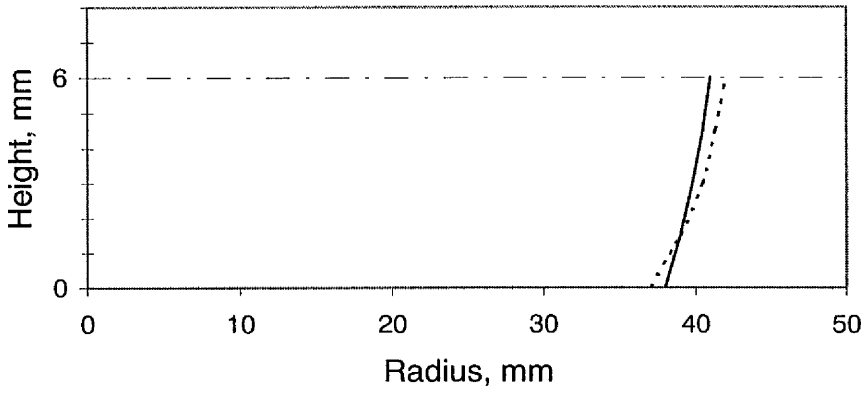

Figure 4.18 When superimposed vibration is applied during upsetting, a reduced specimen barrelling profile (—) observed for D_0 = 60 mm after 8 mm reduction in height, compared with the profile under static loading only (---).

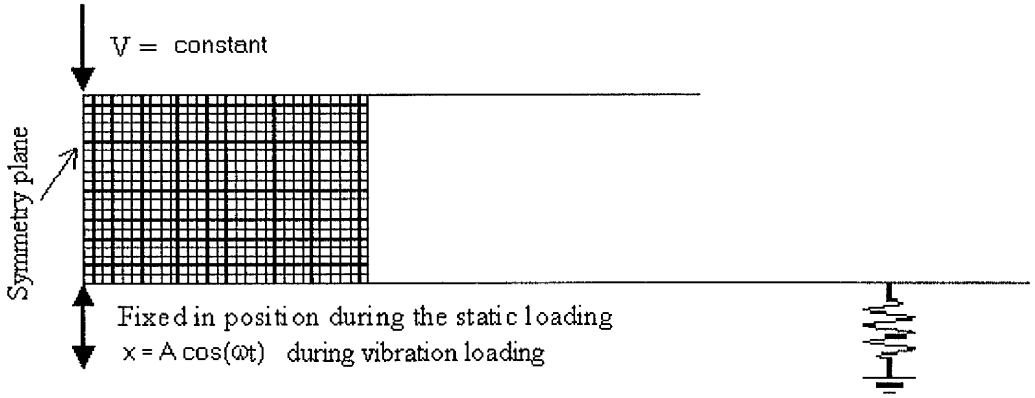

Figure 4.19 The finite element mesh for simulation of the upsetting process.

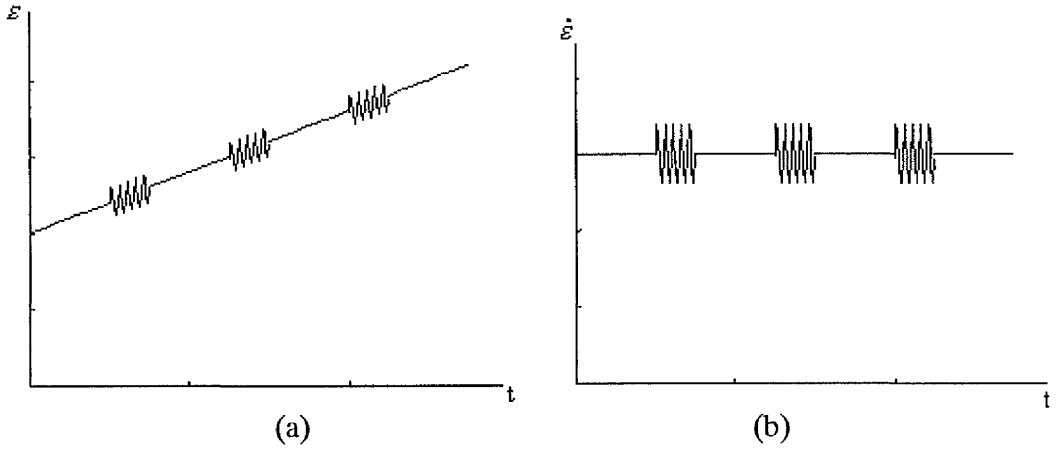

Figure 4.20 (a) Computed strain history and (b) strain rate history during oscillatory upsetting.

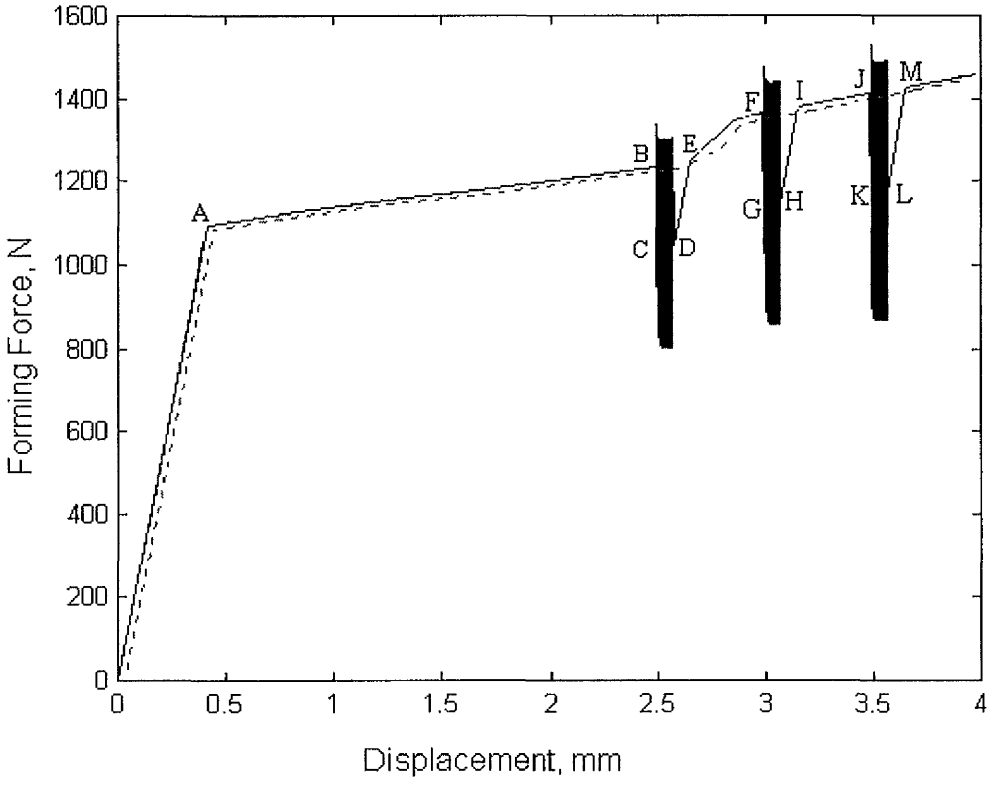

Figure 4.21 Force-displacement data under static-oscillatory loading with amplitude 20 μm and frequency 10Hz.

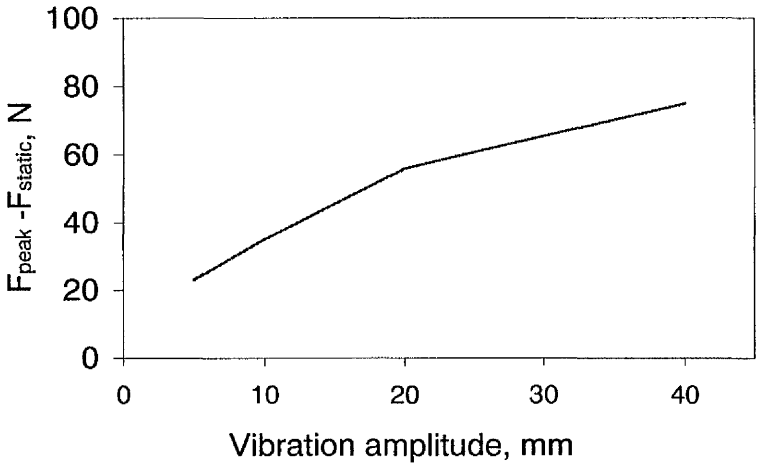

Figure 4.22 $F_{peak} - F_{static}$ as a function of vibration amplitude, predicted by finite element model for oscillatory upsetting at 10 Hz.

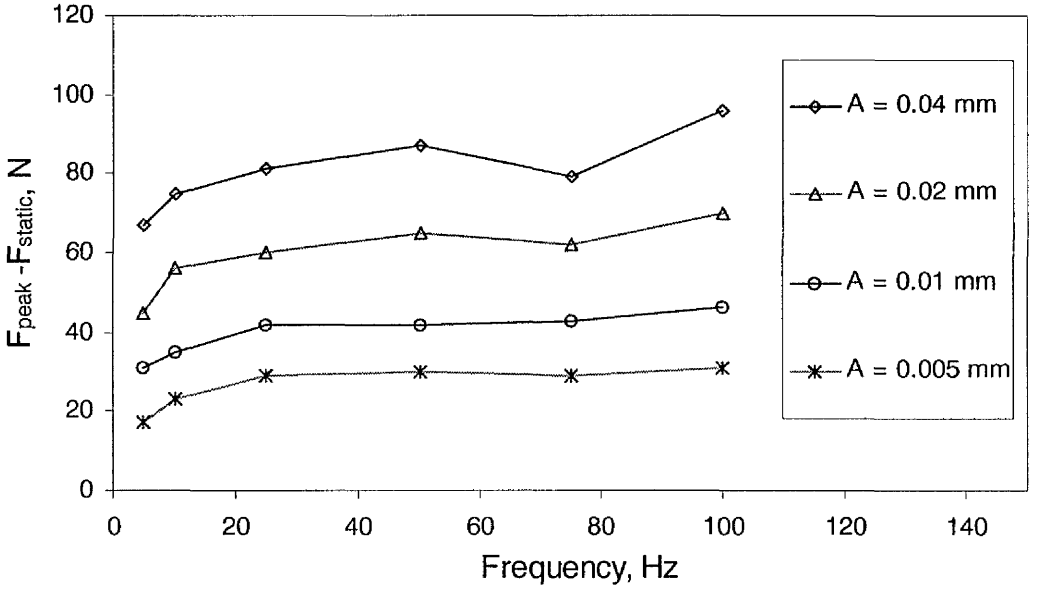

Figure 4.23 $F_{peak} - F_{static}$ as a function of vibration frequency predicted by finite element model for oscillatory upsetting at different amplitudes.

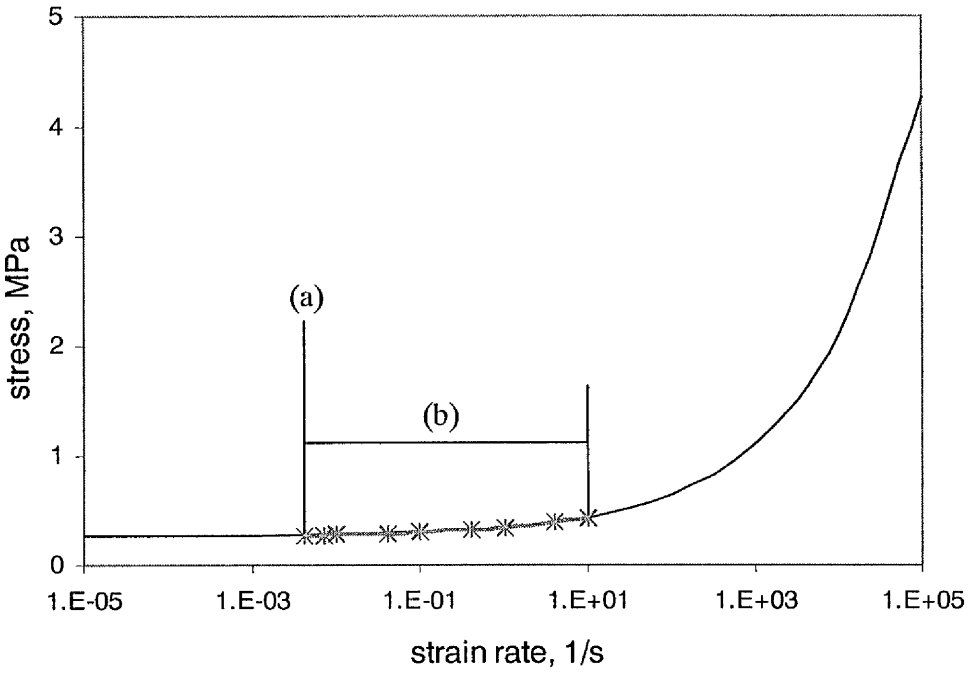

Figure 4.24 Stress-strain rate curve for Plasticine. (a) Strain rate without superimposed vibration (b) strain rate range under superimposed vibration.

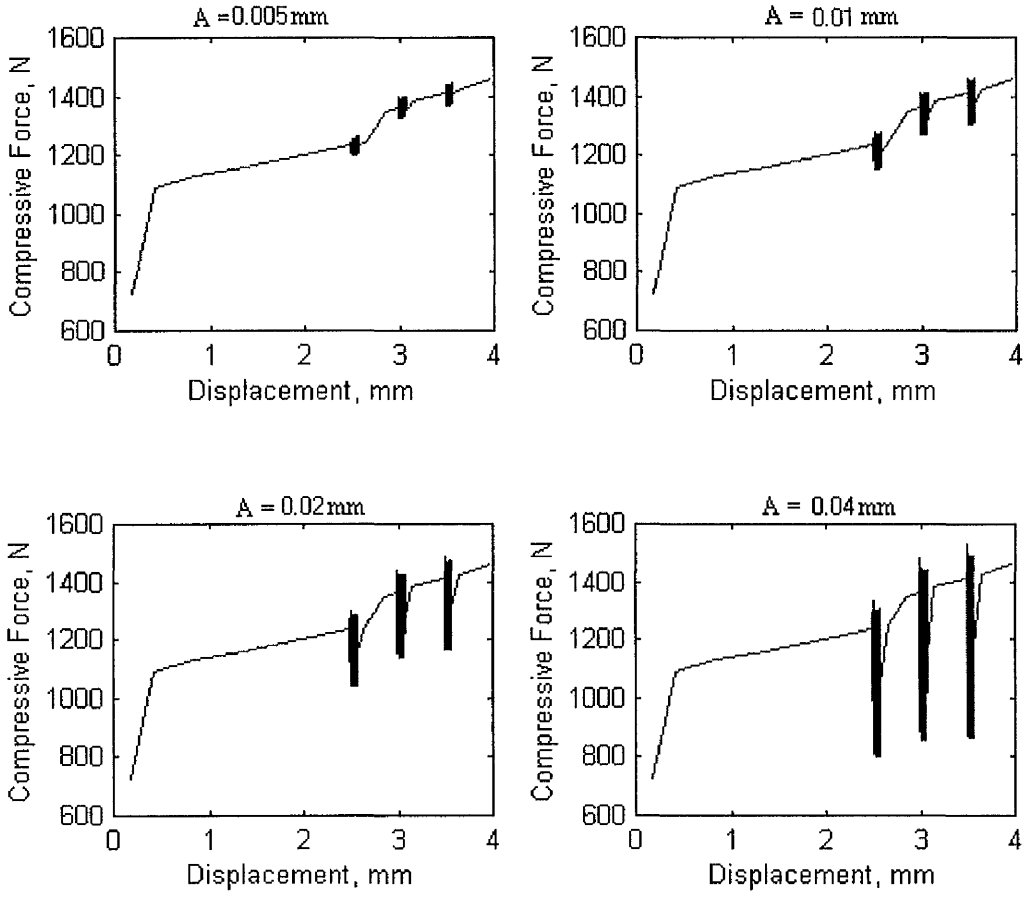

Figure 4.25 Forming force-displacement curves for a Plasticine specimen subject to oscillatory loading at 4 different vibration amplitudes and frequency of 10Hz.

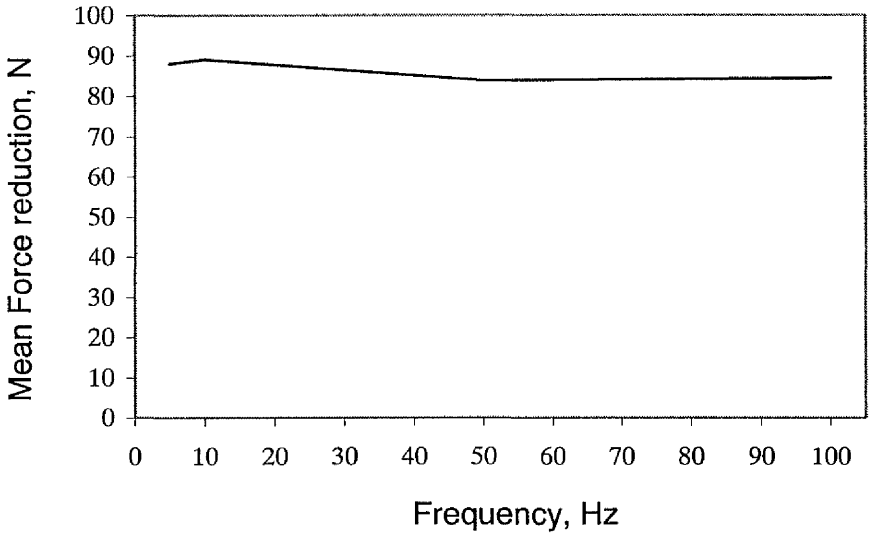

Figure 4.26 Force reduction in relation to the frequency of vibration loading with amplitude of 20 μm.

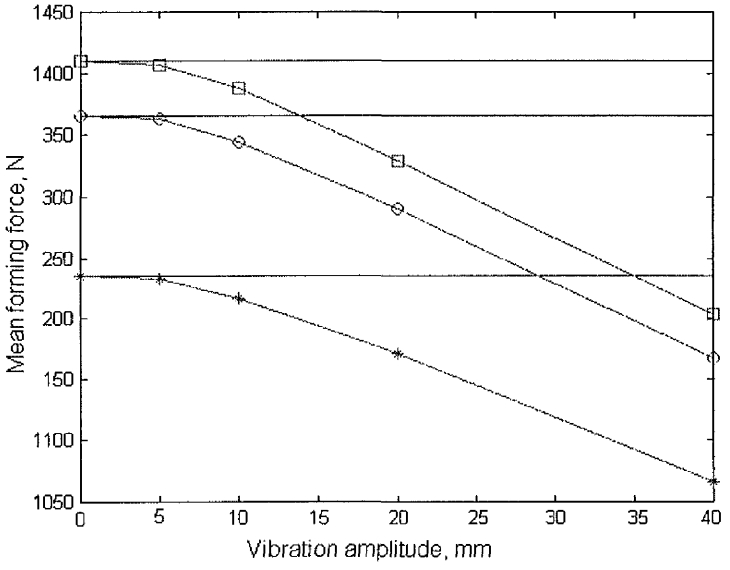

Figure 4.27 Forming force vs. vibration amplitude for true strains of 0.142 (-*-), 0.176 (-o-) and 0.211 (-□-) under no-slip boundary condition. The horizontal straight lines represent static loading only.

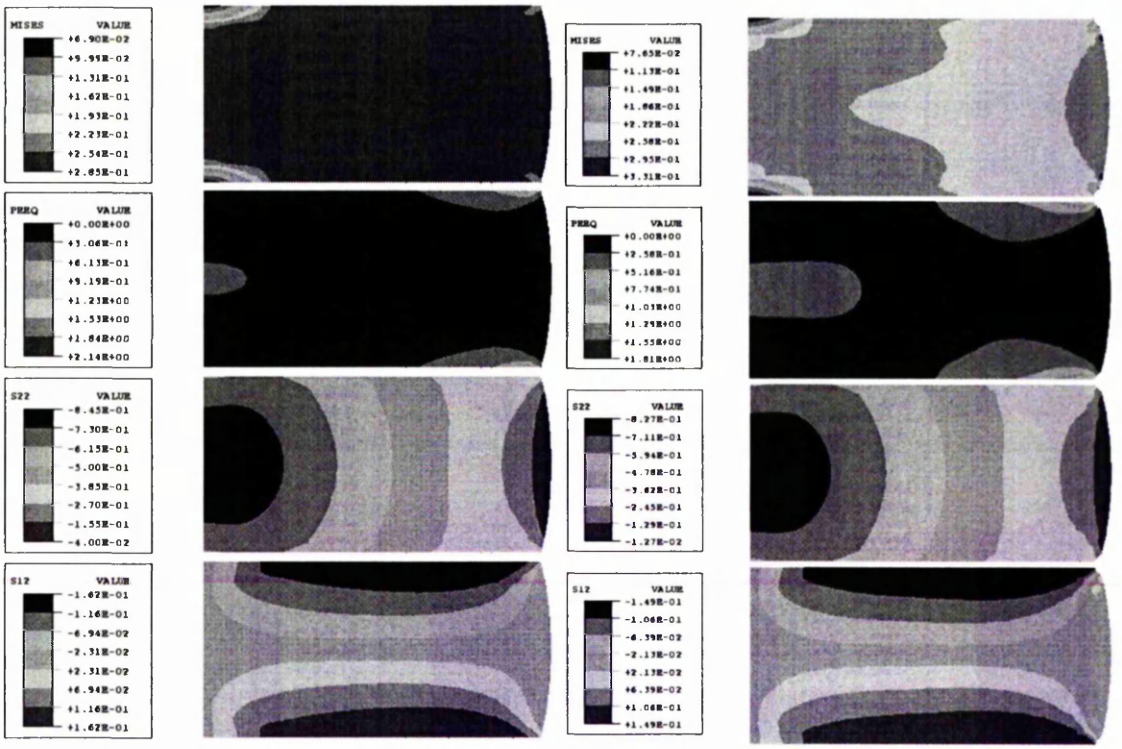

(a) (b)

Figure 4.28 Contours of effective stress, plastic strain, axial stress and shear stress at 17 % reduction in height of the specimen, (a) without vibration, (b) after superimposed vibration of 20 μm at 10 Hz.

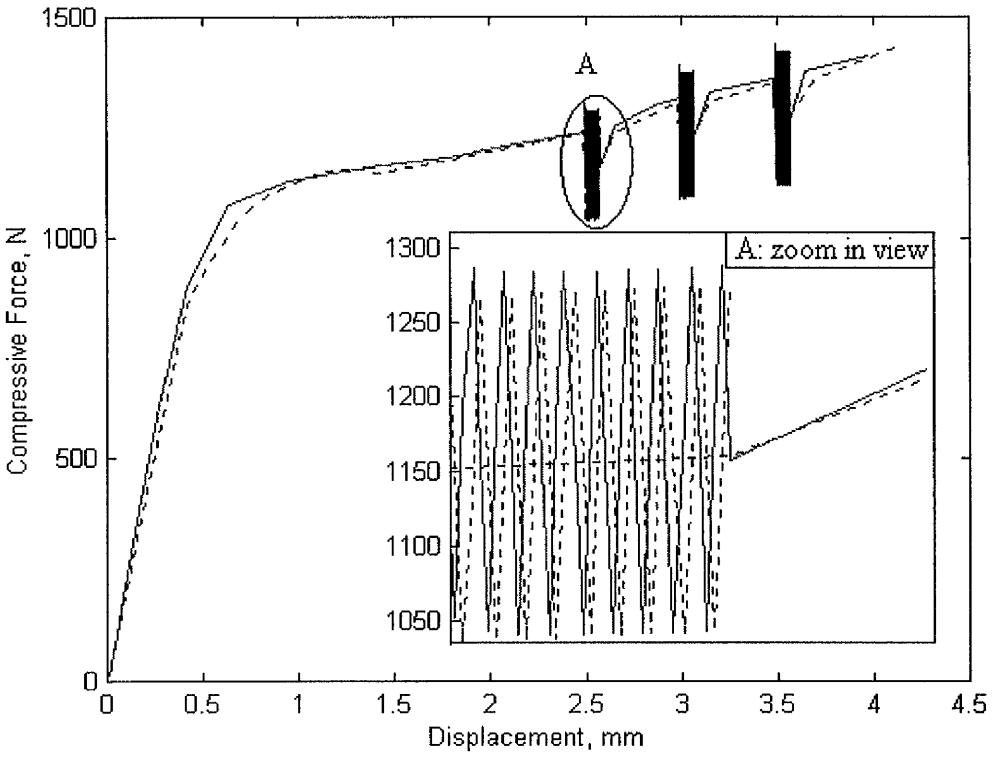

Figure 4.29 Force–displacement data for D_0 = 60 mm Plasticine specimen obtained from FE simulation (—) and experimental measurement (---), under no-slip boundary conditions.

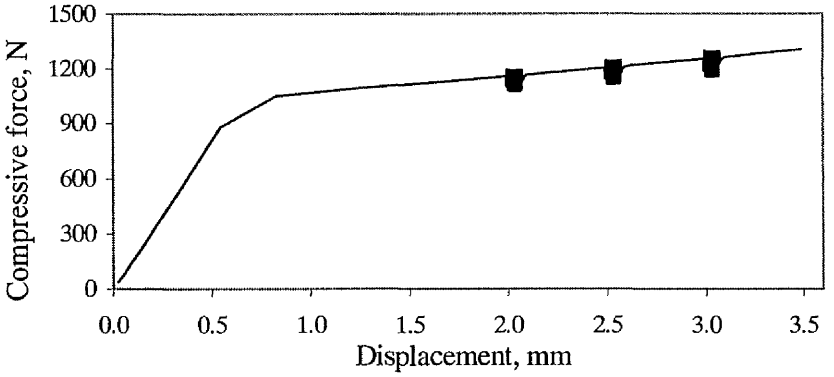

(a)

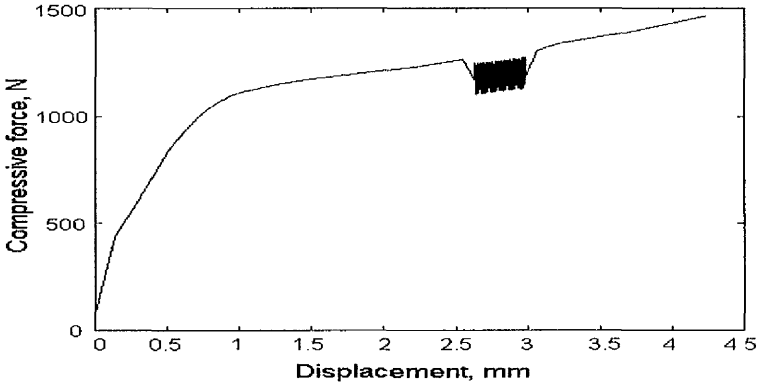

(b)

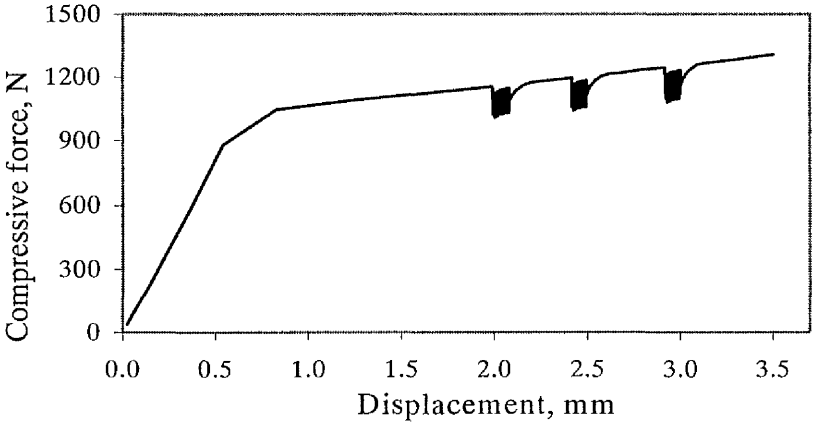

(c)

Figure 4.30 Force-displacement relationship obtained from (a) initial FE model, (b) experiment and (c) updated FE model for upsetting a D_0 = 60 mm specimen under static-oscillatory loading with a lubricated wall boundary condition.

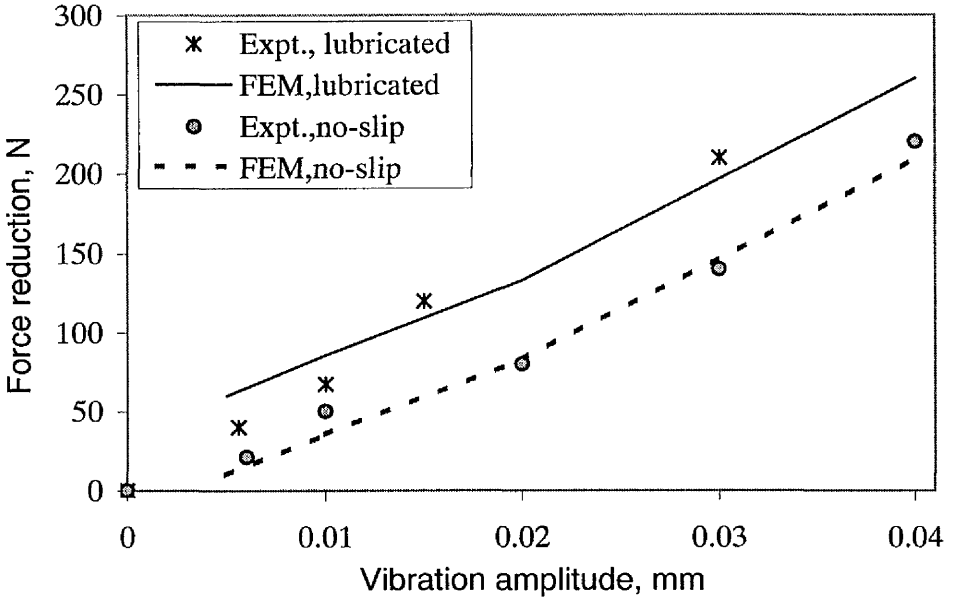

Figure 4.31 Finite element simulation and experimental measurements showing force reduction as a function of vibration amplitude with frequency of 20 Hz for upsetting D_0 = 60 mm specimens under no-slip and lubricated boundary conditions.

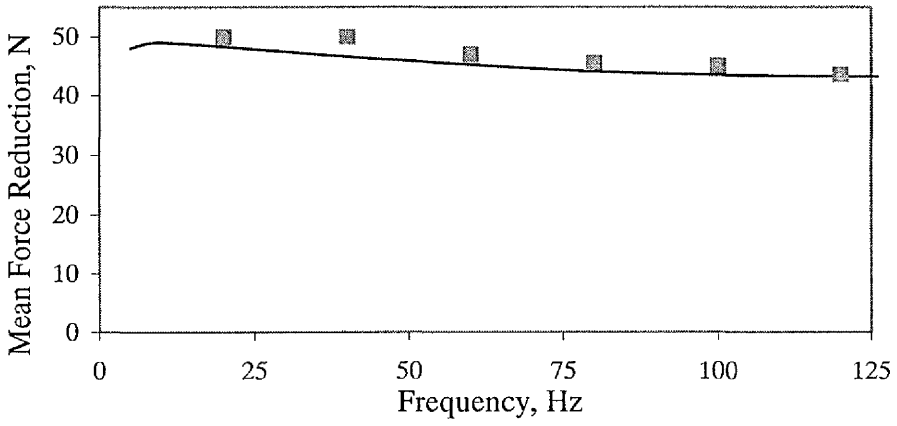

Figure 4.32 Force reduction in relation to the frequency of the oscillatory load with a die amplitude of 10 μm under no-slip boundary conditions, obtained from FE (—) and experimental (▪) results for D_0 = 40 mm specimens.

CHAPTER 5

APPLICATION OF OSCILLATION TO INDENTATION

The first part of this chapter describes an experimental and analytical study carried out to characterise the material properties of the model material, Plasticine, from spherical and conical indentation measurements. An analytical relationship is derived based on the widely used Box-Cox transformation for curve fitting and the Oliver and Pharr procedure for extracting the required material characteristics and minimising the influence of the error inherent in compliance methods.

The second part describes a series of axisymmetric indentation simulations carried out for Plasticine, using the finite element method in order to gain insight into the bulk mechanical flow of the material and the interface frictional characteristics for rigid spherical indenters. Experiments were conducted to obtain selected data as a basis for successful validations of the numerical simulations. Subsequently, a validated study of superimposed vibration loading on standard indentation measurements is described, which investigates the effect on interfacial conditions. Results show that the reduction in indentation load by superimposed oscillations may be explained by a combination of stress superposition and friction reduction.

5.1 Introduction

In this study, the benefits of superimposed oscillations on the bulk mechanical flow and interface frictional characteristics for a model elasto-viscoplastic material

are investigated by adopting indentation testing as a standard method which can be readily adapted for practical studies of the oscillation effects.

Indentation tests are a convenient means of assessing several mechanical properties of solids as they provide a simple and objective test method using small volume specimens. In the traditional hardness test, a diamond indenter is pressed into the surface of a solid specimen with a prescribed load, P, and either the depth of penetration, d, is measured or a characteristic length of the indent such as the contact radius, a. Various shapes of indenter may be used in practice. The most common geometries are spherical (Brinell test), conical (Rockwell test) and a rectangular pyramid (Vickers test). Indentation provides a simple and non-destructive means of assessing the mechanical properties of the material. Although the test is easy to perform, an interpretation in terms of the resulting stress-strain relationship is not straightforward due to the complex strain field produced by the indentation process.

The pioneering work on interpreting the results of indentation procedures was carried out by Tabor [75] who studied the indentation of a number of metals deformed by hardened spherical indenters. A similar study was subsequently undertaken by Stillwell and Tabor [76] to examine the behaviour of conical indenters. One particularly important observation from these studies concerns the shape of the hardness impression after the indenter is unloaded and the material recovers elastically. Tabor also used these results to show that the shape of the entire unloading curve and the total amount of recovered displacement can be accurately related to the elastic modulus and the size of the contact impression for both spherical and conical indenters.

The general response of an elasto-plastic material to indentation is governed by the ratio of the imposed strain to the yield strain of the material, $(E/\sigma_0)\ tan\beta$, where β is the angle of inclination of the indenter to the sample surface, σ_0 and E are the

yield stress and elastic's modulus respectively. For $2 < (E/\sigma_0)\ tan\beta < 50$, the response is elasto-plastic [77]. Plastic deformation is initiated in a small contained region beneath the centre of the indenter at a pressure *ca.* $1.1\sigma_0$ and this region expands with increasing values of $(E/\sigma_0)\ tan\beta$. With cylindrical or spherical indenters this expansion is brought about by an increase in load. When the mean contact pressure, p_m, has increased to about $2.85\sigma_0$, full plastic flow allows the contact radius to grow at a rate sufficient to maintain a constant value of p_m/σ_0, in the manner suggested by rigid-plastic theory. Viscoplastic materials appear to follow a similar pattern, although the relationship between the load and the contact radius is modified once plastic flow has fully developed. Unloading during this stage results in a permanent residual depression with a depth that depends on the maximum applied load. Tabor [75] has shown that the radius of the indent at the surface of a specimen does not change significantly during unloading.

Interest in load and displacement sensing indentation testing began in the early 1970's. For the contact compliance method, in which the reaction force of the indenter is measured as a function of an imposed displacement, the result is a set of loading and unloading curves. For an elasto-viscoplastic response, the unloading curve is elastic but the loading curve contains an irreversible viscoplastic component. The relationships between the applied force and the depth of indentation as a function of the indenter geometry and the effective elastic modulus are described in the next section as a basis for obtaining the elastic modulus from the unloading curves. Methods for independently estimating the contact area from the indenter shape function are then used to calculate the hardness or the mean pressure over the circle of contact. In recent years, depth sensing indentation tests have also been used to characterise a wide variety of material properties, such as creep resistance [78], stress relaxation [79], elastic's modulus [80] and subsurface damage [81].

In using indentation to measure the elastic and plastic properties of a material, it is often assumed that contact is frictionless between the indenter and specimen

[80,82]. However, plastic deformation often produces a permanent indent in the form of a cavity, and friction between the face of the indenter and the material significantly influences the mode of deformation and the force of adhesion [83]. Evidence of the effect of friction induced by the wall roughness on the measurement of elastic's modulus and other mechanical properties has been reported [84,85].

Computer simulation offers a fundamental understanding of the indentation process and the capability to predict a detailed material deformation history. In particular, a detailed knowledge of the deformed configurations at any instant during the indentation process can be derived through a combination of experimentation and finite element simulation. However, modelling indentation contact is a complex problem, since the constitutive equations are non-linear and a number of material parameters must be included to describe material behaviour.

This chapter presents a study of the deformation of an incompressible elasto-viscoplastic solid, which is indented by a rigid spherical indenter with a thinly lubricated wall (ca. 20 μm thickness). The effect of the application of an oscillation to the indenter during penetration has been investigated on the basis of measurements of the indentation load as a function of the depth. The emphasis is on the effects of oscillation on the friction induced by the interaction between the rigid spherical indenter and the specimen. A simple Coulombic wall boundary condition is assumed to be imposed along the wall with a friction coefficient, μ. The vibration indentation problem was investigated by both finite element contact techniques using ABAQUS and a new indentation experiment developed to allow the application of a superimposed oscillatory load.

5.2 Static Indentation

This section describes an experimental and analytical study of contact compliance data for Plasticine obtained from spherical and conical indentation measurements.

An analytical model is employed to determine the elastic's modulus and yield stress from the experimental data. The widely used procedure proposed by Oliver and Pharr and the Box-Cox transformation have been adapted in the analytical description of the data to extract the required material characteristic data and minimise the influence of the errors inherent in compliance methods, such as errors involves in the extrapolation, the assumed indenter geometry and the shape of the impression. The material characteristics deduced for Plasticine are shown to be consistent with the values reported in the literature for this material. With the development of computer based numerical modelling techniques, such as finite element methods, it is possible to develop a more detailed understanding of the indentation process and to predict detailed material deformation history. The results of the application of such a method are also described here.

5.2.1 Analysis of the Contact Compliance

The general relationship between the applied load, P, and the penetration depth, h, may be described by [86],

$$P = mh^{N} \tag{5.1}$$

where the constants m and N are geometric and material property factors respectively. At small imposed depths, for a spherical indenter, the response of an elasto-plastic material will be elastic with the index N being equal to 3/2 which corresponds to Hertzian deformation [77]. At indentation depths exceeding the yield strain, the index will be unity, which corresponds to plastic deformation. In the case of a conical indenter, $N = 2$ irrespective of whether the cone angle corresponds to elastic or plastic deformation. For an elasto-viscoplastic material, the index is reduced by a value that is equal to the strain rate index [87].

The experimental parameters needed to determine hardness and modulus are shown in the schematic load-depth curve in figure 5.1. For an elasto-viscoplastic

contact, the characteristics of the unloading curve reflects the elastic response of both the bulk, relatively undeformed material around the region of gross indentation and also the elastic recovery within the plastically deformed indent itself. The former component is predominant in the initial portion of the unloading curve, which is approximately linear, and the latter contribution is manifested towards the final part of the unloading curve. This latter portion is remarkably non-linear in its character. As a consequence, neither the depth of the penetration at the maximum load, h_{max}, nor the residual depth of penetration, h_r, provide directly a means of determining the area of the plastically deformed contact region. If the depth of penetration, corresponding to the elastic recovery of the bulk material around the indent, is extracted from the value of h_{max}, then the remainder, h_p, may now be used to define the geometry of the plastic indentation. The area of the plastically deformed contact zone may be deduced from the computed numerical value of h_p when the geometry of the indenter is known or assumed (Loubet *et al.* [88]). Figure 5.1 also shows the depth zero error, h_o, which is a significant source of uncertainty in the application of the compliance method.

The initial gradient of the unloading curve, defines the contact stiffness, S, and is given by [80],

$$\frac{dP}{dh} = S = \frac{2}{\sqrt{\pi}} E_r \sqrt{A} \tag{5.2}$$

where A is the contact area projected on the original surface. This projected contact area is distinguished from the apparent area of contact A_{max}, which corresponds to the value computed from the total depth of penetration, h_{max}.

The parameter E_r is the reduced modulus which is defined by the following relationship,

$$\frac{1}{E_r} = \frac{\left(1-\upsilon^2\right)}{E} + \frac{\left(1-\upsilon_I^2\right)}{E_I} \tag{5.3}$$

where E and υ are the elastic's modulus and Poisson's ratio for the specimen and E_I and υ_I are the elastic's modulus and Poisson's ratio for the indenter. By measuring the initial unloading stiffness and assuming that the contact area is equal to the measured area of the hardness impression, the modulus can thus be derived.

In addition to the modulus, the data obtained using this depth sensing method can be used to determine the hardness. The hardness, H, is defined as

$$H = \frac{P_{\max}}{A} \tag{5.4}$$

where P_{max} is the indentation load corresponding to the projected contact area A.

The equations reveal some difficulties associated with the extraction of the material properties from the experimental compliance data. Apart from the obvious effect of the accuracy of the transducers used for the measurement of P and h, other factors which have a considerable influence on the measured compliance are the accuracy of the geometry of the indenter, surface profile of the impression, and the ambiguity in the extrapolation procedure used to describe the linear part of unloading curve. Therefore, the actual geometry of contact and consequent changes in the $P(h)$ relationship need to be modelled more closely for an unequivocal extraction of h_p and S, and thus of the property information.

The effective indenter angle generally does not remain constant with the axial length due to manufacturing tolerances. This error increases rapidly with the semi-

included indenter angle, θ, due to a $tan\theta$ term which defines the imposed strain. The simple tip defect parameter modifies the expected $A(h)$ and $P(h)$ relationships of the indenter, leading to an underestimate of $A(h)$ when the presence of this type of defect is neglected. The presence of this tip defect also results in a simple shift of the effective zero of the compliance curve assumed for the experiment. This generic error may be corrected by using the directly measured value of tip defect as a first order correction, then it may be simply added to the value of h_p and used in a first-order model of the contact geometry.

Zero point of the load-depth data set is defined as $P = 0$ at $h = 0$, but it is determined experimentally by a discernible and subjective change in the force signal as the indenter approaches the test surface at a constant closing velocity. It may be noted that this type of uncertainty generally overestimates the value of h attributed to the corresponding value of P at the chosen zero point. Figure 5.2 shows the nature of the deformation under load. In general, indentation may result in sink-in or pile-up of surface profile, depending on the mechanical properties of the material. The sink-in or pile-up of surface profile can cause difficulties in estimating the contact depth or area.

The associated errors due to the uncertainties of the zero point, the tip defect and the ambiguity of assignment of the linear extrapolation may be greatly minimised by the adoption of the Box-Cox transformation curve-fitting procedure [89] for the experimental compliance data, from which the various values of h and the slopes may be readily obtained. The general $P(h)$ relationship is then obtained as

$$P_1 = m_1(h - h_0)^{n_1}, \quad \text{for the loading curve} \tag{5.5a}$$

$$P_2 = m_2(h - h_r)^{n_2}, \quad \text{for the unloading curve} \tag{5.5b}$$

where h_0 and h_r denote the error or residual values of h in the loading and unloading curves respectively. This method and its application to the analysis of the contact compliance data has been described in detail by Briscoe and Sebastian [82], and a brief account of the method is given in Appendix B. The major advantage of this method is that the computed values of m and n are independent of the magnitude of the zero error and it is possible to derive these value accurately.

We now consider the effects of pile-up of the surface profile on estimating the contact depth or area under load in indentation. Based on the procedure suggested by Oliver and Pharr [80] for estimating the contact depth h_p, from the initial unloading slope, an expression for h_p at the indenter displacement h_{max} can be developed as

$$h_p = h_{\max} - \frac{\xi P_{\max}}{S} \tag{5.6}$$

where P_{max} and S are the respective load at the indenter displacement depth h_{max} and initial slope of the unloading curve respectively. $\xi = 0.72$ for a conical indenter and $\xi = 0.75$ for the spherical indenter [80].

Substituting for P_{max} derived from equation (5.5b), and the slope derived from equation (5.5b), $n_2 m_2 (h_{\max} - h_r)^{(n_2-1)}$, and rearranging equation (5.6) gives

$$h_p = (1 - \frac{\xi}{n_2}) h_{\max} + \frac{\xi}{n_2} h_r \tag{5.7}$$

The contact radius, a, corresponding to an elastic deformation may be obtained as:

$$a = h_p \tan\theta, \qquad \text{for a conical indenter;} \tag{5.8a}$$

$$a = \sqrt{2Rh_p - h_p^2}, \text{ for a spherical indenter,} \tag{5.8b}$$

where θ is the semi-included angle for the conical indenter and R is the radius of the spherical indenter. Since the depth of indentation is large compared to the tip defect, δ, of the conical indenter for all the experiments described in this study, the conical indenters are assumed to be perfect cones and no partial compensation for this type of tip defect is included in the computed value of h_0. The projected contact area may then be obtained as $A = \pi a^2$.

The hardness H and elastic modulus are computed using equations (5.4) and (5.2) respectively.

5.2.2 Conical and Spherical Indentation Experiments

For the indentation studies, 100 mm cubic blocks of Plasticine were prepared and aged for 24 hours at 21°C, as described in Chapter 3. The indenter was lubricated with a thin layer of commercial silicon grease, which has proved to be an effective lubricant in the compressive deformation of Plasticine.

The conical and spherical indenters were made from stainless steel with a polished surface. A range of semi-included angles of 30°, 45°, 60° and 75° with a depth of 10 mm were employed for conical indenters. The radius of the spherical indenters were 2, 3, 5 and 10 mm. The tip defects of conical and spherical indenters were measured using a microscope, and the results are listed in table 5.2.

The indenters were attached to a compression load cell of a mechanical testing machine (LLOYD) and then indented to a depth of 1-2 mm (depending on the size of the indenter) into the Plasticine specimen. The reaction force, P, and the depth of indentation, h, were recorded during loading and unloading of the sample. The indenters were loaded into the specimen with a constant velocity of 1 mm/min, and reversed at the same velocity without any significant dwell time at the maximum depth of penetration. The data were subjected to the curve-fitting procedure described previously.

Figures 5.3 and 5.4 show the force-displacement curves obtained from the conical and spherical indentation tests respectively. Table 5.1 provides the parameters of the Box-Cox type of curves fitted to the data for a maximum depth of 1-2 mm. The values of h_0 indicate the errors in the experimentation, in particular the location of the zero point. When the depth of indentation is large compared to the tip defect, δ, the value of h_0 is the sum of the defect length, δ, and the intrinsic zero error in the measurement of h.

The parameters of the Box-Cox type of the loading and unloading curves is listed in table 5.1 for cones and spheres. The indices of the loading curves are dependent on the geometry of the indenter. The mean value of n_1 is 1.73 for the cones which is less than the expected value of 2 for either elastic or plastic deformation, as discussed previously. In the case of the spherical indenters, n_1 is about unity for the three with the smaller radii, which suggests plastic deformation, and it is about 1.5 for the largest indenters and this is consistent with elastic deformation. For a viscoplastic material like plasticine, it is important to consider the effect of indentation strain rate during loading, as discussed previously. The strain rate-hardness relationship is given as [90],

$$H = \eta \dot{\varepsilon}^{n} \tag{5.9}$$

where η is material constant, n is the material flow index, and $\dot{\varepsilon}$ is the strain rate. For indentation with a cone at a constant velocity, V,

$$\dot{\varepsilon} = V\cot(\theta)/h \tag{5.10}$$

From equation (5.4),

$$P = HA = H\pi a^2 \Rightarrow P \propto Hh^{n_1} \tag{5.11}$$

and by incorporating equations (5.9) and (5.10),

$$P \propto \eta\dot{\varepsilon}^n h^{n_1} \Rightarrow P \propto \eta V^n h^{(n_1-n)} \tag{5.12}$$

Thus, the value of n_1 will be reduced from 2 to (2-n). A linear fit of a log-log plot of H as a function of $\dot{\varepsilon}$ obtained from experimental data, gives a flow index $n = 0.34$. Thus the expected loading index (2-n) is 1.66, which is comparable to the mean value of n_1=1.73.

The abstracted zero error, h_0, also listed in table 5.1, results from the combined contributions of experimental uncertainly in the location of the point of the initial contact and the magnitude of the tip defect of the indenters. Since $h_{max} >> \delta$ for these experiments, the fitted curves describe the compliance characteristics of nearly perfect indenters. The data for the cones generally have a negative value of h_0, which is indicative of the influence of the tip defect. This value of h_0 is then added to the computed value of h_p in order to obtain a more appropriate resolution

of material parameters. In the cases of the spheres, which have a better geometrical accuracy, the variation of the value of h_0 is more likely due to the intrinsic uncertainty of the measured zero point, resulting in a random variation. The residual depth of penetration, h_r, which is also subjected to experimental uncertainties similar to those of the zero point, is explicitly given by the parametric description of the unloading curve.

The efficacy of this procedure is shown in figure 5.5, for the computed values of hardness obtained by the various indenters, as a function of the parameters $0.2cot\theta$ and $0.2a/R$ for cones and spheres respectively, which are a measure of the imposed strain (Johnson [83]). The hardness values shown in figure 5.5 were corrected for the tip defect and deformed surface profile according to the procedure set out previously in section 5.2.1.

The experimental results of hardness H with spheres and cones in figure 5.5 for an elasto-plastic material is as expected, following a steady transition from elastic to fully plastic deformation and reaching an asymptotic value [77]. Then, the hardness may be related to the yield stress, σ_0, of the material in simple compression by an expression based on the theory of indentation by Tabor [91], $H = 2.85\sigma_0$. On this basis, using the asymptotic value of hardness in figure 5.5, which represents the fully plastic case, the yield stress is given as 0.28 MPa. This is a close value to the reported value of 0.26 MPa for Plasticine [5,47], but the difference can be accounted for by the sensitivity of Plasticine to batch, colour, temperature and age.

The value of E may also be obtained by direct application of the $P(h)$ relationship, listed in table 5.1, into equation (5.2). Figure 5.6 shows a plot of the elastic's modulus as a function of the imposed strain calculated from the measured partial unloading data. Assuming $\upsilon = 0.49$, the mean value of elastic's modulus is found

to be 16.5 MPa, which compares favourably with the value of 16 MPa obtained from a simple compression test.

5.2.3 Finite Element Simulation

The finite element code ABAQUS was used to model the *P(h)* relationship during conical indentation and test the analytical procedure for the experimental compliance data described previously. The finite element model is illustrated in figure 5.7. The indenter is assumed to be rigid and the surface of the indenter was defined as an analytical rigid surface with a semi-included angle of 30°, which corresponds to a conical indenter. Contact between the indenter and the specimen was assumed to be frictionless. As a consequence of axisymmetric conditions, the material was modelled using a set of axisymmetric solid elements with four nodes, eight degree-of-freedom, quadrilateral cross-section. A fine mesh in the vicinity of the indenter and a gradually coarser mesh in the far field were used to ensure a high degree of numerical accuracy and an accurate representation of a semi-infinite solid. The constitutive behaviour of Plasticine was treated as non-linear elasto-viscoplastic [6], with the material property parameters obtained from the indentation results in the previous section and compression results in Chapter 3. The yield criterion was that of Von Mises. The material properties for the spherical indenter and the Plasticine are listed in table 5.3 assuming isotropic properties for the Plasticine.

The loading and unloading curves were obtained directly from the output of the total reaction force in the normal direction on the rigid indenter as a function of indenter vertical displacement. A comparison of the *P(h)* relationship obtained from the finite element simulation with the experimental results is shown in figure 5.8, using a conical indenter with a semi-included angle of 30°. The results are in agreement. The corresponding surface profile under load, which is shown in figure 5.9, demonstrates the well-known pile-up phenomenon. The results are consistent with experimental observations of Plasticine. The contact radius, a, may be

obtained directly from the simulation, and is found to be a = 0.75 mm for a maximum indentation depth, h_{max}, of 1.95 mm with a conical indenter with semi-included angle of 30°. Agreement is achieved with the value of a = 0.72 mm obtained from the experimental initial unloading slope using the analytical procedure.

5.3 Static and Superimposed Oscillatory Indentation with Spheres

The oscillatory indentation technique is based on a spherical indentation. Typically, the experimental procedure involves moving the indenter into the specimen under a combination of static and vibration loading, and measuring the forces and displacements associated with the indentation process.

5.3.1 Apparatus

The test apparatus is shown in figure 5.10. Four stainless steel spherical indenters with radii of 2, 3, 5 and 10 mm were used in the study. The static indentation force was provided by a LLOYD testing machine, which is capable of controlling the loading velocity at 1 mm/min and providing a maximum load of 100 N. The mechanical vibration is generated by a signal generator in order to provide a specified vibration amplitude at the working surface of the spherical indenter. The vibration load was therefore superimposed on the static load from the LLOYD test machine.

The load recorded by the force transducer on the crosshead is the mean indentation load since the transducer was not capable of monitoring the oscillatory component of the force response. For measuring the superimposed vibration load, a piezo-electric force transducer was mounted between the vibration exciter and indenter. A non-contact laser Doppler vibrometer (LDV), which monitors the velocity of the target surface, was used to measure indenter vibration. The LDV signal was processed to extract vibration displacement, and post-processed using CADA-X3.2 (LMS International) vibration analysis software. The output of the amplitude

measurement from LDV was fed back such that the driving power for the vibrator was controlled to maintain constant vibration amplitude.

5.3.2 Experimental Procedure

The Plasticine used in this study was prepared as described previously. The specimens used in this study were all 40 mm in height and 60 mm in diameter, which is more than an order of magnitude greater than a characteristic indentation dimension such as the contact depth and the contact radius. Thus the material is treated as a semi-infinite solid.

The vibration assisted experiments were conducted using two different loading arrangements as shown in figure 5.11. During each test, the indenter was loaded statically until a specified depth was reached. A vibration load was then superimposed on the static load until vibration amplitude A was reached. After maintaining constant vibration amplitude of A for 30 s, the oscillation was removed. For case 1, the specimen continued to be deformed under static loading until the indentation reached a specified depth appropriate for the sphere radius, at which point the specimen was unloaded. For case 2, the specimen was unloaded when the oscillations were discontinued. A static indentation test was also conducted (case 3 in figure 5.11). Before each test, the surface of the indenter were cleaned and re-lubricated with a thin layer of silicon oil in order to maintain the lubricant condition. The indentation load-depth data were recorded using dedicated software.

5.3.3 Finite Element Simulation

Finite element simulations using ABAQUS have been carried out to model the oscillatory indentation using the zoned mesh refinement shown in figure 5.12 and for sphere radii equal to those used in the experimental study. As a consequence of the axisymmetric conditions, only the right half cross-section of the axisymmetric

plane was modelled. The surface of the indenter was defined using an analytic rigid surface definition since it may be regarded as much stiffer than the Plasticine. The specimen was modelled using a set of 4-noded bilinear axisymmetric quadrilateral elements and an elasto-viscoplastic constitutive relationship [6]. A fine mesh in the vicinity of the indenter and a gradually coarser mesh away from the indenter was used to ensure a sufficiently accurate representation of a semi-infinite solid.

Between the potential contact surfaces, node-to-node type contact was located. The base of the specimen was fixed, while the load was introduced to the top of the rigid sphere segment. The static load was controlled by constant velocity. Vibration of the indenter was introduced by an oscillatory load superimposed on the static load, and was specified by its sinusoidal displacement amplitude and frequency.

The contact algorithm used iterations to satisfy the stress and displacement contact conditions, as illustrated in figure 5.13. The displacement and stress contact conditions for a rigid sphere are:

$$d_j \geq u_i + h_i;\ p_i > 0 \qquad \text{for points inside the contact area}$$

$$d_j < u_i + h_i;\ p_i \leq 0 \qquad \text{for points outside the contact area}$$

where d_j is the sphere approach, u_i is the deformation of the surface points of the specimen, h_i is the initial gap between the bodies at point i and p_i represents the contact pressure at point i. The reaction forces at the nodes of the contact area are proportional to the contact pressure distribution. If the reaction forces at assumed boundary points of the contact area are positive (representing compression), these points are inside the contact area. If the reaction force is negative (representing tension) the point should be outside the contact area. When contact occurs, a Coulombic coefficient of friction equal to 0.2 was specified for the lubricated boundary condition, which is on the basis of the ring compression test data (details

shown in Appendix C). In this way, the contact area was continuously modified during each iteration and the total normal load, P, was calculated.

5.3.4 Results and Discussion

First, the results for the static indentation (case 3) will be described. The variation of load with indentation depth obtained from the numerical solution and experimental results are presented in figure 5.14. It may be seen that there is agreement between the numerical and experimental values. With the aid of the finite element simulations, it is possible to obtain detailed information at any instant of the deformation. The contours of the effective Mises stress and plastic strain are shown in figure 5.15a and b corresponding to indentation depths of 0.15 and 1.5 mm for the spherical indenter of radius of 5 mm. The contour levels (in MPa) are also indicated in the figures. Comparison of figure 5.15a and b correctly shows a growth of the plastic zone due to additional indentation.

A reduction in the static load required to deform the material was observed and predicted numerically in all cases when there was a superimposed oscillation. Experimental results shown in figures 5.16 and 5.17 clearly indicate that any application of superimposed vibration to the indenter always reduces the mean force. After the interval of vibration, indentation deformation is seen to follow an elastic line and return to the non-oscillatory static loading curve for case 1. For case 2, the specimen is unloaded along the static unloading curve. The load-depth relationships during oscillatory indentation for case 1 loading at different vibration amplitudes and a frequency of 4 Hz are shown in figure 5.18. The FE models, which are developed to simulate the superposition effect due to vibration, agree well with the experimental measurements during static loading but, in each case, the mean load reduction measured experimentally during superimposed vibration loading is greater than the FE prediction. This would suggest that friction conditions are improved during oscillatory loading.

Vibration at higher frequencies was also investigated. A finite element solution for the load-depth relationship is shown in figure 5.19a using the procedure described previously for a specimen indented by a sphere of 5 mm radius at a vibration amplitude of 0.03 mm and frequency of 40 Hz. Figure 5.19b and c shows an expanded view of the loading history during the interval of vibration loading. Again, the measured reduction in mean force is greater than the FE prediction. The difference between the finite element simulation and experimental results may be explained by a further reduction in friction achieved under superimposed vibration. The finite element model only simulates the superposition effect due to the vibration. Updating the finite element model by changing the coefficient of friction from 0.2 to 0.01 during the interval of vibration loading allows closer agreement with experimental data to be achieved, as shown in figure 5.19b and c. This result supports the findings of friction condition improvement by vibration as reported in Chapter 4.

The hardening of the material during vibration loading, which can be seen as the over-stress during period A on the FE curve in figure 5.19a, is due to the strain rate dependency of Plasticine during plastic deformation, as described in Chapter 4. It indicates that a reduction in mean force due to superposition alone is not significant, since for a strain rate dependent material the maximum force can be greater than the static force and both mean and minimum force are following paths parallel to the non-oscillatory force-depth curve. The indentation experiments under superimposed vibration loading, in figure 5.20, show both a reduction in the mean force and a maximum force which is less than the static force. The updated FE simulation shown in figure 5.21, which related this reduction in force to the interface friction, brings a close agreement with the experimental results.

For both the FE simulation and experimental study of vibration indentation, the unloading curves remain unaffected for both loading cases 1 and 2 described in figure 5.11. Also, the elastic curve back to the plastic deformation curve upon cessation of oscillation and the following plastic deformation curve for case 1

remains unaffected. Thus it can be deduced that there is no absolute change in the mechanical properties of Plasticine following the application of vibration.

Figure 5.22 illustrates adhesion forces between the contact bodies measured from the load-depth curves during unloading of case 2. It is clear that a tensile force (negative), the force of adhesion, has to be exerted to separate the surfaces. For the higher vibration frequencies (> 40 Hz in the experiment), the adhesion force exhibited about 20 % reduction from the static value for indentation with superimposed vibration. These observations provide strong evidence that interfacial friction is improved by superimposed vibration with a lubricated boundary condition. There is no absolute change observed in adhesion force for case 1 and for case 2 with the lowest experimental frequency of 4Hz.

5.4 Conclusions

An analytical procedure has been proposed which simulates the entire loading and unloading of an elasto-viscoplastic model material, Plasticine, during indentation. A relationship was derived based on the Box-Cox transformation for curve fitting and the Oliver-Pharr procedure for extracting the required material characteristics and minimising the influence of the error inherent in the compliance method.

In this study, the surface profile, caused by indentation in the model material, has been considered. The procedure proposed by Oliver and Pharr for estimating the contact depth is then evaluated systematically. By comparing the contact depth obtained directly from finite-element calculations with that obtained from the initial unloading slope using the analytical procedure, a close correlation was obtained. For the finite element simulation incorporating the material parameters extracted using the analytical procedure, a close agreement is obtained for the $P(h)$ relationship and the deformed surface profile when compared with the experimental observations of conical indentation.

A detailed finite element simulation and experimental study of spherical indentation has also been conducted for the model material, Plasticine. The finite element solution provides details of the displacement, strain and stress history of the specimen during the indentation. These results are in agreement with the experiments conducted under similar boundary and loading conditions.

Introducing vibration in an indentation test, results in a reduction in the mean forming force required to deform the material. The force reduction may be explained by a combination of stress superposition and friction reduction due to vibration. There was no absolute change observed in the mechanical properties of the material following the application of vibration. These results support the findings of the previous study of an upsetting process.

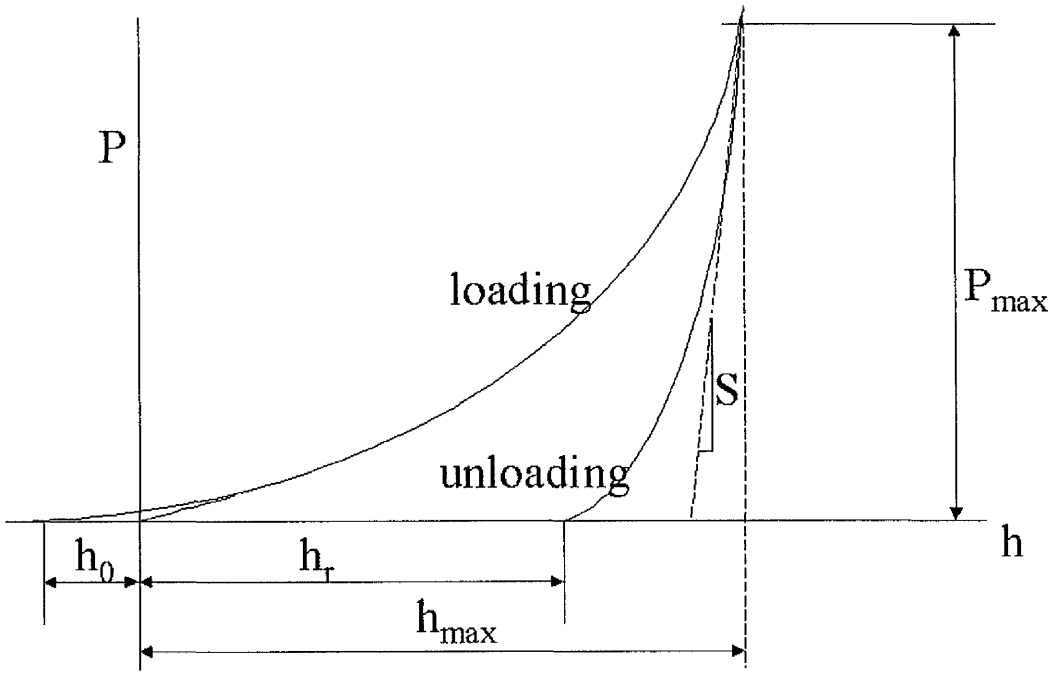

Figure 5.1 Schematic representation of the load as a function of depth for an indentation experiment. The quantities shown are P_{max}, the peak indentation load; h_{max}, the indenter displacement at peak load; h_r, the residual depth of the contact impression after unloading; h_0, the depth zero error and S, the contact stiffness.

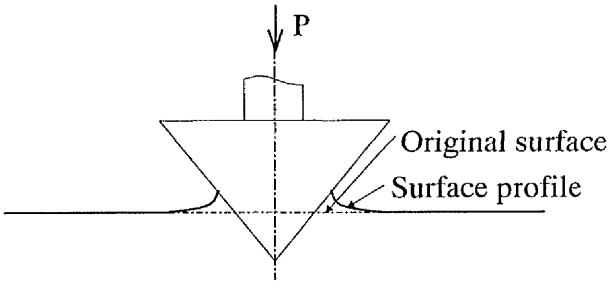

Figure 5.2 Indentation geometry under load.

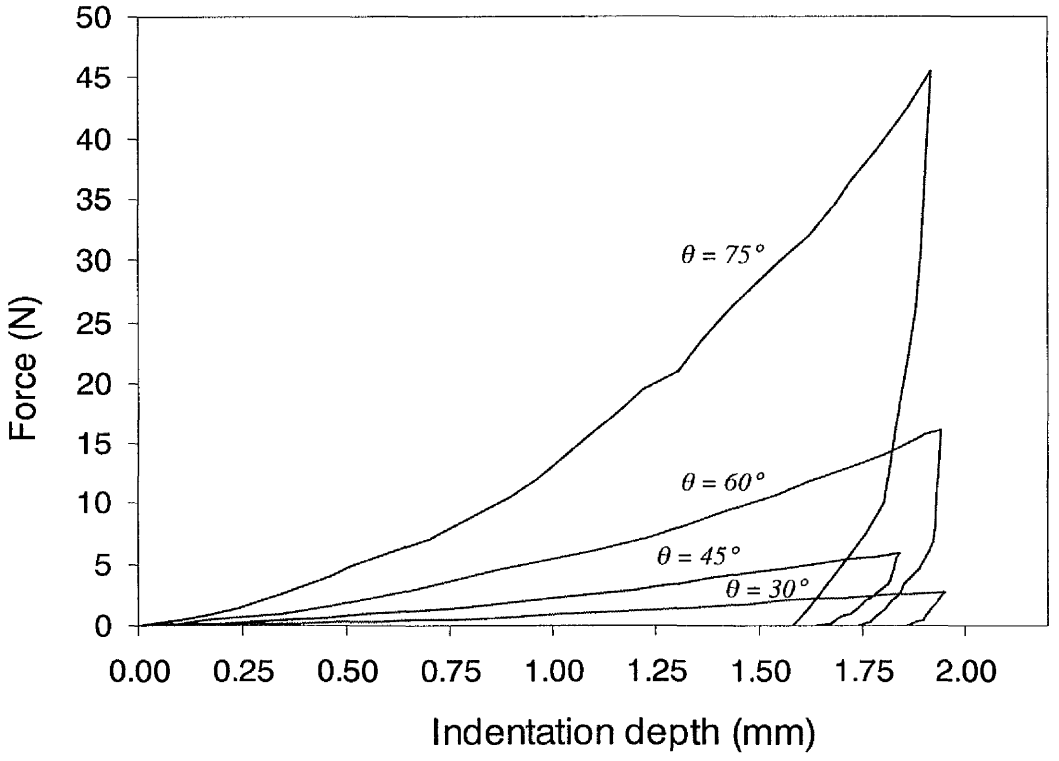

Figure 5.3 Load as a function of displacement for Plasticine indented by cones of various semi-included angles. Each set of data consists of a loading and unloading cycle.

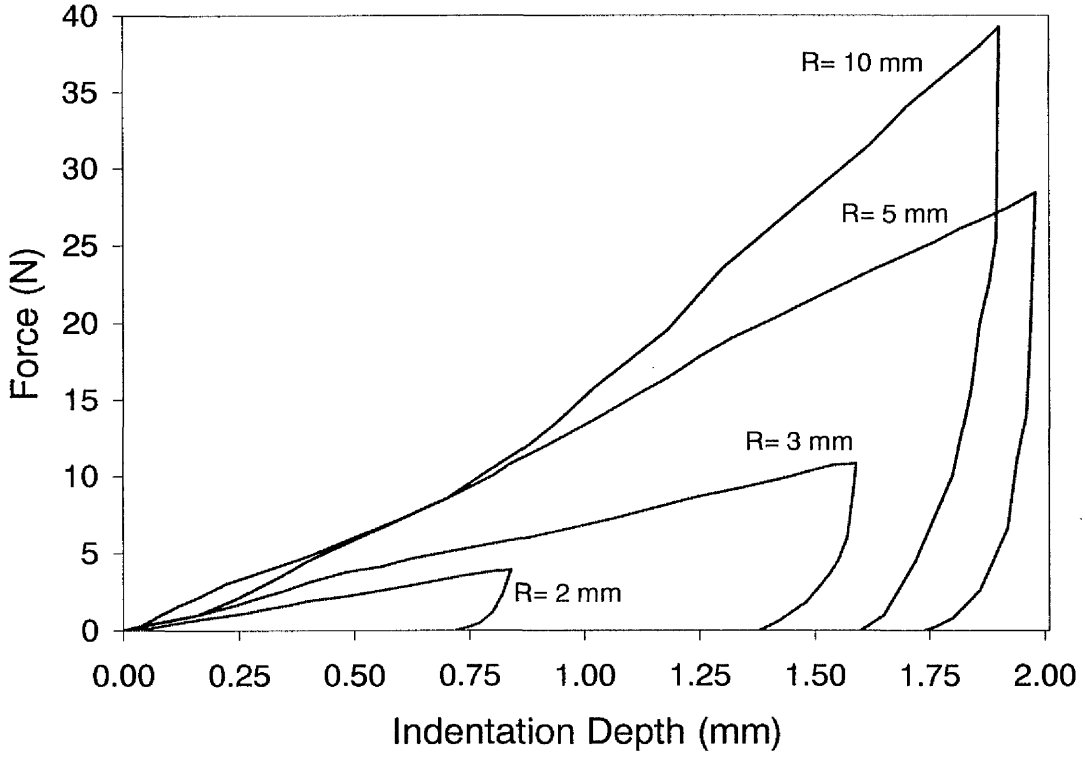

Figure 5.4 Load as a function of displacement for Plasticine indented by spheres of various radii. Each set of data consists of a loading and unloading cycle.

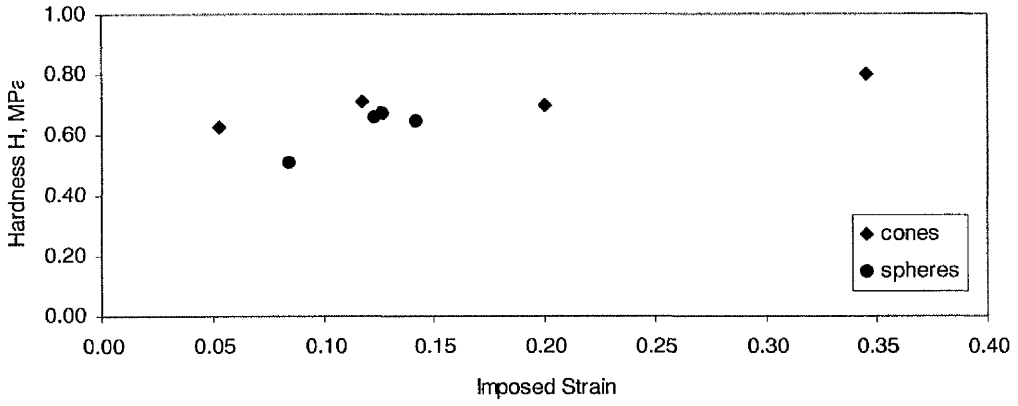

Figure 5.5 Hardness of Plasticine as a function of the imposed strain. Results obtained using spherical and conical indenters.

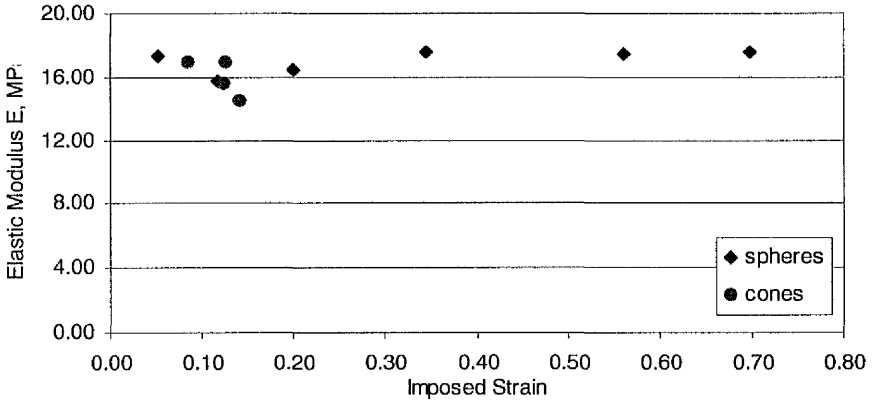

Figure 5.6 Variation of computed elastic modulus of Plasticine with imposed strain. Results obtained using spherical and conical indenters.

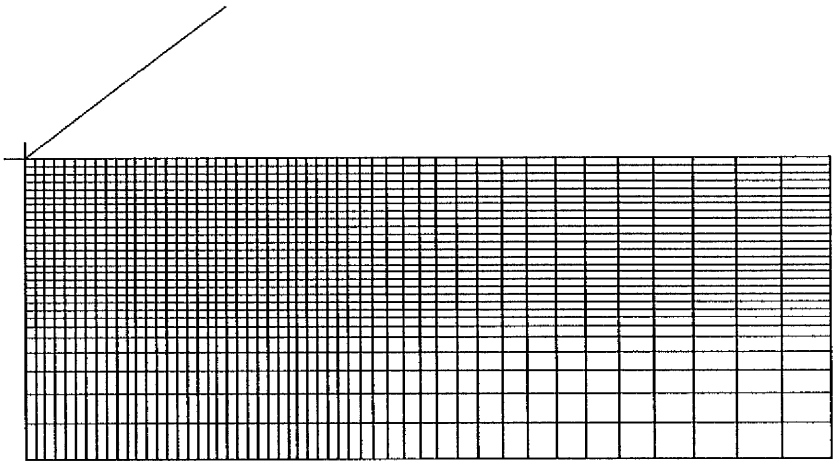

Figure 5.7 Finite element mesh used to model conical indentation.

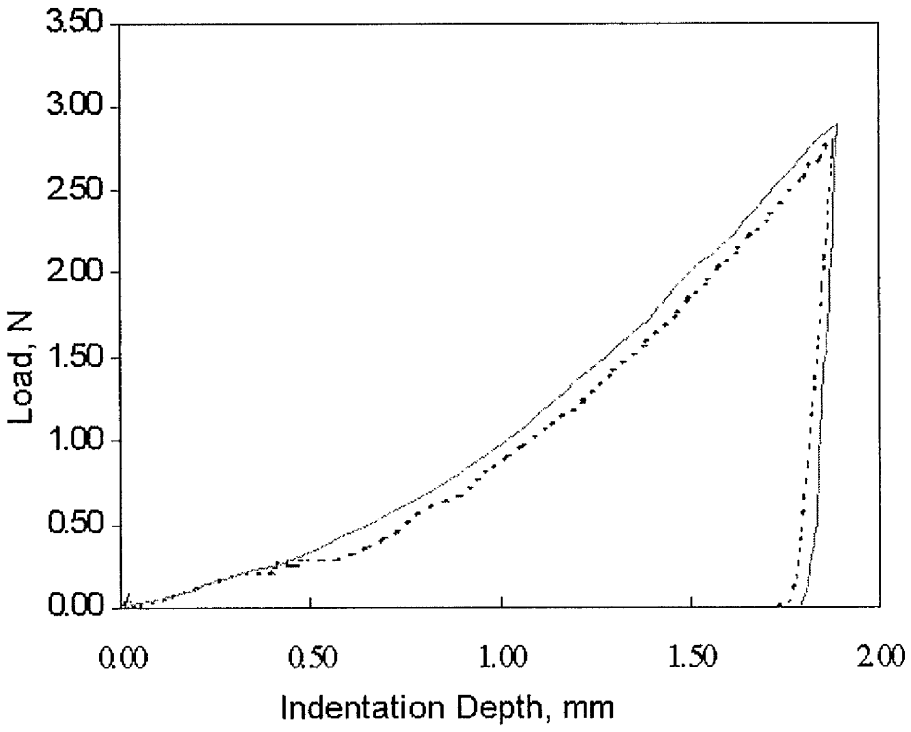

Figure 5.8 Comparison of load as a function of indentation depth obtained numerically (---) and experimentally (—) for a conical indenter with a semi-included angle of 30°.

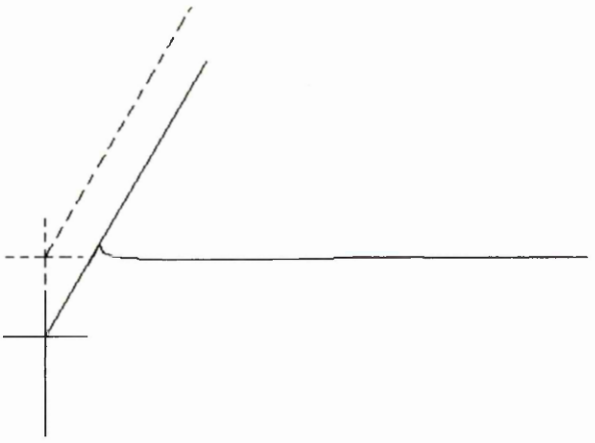

Figure 5.9 The surface profile shows the computed pile-up (—) under load, compared with the original surfaces (---).

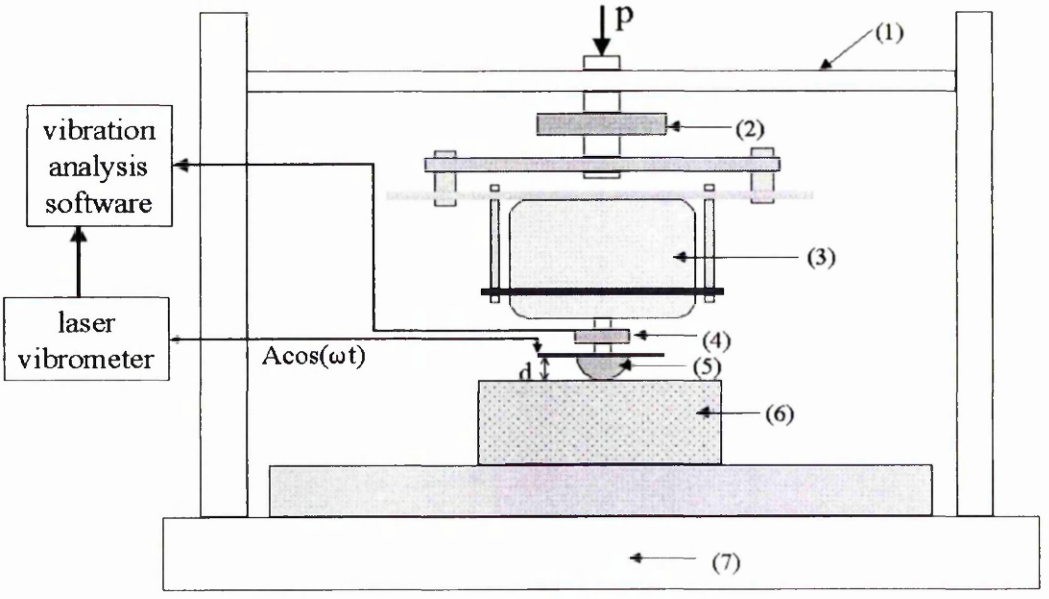

(1) crosshead, (2) load cell, (3) exciter, (4) piezoelectric force transducer, (5) indenter, (6) specimen, (7) LLOYD base.

Figure 5.10 Apparatus for oscillatory indentation.

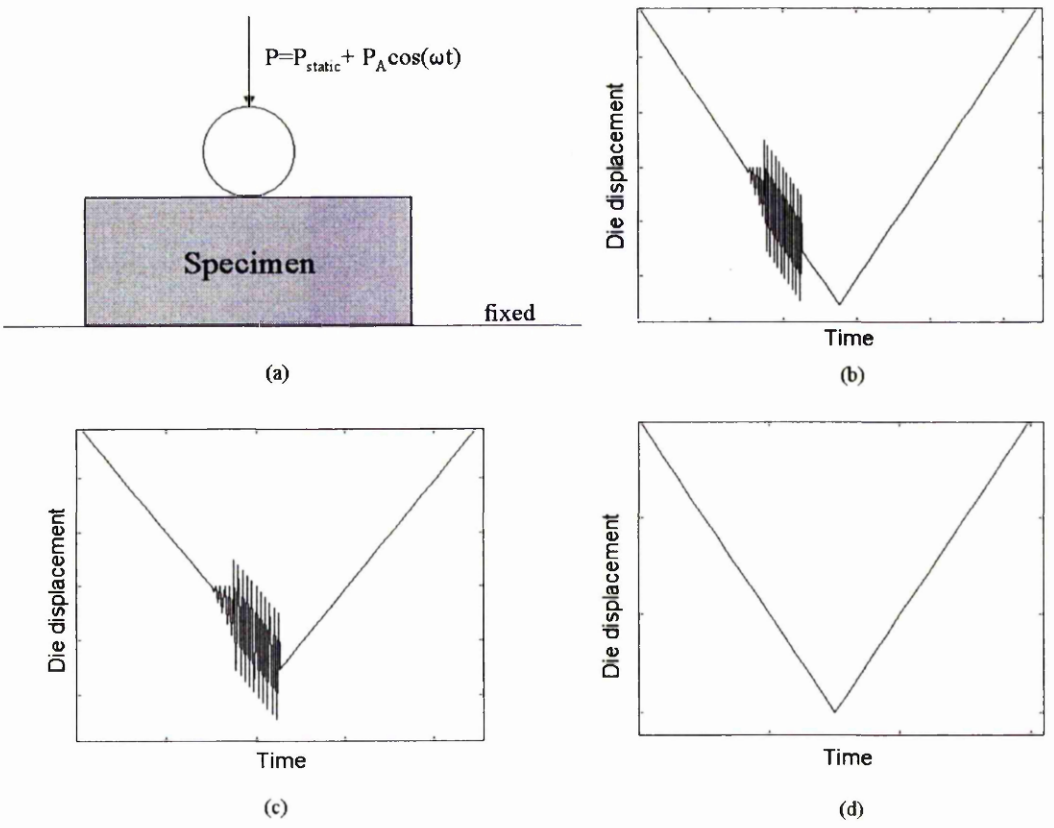

Figure 5.11 (a) Spherical indentation with vibration. Displacement history for (b) case 1, (c) case 2 and (d) case 3.

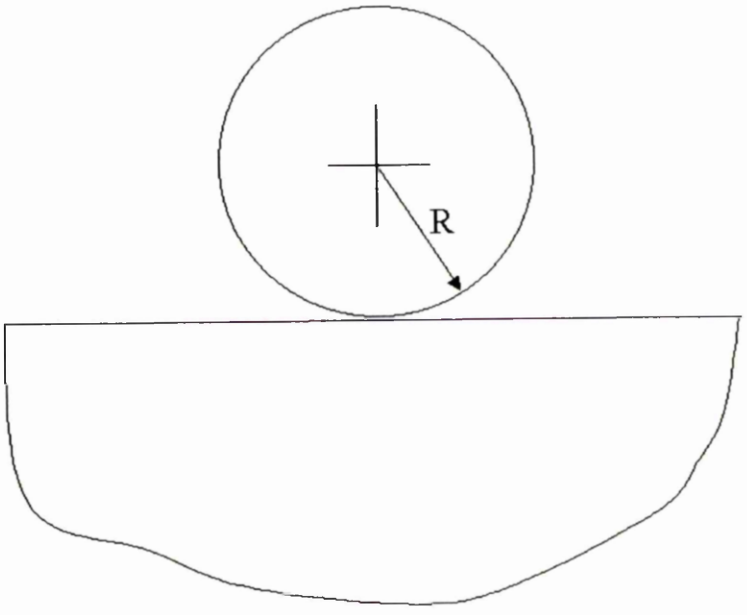

(a)

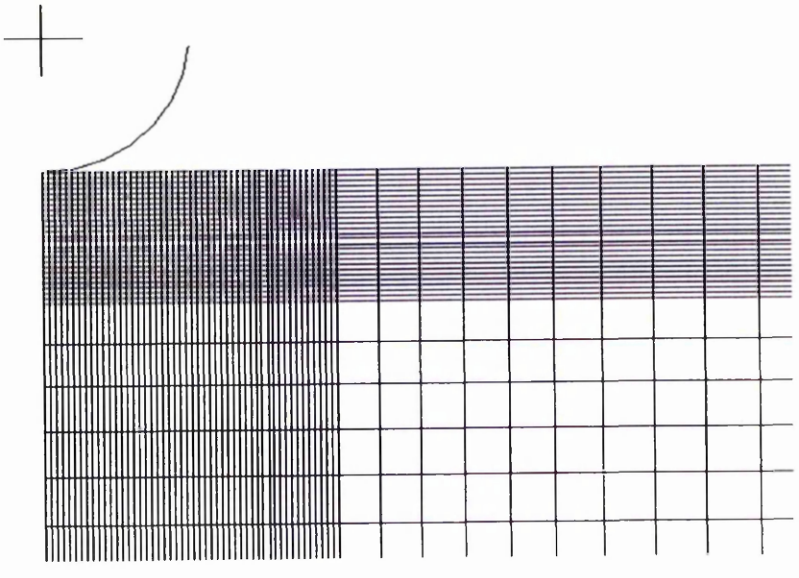

(b)

Figure 5.12 (a) Geometry and (b) undeformed mesh of FE model for axisymmetric spherical indentation.

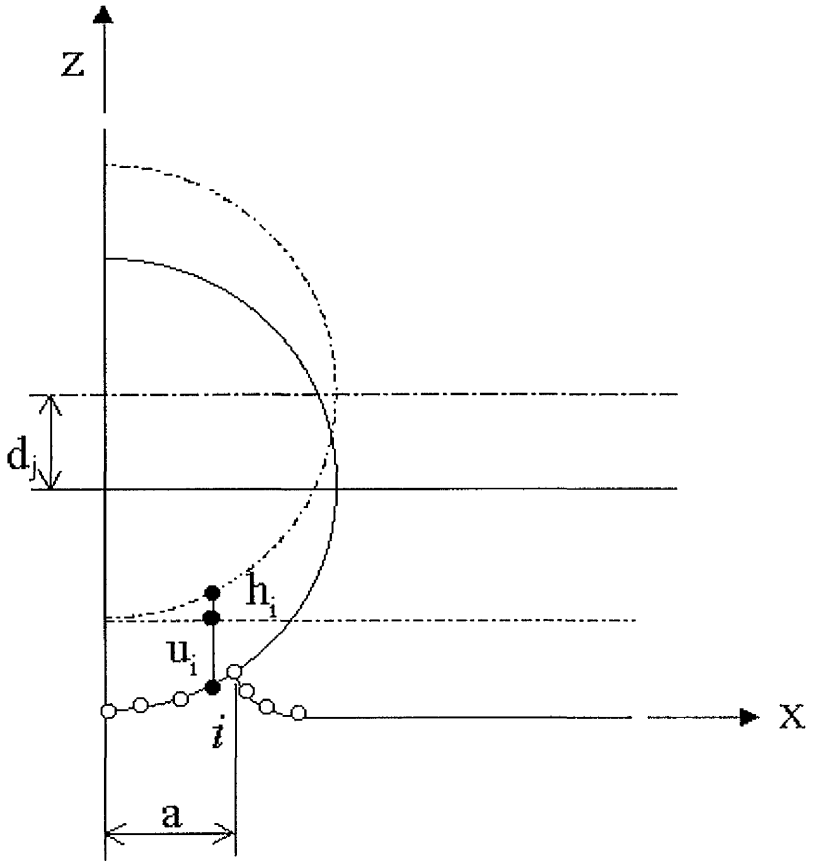

Figure 5.13 Displacement contact condition.

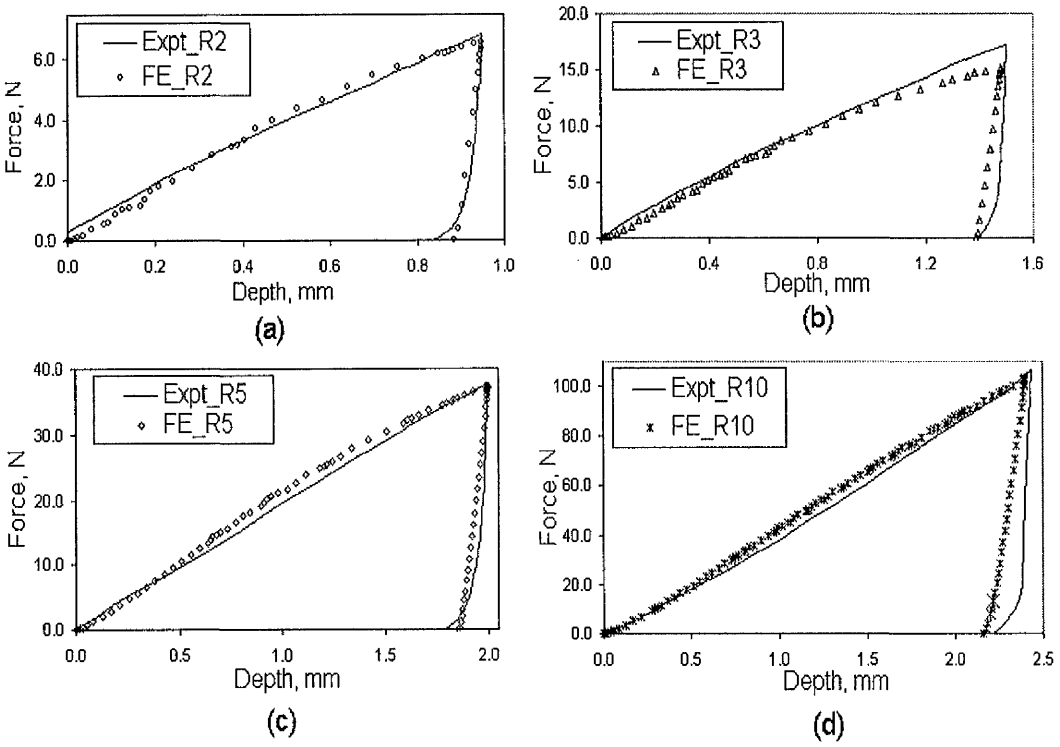

Figure 5.14 Load as a function of indentation depth obtained numerically and experimentally for spherical indenter with radius (a) 2, (b) 3, (c) 5 and (d) 10 mm.

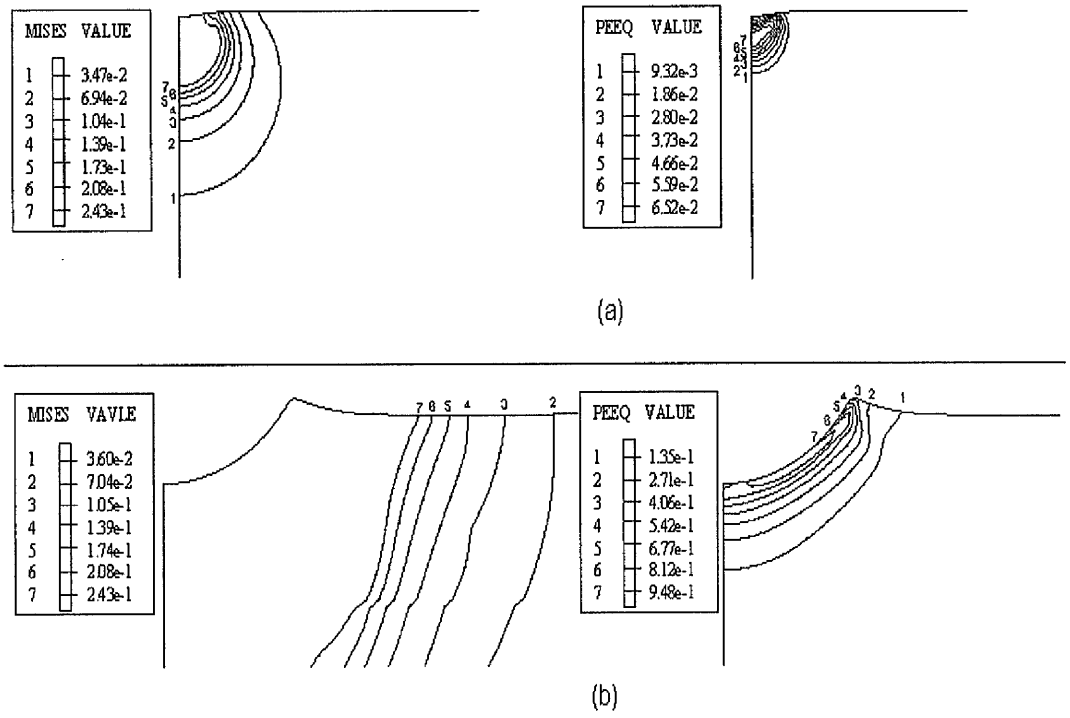

Figure 5.15 Contours of equivalent Mises stress and plastic strain corresponding to indentation depth (a) 0.15 mm and (b) 1.5 mm for a spherical indenter of radius 5 mm.

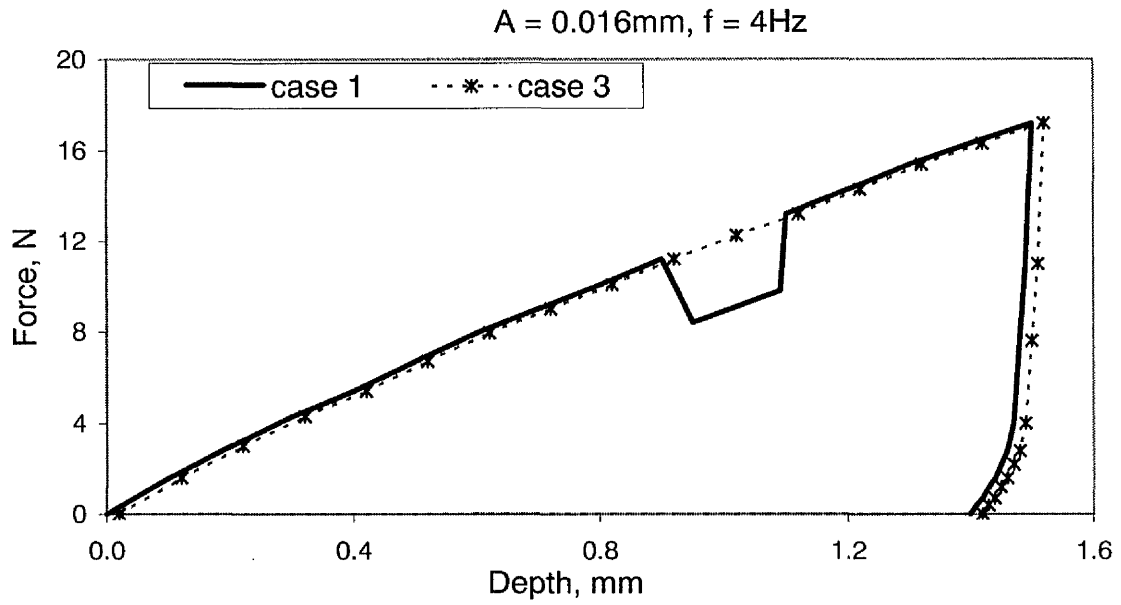

Figure 5.16 Load-depth relationship for R = 3 mm spherical indenter during oscillatory (case 1) and static (case 3) indentation.

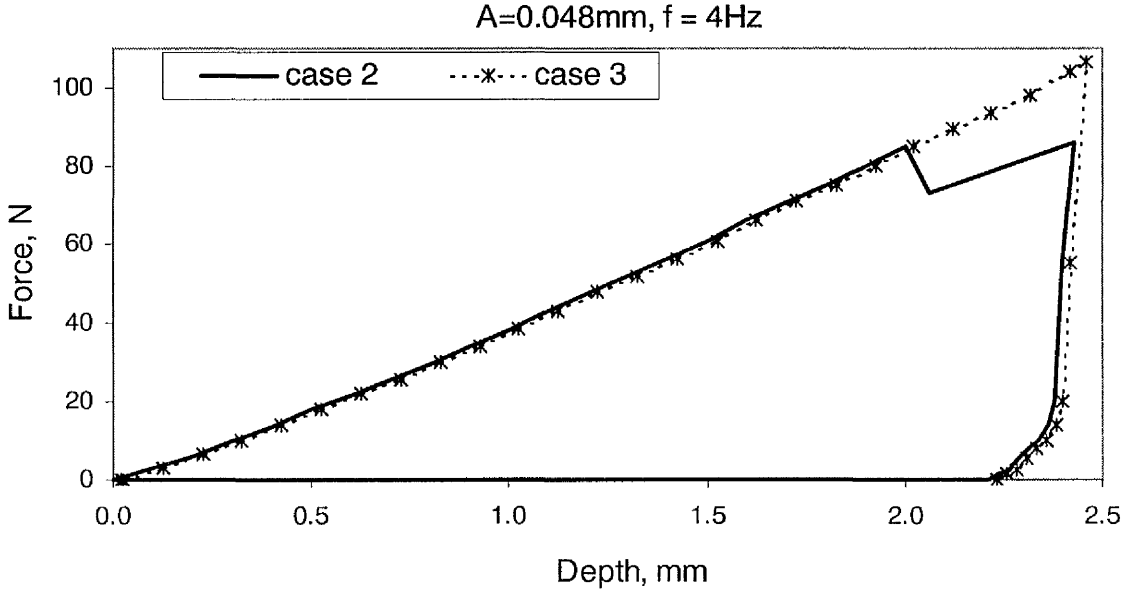

Figure 5.17 Load-depth relationship for R = 10 mm spherical indenter during oscillatory (case 2) and static (case 3) indentation.

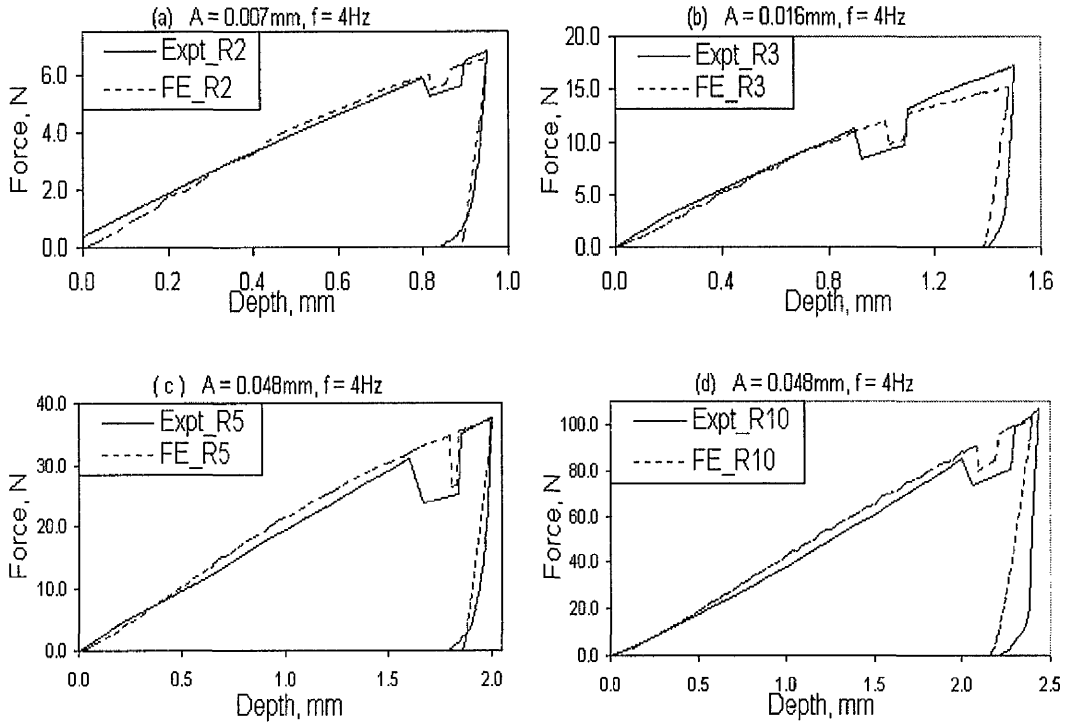

Figure 5.18 Load as a function of indentation depth (for vibration indentation case 1) for a spherical indenter of radius (a) 2 mm, (b) 3 mm, (c) 5 mm and (d) 10 mm, during intervals of vibration with various vibration amplitudes and frequency of 4Hz.

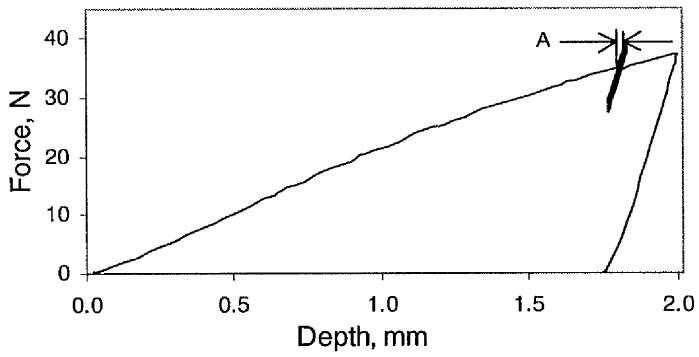

(a)

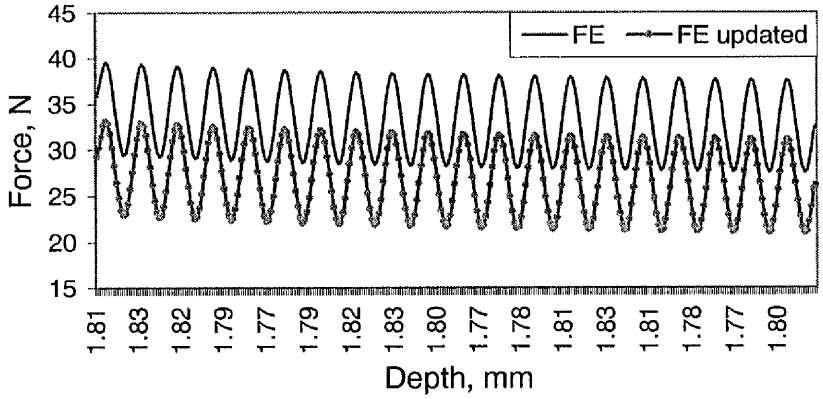

(b)

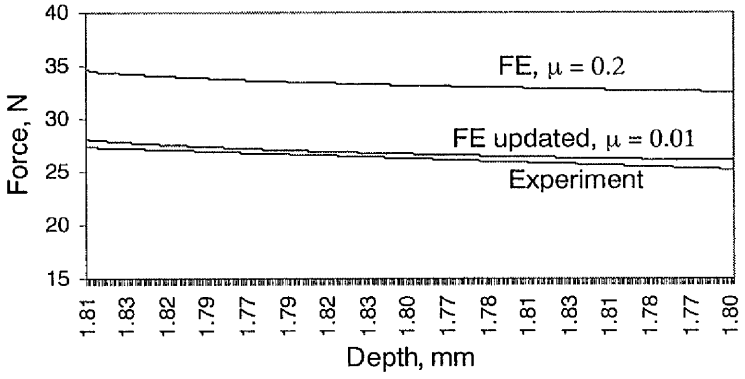

(c)

Figure 5.19 (a) FE simulation of force–depth data for Plasticine indented by a spherical indenter of radius 5 mm, (b) expanded view of interval A and, (c) the mean force value during interval A of vibration loading at an amplitude of 0.03 mm and frequency of 40 Hz under a lubricated boundary condition.

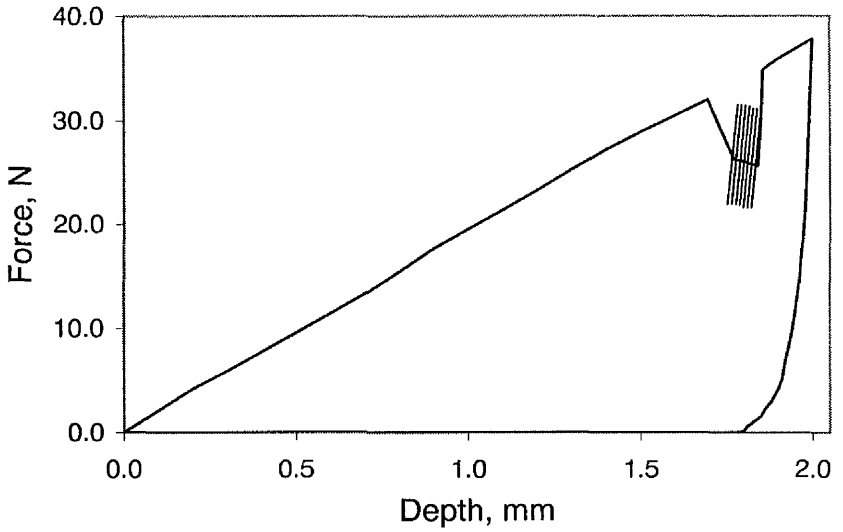

Figure 5.20 measured load-depth data for Plasticine indented by R = 5 mm sphere during oscillatory indentation at amplitude of 0.03 mm and frequency of 40 Hz under a lubricated boundary condition.

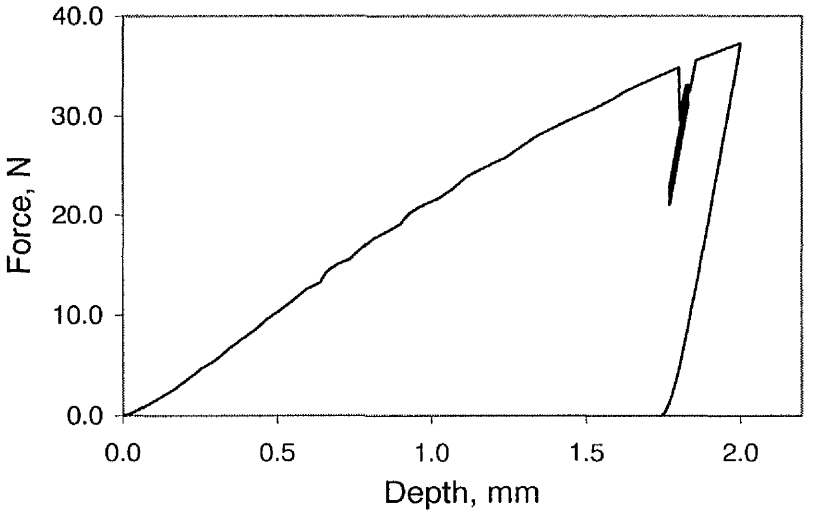

Figure 5.21 Load-depth data obtained from updated FE model, with μ = 0.01, for Plasticine indented by R = 5 mm sphere during oscillatory indentation at amplitude of 0.03 mm and frequency of 40 Hz under a lubricated boundary condition.

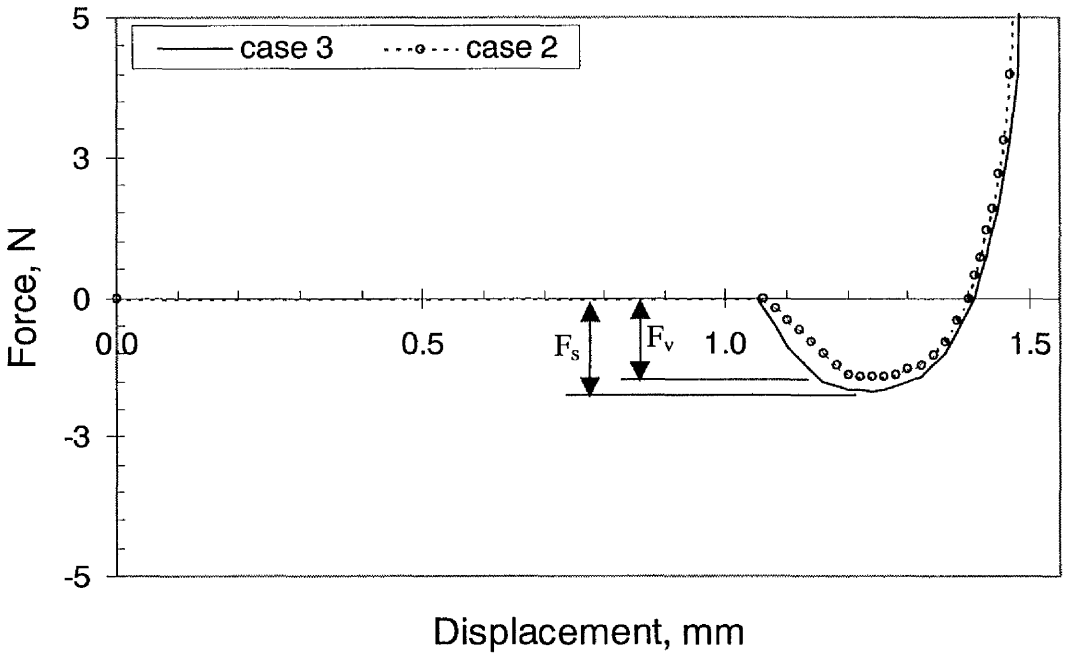

	R = 2mm	R = 3mm	R = 5mm	R = 10mm
F_V (N)	0.2	1.4	1.8	4.0
F_S (N)	0.25	1.8	2.4	5.0
Reduction ($1-F_V/F_S$) (%)	20 %	22 %	25 %	20 %

Figure 5.22 Force-separation curve shows the adhesion force for a spherical indenter with radius 3 mm. The reduced values of adhesion force for all spheres during oscillatory indentation (case 2), F_v, are listed in the table and compared with the values for static indentation (case 3), F_s.

Table 5.1 Parameters from fitted curves for the force displacement data of Plasticine; $h_{max} \approx$ 1-2 mm for the conical and spherical indentations, from equation (5.5).

INDENTER	m_1	n_1	h_o (mm)	m_2	n_2	h_r (mm)
R =2 mm	4.74	1.02	0.017	14.06	2.19	0.72
R =3 mm	8.04	0.94	0.012	14.64	1.92	1.37
R =5 mm	9.79	1.13	-0.020	11.02	2.50	1.68
R =10 mm	6.05	1.50	-0.015	14.98	2.13	1.58
$\theta = 30°$	0.92	1.77	-0.027	17.86	1.82	1.85
$\theta = 45°$	1.62	1.60	-0.026	9.03	2.17	1.60
$\theta = 60°$	2.58	1.69	-0.044	9.95	2.27	1.66
$\theta = 75°$	3.82	1.87	-0.064	16.28	2.00	1.55

Table 5.2 Dimensions and tip defects of the indenters used in the experimental study.

Spheres				
R (mm)	2.005	3.024	5.14	9.98
δ (mm)	0.0024	0.020	0.019	-0.0008
Cones				
θ (°)	30.05	45.04	59.66	75.16
δ (mm)	-0.021	-0.044	-0.0081	-0.018

Table 5.3 Material properties of indenter and Plasticine.

	E (MPa)	σ_0 (MPa)	ρ (Kg/m^3)	ν	n	K_{sc} (MPaS^n)
Spherical indenter	193000	200	7833	0.33		
Plasticine	16.5	0.28	1878	0.49	0.34	0.039

CHAPTER 6

CONCLUSIONS AND FUTURE WORK

6.1 Conclusions

This thesis has presented experimental and finite element analytical results of kinematic and low frequency oscillatory deformation of soft solid materials. Soft solids, which are also referred to as pastes, are dispersions of solid particles in a liquid medium. The response of the material and friction at the die/workpiece interface under different external constraints have been studied for efficient process operation design and optimisation, in terms of process speed, reliability and quality. This study used uniaxial upsetting and an indentation technique to investigate the effects of a superimposed oscillatory mechanism, and to establish a fundamental understanding of the contribution of stress superposition, and changes in the coefficient of friction, to improve interfacial conditions in vibration assisted processing of generic soft solid material.

Innovations in this research include:

(1) the characterisation of material flow during kinematic and vibration assisted processes, by finite element models which incorporate measurement data to provide a detailed knowledge of interfacial conditions, deformation history and stress-strain relationships of specimens,

(2) the design and control of the oscillating system to deliver identified optimum vibration loading parameters and to be adaptable to accommodate the requirement of supporting the high compression loads and the need to

achieve vibration amplitude constancy and uniformity throughout the process,

(3) characterisation and monitoring of tool vibration performance, providing data acquisition and analysis from LDV measurements and LMS software,

(4) definitive knowledge of the beneficial mechanisms of low frequency oscillation assistance in forming soft-solid materials.

This thesis considered various aspects of static deformation characteristics from upsetting and indentation of the soft plastic solid material, Plasticine, with well defined geometrical shapes. The successful simulations of the model material were created by the accurate and validated FE models which included the effects of elasticity, viscoplasticity, strain rate, large strains and a coulombic stress boundary condition in the presence of a lubricant. An analytical curve-fitting procedure has been derived to extract the indentation force-depth data. There was close agreement between the FE results and those obtained from upsetting and indentation experiments with respect to the force-displacement curves and deformed configurations for a range of friction coefficients, specimen sizes and platen velocities.

The application of low frequency axial oscillations to the tools in upsetting and indentation have been studied, which aimed to establish a fundamental understanding of the contribution of the oscillation effects on the material deformation and the interfacial boundary conditions. The FE models were developed, based on the accurate and validated models created for the kinematic deformation study, to simulate the superposition of oscillatory loading on the kinematic load in vibration assisted deformation of Plasticine. The models relied on experimental investigations to incorporate a realistic assessment of the reduction in the coefficient of friction, and resulted in a description of the beneficial mechanisms of oscillation assisted tooling.

The oscillatory tools have been successfully designed to provide the requirement of supporting the high deforming load and the need to achieve vibration amplitude constancy and uniformity throughout the process. Tool design relied initially on FE models to predict vibration behaviour. Models were validated by modal testing and updated to achieve the required vibration response in the experimental frequency range.

A series of upsetting and indentation experiments have been conducted with a range of Plasticine specimens. Measurement of reaction force, force oscillations, deformation and tool vibration response, and flow visualisation and surface inspections, provide all the deformation history for FE validation and allow identification of bollarding and barrelling effects consistent with different friction regimes.

The relationship between vibration condition and soft solid material flow is established. Vibration assisted forming results in a significant reduction in resistance of the forming material to deformation, by a combination of the stress superposition effect and a reduction in interface friction. The reduction in mean force is largely dependent on the vibration amplitude and shows a weak dependence on frequency.

In the final conclusion, these various specific achievements may be summarised as follows.

The rheological and interfacial parameters exhibited by the soft solid materials have been predicted by the validated finite element simulation with confidence. For a range of specimen sizes, platen velocities and friction coefficients, the predictions of the deformed configurations and interfacial and bulk stress, based upon the assumption of prevailing homogeneous deformation conditions and established Herschel-Bulkley mathematical models, does provide a generally accurate description of the overall magnitude of frictional and bulk forces

involved. The various data for these parameters have been found to be mutually consistent between the experimental methods and the FE procedures applied.

The FE models were subsequently developed to simulate the processes under superimposed vibration loading of the forming tools. The application of low frequency coaxial oscillations to the die in upsetting or indentation causes the material to be deformed intermittently once every cycle and elastically off-loaded during the remainder of the cycle. This results in an apparent reduction in the mean forming force. It is proposed that this will only be achieved when the peak velocity of the die exceeds the speed of forming. The reduction in mean force is largely dependent on the vibration amplitude and shows a weak dependence on frequency. These results are explained by stress superposition, where a vibration stress is superimposed on a non-oscillatory static stress. However, reduction in mean force by superposition alone is not commercially significant since, for strain rate dependent materials, the maximum stress can exceed the static value, and this overstress is due to the increase in strain rate by superimposed vibration.

More importantly, in processes where a lubricant is applied at the interface between the die and specimen, then the deformation produced by superimposed oscillation of the die enables real reductions in forming force to be realised. This is achieved since the deformation proceeds with a reduced mean forming force and a reduced maximum stress, such that the specimen never experiences a force exceeding that necessary to maintain static plastic deformation. The reduction in maximum force achieved is related to an improved friction condition at the die/specimen interface.

Finally, no change in the bulk material properties of the specimen when low frequency oscillations were applied.

It is believed that the processes of compressive forming with oscillations produce a reduction in the forming force and a beneficial change in the interfacial friction

conditions, and hence provide the opportunity for oscillatory energy to be applied with commercial success to optimising some soft solid material deformation processes.

6.2 Future Work

The current research has demonstrated the benefits of applying coaxial vibration of forming tools in soft solid forming processes using Plasticine as a model material. This work has concentrated on low frequency, low amplitude vibration in the first instance, due to the relative ease of control of the vibration input using conventional test equipment. Both FE and experimental results show that the beneficial effect of vibration has a weak influence due to frequency variations. Therefore, this research may be extended to an investigation of high power ultrasonic oscillations in soft solid material forming processes in the low ultrasonic range (20-40 kHz). In fact, vibration is more effectively applied to tooling when the system is resonant and this also allows much greater flexibility in conducting a range of forming experiments at sufficiently high vibration velocities. As the excitation force required to sustain resonance is low, significant energy benefits are also gained in ultrasonic applications. A further advantage of low ultrasonic frequencies to industrial users is the reduced noise contamination compared with sonic frequencies. Further, it has been postulated that beneficial changes in interfacial friction conditions are maximised at ultrasonic frequencies with little effect on the bulk characteristics [17].

Therefore, it is suggested that a fundamental understanding of the contributions of stress superposition, friction vector effect and changes in the coefficient of friction in ultrasonically assisted processes may be achieved by basing new studies on the wealth of knowledge from this current research. At ultrasonic frequencies, the temperature effects due to vibration will be significant and probably highly localised. Therefore, a new finite element model should be developed to incorporate a study of a coupled thermo-mechanical analysis. Also, a customised

tuned tooling design should be conducted to provide identified optimum vibration performance parameters for ultrasonically assisted upsetting.

The effects of coaxial vibration have been demonstrated in this thesis. A new understanding of the significance of tangential vibrations on interfacial friction would allow further evidence of friction effects to be predicted. No attempt was made to measure the local stresses at the die/specimen interface directly in this thesis. Thus, development of a directed stress measurement technique may provide further evidence of the changes in friction due to superimposed vibration.

Finally, verifying the benefits and widening the applicability of the technology may be achieved by using alternative materials and different standard tests including wedge indentation and extrusion.

APPENDICES

Appendix A Mathematical Transformation of Viscoplasticity

The viscoplastic associated flow rule is given by [71]

$$\dot{\varepsilon}_{ij}^{vp} = D^{*}\Phi(F)\frac{\partial F}{\partial \sigma_{ij}} \tag{A1}$$

where D^{*} is a physical constant for the material, σ_{ij} is the stress tensor and the force function $\Phi(F)$ defines the yield condition such that

$$\Phi(F) = 0 \text{ if } F \leq 0 \text{ and } \Phi(F) \neq 0 \text{ if } F > 0 \tag{A2}$$

Equation (A1) has been termed a viscoplastic stress overshoot model since the rate of increase of the viscoplastic components of the strain tensor depends upon the magnitude of the stresses in excess of the static yield condition. That is, the yield surface increases in size during loading. The static yield surface has a radius $\sqrt{2}\tau_0$ as defined by Von Mises yield criterion:

$$F = \frac{J_2^{1/2}}{\tau_0} - 1 \tag{A3}$$

where τ_0 is the static shear stress and $J_2^{1/2} = S_{ij}S_{ij}/2$ where J_2 is the second invariant of the stress deviation tensor and S_{ij} is the deviation components of the stress. Substitution of equation (A3) into equation (A1) leads to

$$\dot{\varepsilon}_{ij}^{vp} = \frac{D^*}{2\tau_0}\Phi(F)\frac{S_{ij}}{J_2^{1/2}} \tag{A4}$$

We will assume that $\Phi(F)$ takes the following general form [71]:

$$\Phi(F) = F^{1/n} = \left(\frac{J_2^{1/2}}{\tau_0} - 1\right)^{1/n} \tag{A5}$$

which on substitution into equation (A4) leads to

$$\dot{\varepsilon}_{ij}^{vp} = \frac{D^*}{2\tau_0}\left(\frac{J_2^{1/2}}{\tau_0} - 1\right)^{1/n}\frac{S_{ij}}{J_2^{1/2}} \tag{A6}$$

Equation (A6) may be writen in the following form:

$$\sqrt{I_2} = \frac{D^*}{2\tau_0}\left(\frac{J_2^{1/2}}{\tau_0} - 1\right)^{1/n} \tag{A7}$$

where $I_2\left(\dot{\varepsilon}_{ij}^{vp}\dot{\varepsilon}_{ij}^{vp}/2\right)$ is the second invariant of the strain rate tensor. Equation (A7) may be further rearranged as follows:

$$\dot{\varepsilon}^{vp} = D\left(\frac{\overline{\sigma}}{\sigma_0} - 1\right)^{p} \tag{A8}$$

where σ_0 is the uniaxial yield stress, $D = D^* / \sqrt{3}\tau_0$, $p = 1/n$. $\bar{\sigma}(= \sqrt{3J_2})$ and $\dot{\varepsilon}^{vp}(= 2\sqrt{I_2/3})$ are the effective stress and strain rates respectively. Equation (A8) leads to equation (3.1) where (σ_0 / D^n) is equivalent to the uniaxial plastic flow consistency, k.

Appendix B: Application of The Box-Cox Transformation

The dependent variable in the *P(h)* relationship is transformed using the Box-Cox transformation, and is given by:

$$Z_i(\lambda) = \frac{P_i^{\lambda} - 1}{\lambda \hat{P}^{(\lambda-1)}} \tag{B1}$$

where $Z_i(\lambda)$ is the normalised transformed variable, λ is a transformation parameter and $\hat{P}$ is the geometric mean of all P_i, $P_i > 0$. The magnitude of the transformation parameter, λ, is then determined by a criterion that is normally the minimisation of the sum of the squares of the residuals, $\sum \varepsilon_i^2$. The transformed variable $Z(\lambda)$ satisfies the required statistical conditions on the error distribution and linearises the functionality of the dependent variable. A linear relationship is then used to interrelate, by least squares fitting, the transformed variable, $Z_i(\lambda)$, and the independent variable h_i, which is of the form

$$Z(\lambda) = c' + m'h \tag{B2}$$

Such that $\sum_i \varepsilon_i^2(\lambda) = \sum_i [Z_i^{\lambda}(\lambda) - (c' + m'h_i)]^2$.

Substituting this equation into equation (B1) gives

$$P = (c + mh)^N \tag{B3}$$

where $c = c'\lambda\hat{P}^{(\lambda-1)} + 1$, $m = m'\lambda\hat{P}^{(\lambda-1)}$ and $N = 1/\lambda$.

Using the boundary conditions: $h = h_0$, at $P_1 = 0$ and $h = h_r$, at $P_2 = 0$, where h_0 and h_r denote the error and residual value of h in the loading and unloading curves respectively, equation (B3) may be written as

$$P_1 = m_1(h - h_0)^{n_1} \tag{B3a}$$

$$P_2 = m_2(h - h_r)^{n_2} \tag{B3b}$$

for the loading and unloading curves respectively.

Appendix C: Coefficient of Friction Determined From Ring Compression Test

Ring compression tests were carried out to obtain specific coefficients of friction under different lubrication conditions for the Plasticine used in this thesis.

The experimental procedure for a ring compression test was as follows:

1. The Plasticine test specimens were prepared and cut to the chosen diameter using a special ring cutter and then aged for 24 hours at 20°C, as described in Chapter 3. The dimensions of the specimen used in this study were 60 mm, 30 mm, and 20 mm in outer diameter, inner diameter, and height, respectively.
2. The ring compression tests were conducted by placing the specimens between two parallel stainless steel platens.
3. Abrasive paper, wax paper, talcum powder with silicon oil, and silicon grease were used to provide different friction boundary conditions.
4. To achieve a calculated determination of friction coefficient, a finite element analysis was developed for an interface with a constant coefficient of friction.
5. Specific friction calibration curves for Plasticine were reconstructed using the finite element results. The finite element analysis modelled the behaviour of Plasticine by means of a constitutive equation referred to in Chapter 3 of this thesis.

Finite element models were adopted to reproduce friction calibration curves for this thesis since the classical friction calibration curves generated by Male and Cockcroft [52] cannot provide accurate friction data. The reasons are discussed in Chapter 2. On the basis of experimental results obtained from the ring test and the computed calibration curves, specific coefficients of friction for the test conditions were obtained. These results are shown in figure A1. The coefficients of friction of 0.577, 0.3, 0.2, and 0.05 were selected for Plasticine utilising abrasive paper, wax paper, talcum powder with silicon oil, and silicon grease as friction boundary conditions respectively. These coefficients of friction were then used to model the behaviour of Plasticine deforming between the die/specimen interface.

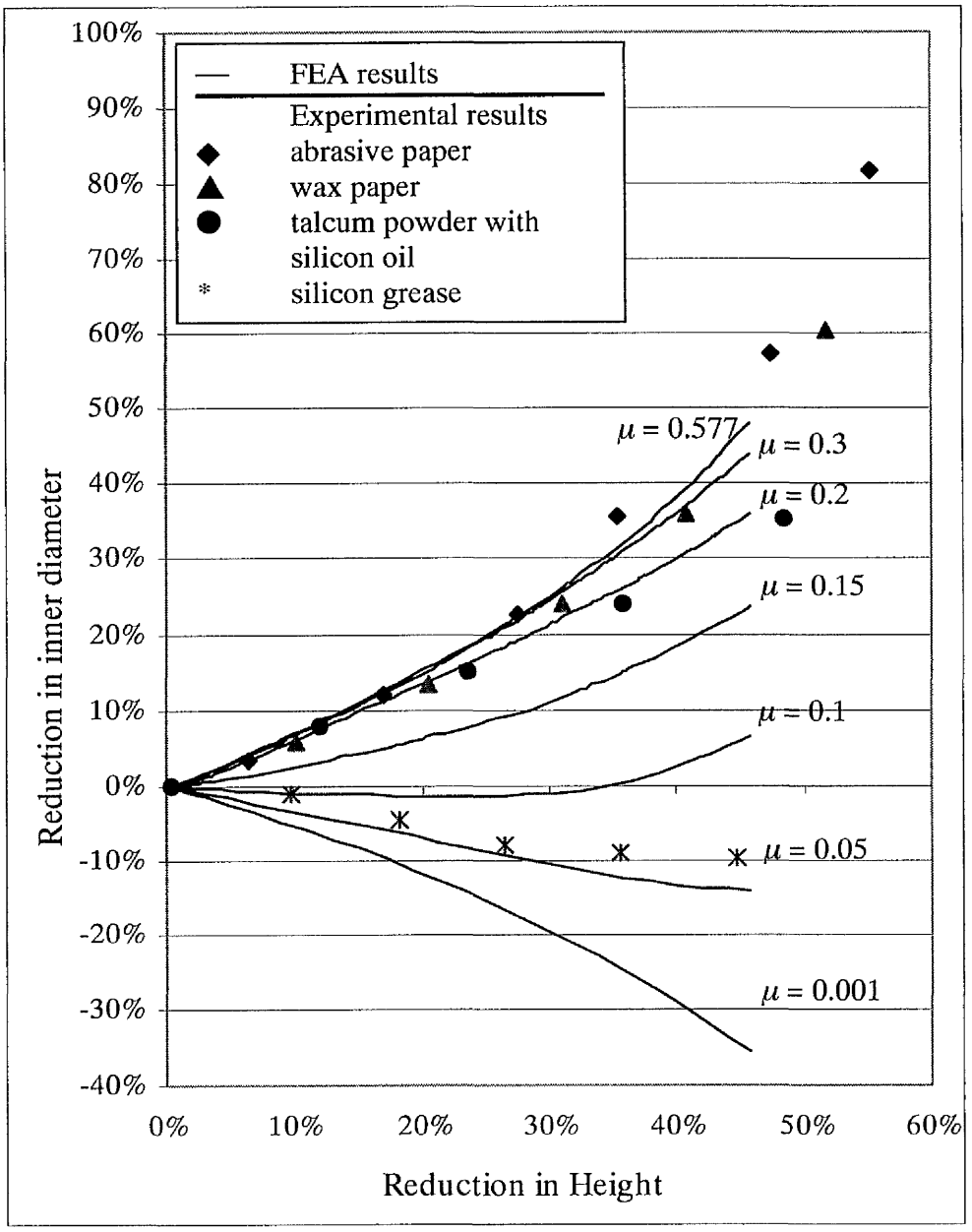

Figure A1 Friction calibration curves for Plasticine obtained from the finite element analysis (FEA) and experimental results.

Appendix D: List of Publications

1. Huang, Z., Lucas, M. and Adams, M.J., Viscoplastic material upsetting with oscillating dies, Proceedings of the SEM IX International Congress & Exposition on Experimental Mechanics, Orlando, USA, 2000, 434-437, ISBN: 0-912053-71-2.
2. Huang, Z., Lucas, M. and Adams, M.J., Effect of vibration on axisymmetric indentation of a model elasto-viscoplastic material, Proceedings of the 16th International Conference on Computer-Aided Production Engineering, Edinburgh, UK, 2000, 353-362, ISBN: 1-86058-263.
3. Huang, Z., Lucas, M. and Adams, M.J., The elasto-viscoplastic response of plasticine to indentation, Proceedings of the Fourth International Conference on Modern Practice in Stress and Vibration Analysis, Nottingham, UK, 2000, 469-480, ISBN 1-901537-21-8.
4. Huang, Z., Lucas, M. and Adams, M.J., Modelling wall boundary conditions in an elasto-viscoplastic material forming process, Journal of Material Processing Technology, Vol. 107 (1-3), 2000, 267-275.
5. Huang, Z., Lucas, M. and Adams, M.J., Finite element squeeze flow simulation of a viscoplastic material, Proceedings of the SEM Annual Conference on Theoretical, Experimental and Computational Mechanics, Cincinnati, USA, 1999, 471-474, ISBN: 0-912053-66-6.
6. Huang, Z., Lucas, M. and Adams, M.J., Influence of vibration on squeeze flow of a viscoplastic material, Proceedings of the SEM Annual Conference on Theoretical, Experimental and Computational Mechanics, Cincinnati, USA, 1999, 483-486, ISBN: 0-912053-66-6.
7. Huang, Z., Lucas, M. and Adams, M.J., A finite element study for optimising wall boundary conditions in an elasto-viscoplastic material forming process, Proceedings of the 15th International Conference on Computer-Aided Production Engineering, Durham, UK, 1999, 117-124, ISBN: 0-9535558-0-1.

8. Huang, Z., Lucas, M. and Adams, M.J., Vibration assisted forming of a paste, in Material Microstructure Properties and Modern Processing Techniques, (Eds.) J. Xie and Q. Zhu, 1999, 51-54, Chemistry Industrial Press, ISBN 7-5025-2692-7.

9. Huang, Z. and Lucas, M., Validated finite element simulation of thermal effect of viscoplastic material in upsetting, Journal of Material Technology, in press.

10. Huang, Z. and Lucas, M., Forming process optimisation and finite element method, Chinese Journal of Material Science, in press.

11. Huang, Z., Lucas, M. and Adams, M.J., Computer simulation of vibration effects on soft solid processing, The Sixth Chinese Materials Association (UK) Annual Congress and The First Symposium on Materials Science and Technology, London, October, 1998.

12. Huang, Z. and Lucas, M., Viscoplastic material flow in upsetting, The Seventh Chinese Materials Association (UK) Annual Congress, London, September, 1999 .

13. Huang, Z. and Lucas, M., Modelling of viscoplastic material properties and heat transfer of upsetting, The Second Materials Science and Technology Symposium of Chinese Youth Scholars, Hangzhou, China, October, 1999, N5.

REFERENCES

[1] Adams, M.J. and Briscoe, B.J., The optimisation of solid food processing operations, Trans. IChemE, Vol. 71, Part C, 251-263, 1993.

[2] Benbow, J.J., Lawson, T.A., Oxley, T.A. and Bridgwater, J., The prediction of paste extrusion pressure, American Ceramic Bull., 1821-1824, 1989.

[3] Benbow, J.J., The influence of liquid phase rheology on particulate paste extrusion, Third European Rhe. Conf. and Golden Jubilee Meeting of the British Society of Rheology, 50-53, 1990.

[4] Benbow, J.J. and Bridgwater, J., The influence of formulation on extrudate structure and strength, Chem. Eng. Sci., Vol. 42, 753-766, 1987.

[5] Adams, M.J., Briscoe, B.J. and Sinha, S.K., Interfacial and bulk rheological characterisations of paste materials in extrusion flow, 27th International SAMPE Technical Conference, 877-890, 1995.

[6] Adams, M.J., Edmondson, B., Caughey, D.G. and Yahya, R., An experimental and theoretical study of the squeeze-film deformation and flow of elastoplastic fluids, Journal of Non-Newtonian Fluid Mechanics, Vol. 51, 61-78, 1994.

[7] Barnes, H., The yield stress – a review or 'παντα ρει' – everything flows?, J. Non-Newtonian Fluid Mech., Vol. 81, 133-178, 1999.

[8] Adams, M.J., Briscoe, B.J. and Kamyab, M., The deformation and flow of highly concentrated dispersions, Advances in Colloid and Interface Science, Vol. 44, 143-182, 1993.

[9] Kamyab, M., Deformation of soft plastic solid by rigid walls, PhD thesis, Imperial College, London, 1992.

[10] Sherwood, J.D. and Durban, D., Squeeze flow of a power-law viscoplastic solid, J. Non-Newtonian Fluid Mech., Vol. 62, 35-54, 1996.

[11] Blaha, F. and Langenecker, B., Dehnung von Zink-Kristallen unter ultraschalleinwirkung, Z. Naturwiss., Vol.20, 556, 1955.

[12] Blaha, F. and Langenecker, B. and Oelschlagel, D., Plastic behaviour of metals under ultrasonics, Zeitshrift für Metallkunde, Vol. 51, 636, 1960.

[13] Izumi, O., Oyama, K. and Suzuki, Y., Effects of superimposed ultrasonic vibration on compressive deformation of metals, Trans. JIM, Vol. 7, 162-167, 1966.

[14] Winsper, C.E., Dawson, G.R. and Sansome, D.H., An introduction to the mechanics of oscillatory metalworking, Metals and Materials, 158-162, April, 1970.

[15] Langenecker, B., Effects of ultrasound on deformation characteristics of metals, IEEE Transaction on Sonic and Utrasonics, Vol. 13, No. 1, 1-8,1966.

[16] Kristoffy, I., Metal forming with vibrated tools, Transactions of the ASME, Journal of Engineering for Industry, 1168-1174, November 1969.

[17] Eaves, A.E., Smith, A.W., Waterhouse, W.J. and Sansome, D.H., Review of the application of ultrasonic vibrations to deforming metals, Ultrasonics, 162-170, July 1975.

[18] Dawson, G.R., Winsper, C.E. and Sansome, D.H., Application of high- and low- frequency oscillations to the plastic deformation of metals (part 1), Metal Forming, 234-238, August 1970.

[19] Dawson, G.R., Winsper, C.E. and Sansome, D.H., Application of high- and low- frequency oscillations to the plastic deformation of metals (part 2), Metal Forming, 254-261, September 1970.

[20] Lee, D., Sata, T. and Bakofen, W.A., The reduction of compressive deformation resistance by cyclic loading, J. Inst. Metals, Vol. 23, 418-422, 1964-65.

[21] Kariyawasam, V.P., Young, M.J.R. and Sansome, D.H., An experimental and design study of fixed-plug tube-drawing with radial ultrasonic vibration of the die, Wire Industry, Vol. 46, 104-116, 1979.

[22] Nerubai, M.S. and Usov, V.P., Use of ultrasonics when rolling internal threads, Russian Engineering Journal, Vol. 54, No. 10, 60-61, 1974.

[23] Sansome, D.H., Ultrasonic techniques, Metal Forming, Edited by Beadle, J.D., Chapter 21, 1971.

[24] Hurtado, J.F. and Melkote, N., Workpiece-fixture static friction under dynamic loading, Wear, Vol. 231, 139-152, 1999.

[25] Nevill, G.E. and Brotzen, F.R., The effect of vibrations on the static yield strength of low carbon steel, Proceedings of the American Society for Testing and Materials, Vol. 57, 751-758, 1957.

[26] Jones, J.B., Tube drawing, draw ironing, flare and flange forming with an ultrasonic assist, Metal Progress, Vol. 93, 103-107, 1968.

[27] Pohlman, R. and Lehfeldt, E., Influence of ultrasonic vibration on metallic friction, Ultrasonics, 178-185, October 1966.

[28] Balamuth, L., Ultrasonic motors fabricate metals and plastics, S.A.E. J., Vol. 74, No. 6, 72-76, 1966.

[29] Rees, T.W. and Rippon, D.J., The application of ultrasonic vibrations in tube drawing, Developments in the Drawing of Metals, 132-140, 1983.

[30] Sansome, D.H., Engineering developments in ultrasonic tube-draw equipment, ITA Conf. Tube 89, Singapore, 1-16, 1989.

[31] Siegert, K. and Möck, A., Wire drawing with ultrasonically oscillating dies, Journal of Materials Processing Technology, Vol. 60, 657-660, 1996.

[32] Astashev, V.K., Effect of ultrasonic vibration of a single-point tool on the process of cutting, Journal of Machinery manufacture and Reliability, No. 3, 65-70, 1992.

[33] Smith, A.C., Lucas, M, Nurse, A.D. and Graham, G., Ultrasonic cutting – a fracture mechanics model, Ultrasonics, Vol. 34, No. 7, 197-203, 1996.

[34] Tsujino, J., Recent developments of ultrasonic welding, IEEE Ultrasonics Symposium, Vol. 2, 1051-1060, 1995.

[35] Godfrey, D., Vibration reduces metal to metal contact and an apparent reduction in friction, A.S.L.E. Trans., Vol. 10, 183-192, 1967.

[36] Lenkiewicz, W., The sliding friction process – effect of external vibrations, Wear, Vol. 13, 99-108, 1969.

[37] Mitskevich, A.M., Motion of a body over a vibrating surface, Soviet Physics: Acoustics, Vol. 13(3), 348-351, 1968.

[38] Sansome, D.H., Recent developments in oscillatory metal working, Engineering, 243-247, April 1973.

[39] Kirchner, H.O.K., Kromp, W.K., Prinz, F.B. and Trimmel, P., Plastic deformation under simultaneous cyclic and unidirectional loading at low and ultrasonic frequencies, Materials Science and Engineering, Vol. 68, 197-206, 1984.

[40] Fridman, H.D. and Levesque, P., Reduction of static friction by sonic vibration, Journal of Applied Physics, 1572-1575, October 1959.

[41] Benbow, J.J. and Bridgwater, J., The role of frictional forces in paste extrusion, Tribology in Particle Technology, Chapter 1.5, Briscoe, B.J. and Adams, M.J., Eds. Adam Hilger, U.K., 80-90, 1987.

[42] Adams, M.J., Biswas, S.K., Briscoe, B.J. and Kamyab, M., The effects of interface constraints on the deformation of pastes, Powder Technology, Vol. 65, 381-392, 1991.

[43] Herschel, W.H. and Bulkley, R., Measurement of consistency as applied to rubber-benzene solutions, Proceedings of the American Society for Testing Materials, 621-633, 1926.

[44] Briscoe, B.J., Biswas, S.K., Sinka, S.K. and Panesar, S.S., The scratch hardness and friction of a soft rigid plastic solid, Tribology Int., Vol. 26, 183-193, 1993.

[45] Huang, Z., Lucas, M. and Adams, M.J., The elasto-viscoplastic response of plasticine to indentation, Proceedings of the Fourth International Conference on Modern Practice in Stress and Vibration Analysis, 469-480, Nottingham, 2000.

[46] Rooyen, G.T. and Backofen, W.A., A study of interface friction in plastic compression, Int. J. Mech. Sci., Vol. 1, 1-27, 1960.

[47] Adams, M.J., Aydin, I., Briscoe, B.J. and Sinha, S.K., A finite element analysis of the squeeze flow of an elasto-viscoplastic paste material, J. Non-Newtonian Fluid Mech., Vol. 71, 41-57, 1997.

[48] Vertin, K.D. and Majlessi, S.A., Finite element analysis of axisymmetric upsetting process using the deformation theory of plasticity, ASME Journal of Engineering for Industry, Vol. 115, 450-458, 1993.

[49] Carter, W. T. and Lee, D., Further analysis of axisymmetric upsetting, ASME Journal of Engineering for Industry, Vol. 108, 198-204, 1986.

[50] Sofuglu, H. and Rasty, J., On the measurement of friction coefficient utilizing the ring compression test, Tribology International, Vol. 32, 327-335, 1999.

[51] Moon, Y.H. and Tyne, V., Validation via FEM and plasticine modelling of upper bound criteria of a process-induced side-surface defect in forgings, Journal of Materials Processing Technology, Vol. 99, 185-196, 2000.

[52] Male, A.T. and Cockcroft, M.G., A method for the determination of the coefficient of friction of metals under conditions of bulk plastic deformation, Journal of the Institute of Metals, Vol. 93, 38-47, 1964.

[53] Sofuglu, H. and Rasty, J., On the measurement of friction coefficient utilizing the ring compression test II: effects of deformation speed, strain rate and barreling, PD-Vol. 75, Engineering Systems Design and Analysis, Vol. 3, 189-197, ASME 1996.

[54] Rudkins, N.T., Hartley, P., Pillinger, I. and Petty, D., Friction modelling and experimental observations in hot ring compression tests, Journal of Materials Processing Technology, Vol. 60, 349-353, 1996.

[55] Yagishita, K., Tsukamoto, H., Egawa, T., Oomori, S. and Ibushi, J., Study of simulative model test for metal forming using plasticine, Mitsubishi Heavy Industries, Mitsubishi Tech. Bull., 1-11, 1974.

[56] Wong, S.F., Hodgson, P.D., Chong, C.-J. and Thomson, P.F., Physical modelling with application to metal working, especially to hot rolling, Journal of Materials Processing Technology, Vol. 62, 260-274, 1996.

[57] So, H., Lin, Y.F. and Huang, K.W., Comparison of flow patterns between plasticine and aluminium alloys in hot-precision forging, Journal of Materials Processing Technology, Vol. 66, 39-48, 1997.

[58] Segawa, A. and Kawanami, T., Rolling-deformation characteristics of clad materials determined by model experiment and numerical simulation:

experimental rolling tests using plasticine, Journal of Materials Processing Technology, Vol. 47, 375-384, 1995.

[59] Sofuoglu, H. and Rasty, J., Three-dimensional analysis of extrusion process utilizing the physical modelling technique, ASME Journal of Energy Resources Technology, Vol. 115, 32-40, 1993.

[60] Green, A.P., The use of plasticine models to simulate the plastic flow of metals, Philosophical Magazine, Vol. 42, No. 327, 365-373, 1951.

[61] Keife, H., Extrusion through two die openings: a 2D upper-bound analysis checked by plasticine experiments, Journal of Materials Processing Technology, Vol. 37, 189-202, 1993.

[62] Wanheim, T et al., Physical modelling of metal forming processes, Process Modelling, Proceedings of ASM Process Modelling Sessions, Materials and Processing Congresses, ASM 146, 1978-1979.

[63] Arentoft, A., Gronostajski, Z., Niechjowicz, A. and Wanheim, T., Physical and mathematical modelling of extrusion processes, Journal of Materials Processing Technology, Vol. 106, 2-7, 2000.

[64] Boucly, P., Oudin, J. and Ravalard, Y., Simulation of ring rolling with new wax-based model materials on a flexible experimental machine, Journal of Mechanical Working Technology, Vol. 16, 119-143, 1988.

[65] Bramley, A.N. and Mynors, D.J., The use of forging simulation tools, Materials and Design, Vol. 21, 279-286, 2000.

[66] Hacquin, A., Montmitonnet, P and Guillerault, J.P., A steady state thermo-elastoviscoplastic finite element model of rolling with coupled thermo-elastic

roll deformation, Journal of Materials Processing Technology, Vol. 60, 109-116, 1996.

[67] Shih, A.J.M. and Yang, H.T.Y., Experimental and finite element simulation methods for rate-dependent metal forming process, International Journal for Numerical Methods in Engineering, Vol. 31, 345-367, 1991.

[68] Balaji, P.A., Sundararajan, T. and Lal. G.K., Viscoplastic deformation analysis and extrusion die design by FEM, ASME Journal of Applied Mechanics, Vol. 58, 644-650, 1991.

[69] Johnson, W. and Mellor, P.B., Engineering Plasticity, Van Nostrand Reinold, 1973.

[70] Hsu, T., A study of the compression test for ductile materials, Materials Research and Standards, Vol. 9, 20-25, December 1969.

[71] Perzyna, P., The constitutive equations for rate sensitive plastic materials, Quart. Appl. Maths., Vol. 20, 321-332, 1963.

[72] O'Shea, K, Enhanced vibration control of ultrasonic tooling using finite element analysis, Vibration Analysis-Analytical and Computational ASME, Vol. 37, 259-265, 1991.

[73] Lucas, M., Vibration sensitivity in design of ultrasonic forming dies, Ultrasonics, Vol. 34, 35-41, 1996.

[74] Nicoletti, N., Aubry, E., Fendeleur, D. and Renner, M., Natural frequencies of a tensioned circular plate, Proceedings of the International Modal Analysis Conference, Vol.1, 332-335, 1997.

[75] Tabor, D., A simple theory of static and dynamic hardness, Proc. R. Soc. A, Vol. 192, 247-274, 1948.

[76] Stillwell, N.A. and Tabor, D., Elastic recovery of conical indentations, Proc. Phys. Soc. London, Vol. 78, 169-179, 1961.

[77] Johnson, K.L., The correlation of indentation experiments, J. Mech. Phys. Solids, Vol. 18, 115-126, 1970.

[78] Bower, A.F., Fleck, N.A., Needleman, A. and Ogbonna, N., Indentation of a power law creeping solid, Proc. R. Soc. Lond. A., Vol. 44, 97-124, 1993.

[79] Lawrence, C.J., Adams, M.J., Briscoe, B.J. and Kothari, D.C., Wedge indentation and stress relaxation of a viscoelastic paste, Proceedings of the 3rd World Congress on Particle Technology, No. 60, 1-10, 1998.

[80] Oliver, W.C. and Pharr, G.M., An improved technique for determining hardness and elastic modulus using load and displacement sensing indentation experiments, J. Mater. Res., Vol. 7, No. 6, 1564-1583, 1992.

[81] Chaudhri, M.M., Subsurface deformation patterns around indentations in work-hardened mild steel, Philosophical Magazine Letter, Vol. 67, No. 2, 107-115, 1993.

[82] Briscoe, B.J. and Sebastian, K.S., The elastoplastic response of poly (methylmethacrylate) to indentation, Proc. R. Soc. Lond. A, Vol. 452, 439-457, 1996.

[83] Johnson, K.L., Contact mechanics, Cambridge University Press, 1985.

[84] Adams, M.J., Briscoe, B.J., Kothari, D.C. and Lawrence, C.J., Plane-strain wedge indentation of a soft plastic solid, The 1997 Jubilee Research Event, 317-320, 1997.

[85] Yang, F. and Li, J.C.M., Effect of friction and cavity depth on the elastic indentation of a cylindrical rod, Mechanics and Materials, Vol. 25, 163-172, 1997.

[86] Sneddon, I.N., The relation between load and penetration in the axisymmetric bousinesq problem for a punch of arbitrary profile, Int. J. Engng. Sci., Vol. 3, 47-57, 1965.

[87] Adams, M.J., Gorman, D.M. and Johnson, S.A., Nanoindentation of of poly (methyl methacrylate), To be published in the Proceedings of the Mater. Res. Soc. Symp. 'Fundamentals of Nanoindentation and Nanotribology II', Boston, 27 - 30th Nov. 2000.

[88] Loubet, J.L., Georges, J.M., Marchesini, O. and Meille, G., Vickers indentation curves of MgO, Trans. ASME: J. Tribol., Vol. 106, 43-48, 1984.

[89] Box, G.E.P. and Cox, D.R., An analysis of transformations, J. Roy. Statistical Soc. London, Vol. 26, 211-252, 1964.

[90] Adams, M.J., Briscoe, B.J. and Sinha, S.K., An indentation study os an elastoviscoplastic material, Philosophical Magazine, Vol. 74, No. 5, 1225-1233, 1996.

[91] Tabor, D., Hardness of Metals, Oxford University Press, 1951.